11 A Global View of Remote Sensing of Rangelands

Evolution, Applications, Future Pathways

Matthew Reeves, Robert Washington-Allen, Jay Angerer, E. Raymond Hunt Jr., Wasantha Kulawardhana, Lalit Kumar, Tatiana Loboda, Thomas Loveland, Graciela Metternicht, R. Douglas Ramsey, Joanne V. Hall, Trenton Benedict, Pedro Millikan, Angus Retallack, Arjan J.H. Meddens, William K. Smith, and Wen Zhang

ACRONYMS AND DEFINITIONS

ATSR	Along-Track Scanning Radiometer
ENVISAT	Environmental Satellite
ERTS	Earth Resources Technology Satellite
ESRI	Environmental Systems Research Institute
ETM+	Enhanced Thematic Mapper Plus
EVI	Enhanced Vegetation Index
FAO	Food and Agriculture Organization of the United Nations
fPAR	Fraction of Photosynthetically Active Radiation
GIMMS	Global Inventory Modeling and Mapping Studies
GPP	Gross Primary Production
ICESat	Ice, Cloud, and Land Elevation Satellite
LAI	Leaf Area Index
MERIS	Medium Resolution Imaging Spectrometer
MSS	Multispectral Scanner
MODIS	Moderate-Resolution Imaging Spectroradiometer
NASA	National Aeronautics and Space Administration
NDBR	Normalized Difference Burn index
NDVI	Normalized Difference Vegetation Index
NIR	Near-Infrared
NOAA	National Oceanic and Atmospheric Administration
NPP	Net Primary Productivity
OLI	Operational Land Imager
SAR	Synthetic Aperture Radar
SAVI	Soil Adjusted Vegetation Index
S-NPP	Suomi National Polar-orbiting Partnership
SST	Sea Surface Temperature
SWIR	Shortwave infrared

DOI: 10.1201/9781003541165-14

TIRS Thermal Infrared Sensor
TNDVI Transformed Normalized Difference Vegetation Index
UAV Unmanned Aerial Vehicles
VIIRS Visible Infrared Imaging Radiometer Suite

11.1 INTRODUCTION

The term “rangeland” is rather nebulous and there is no single definition of rangeland that is universally accepted by land managers, scientists, or international bodies (Reeves and Mitchell, 2011; Lund, 2007). Dozens and possibly hundreds (Lund, 2007) of definitions and ideologies exist because various stakeholders often have unique objectives requiring different information. To describe the role of remote sensing in a global context it is, however, necessary to provide definitions to orient the reader. The Food and Agricultural Organization of the United Nations (FAO) convened a conference in 2002 and again in 2013 to begin addressing the issue of harmonizing definitions of forest-related activities. Based on this concept, here rangelands are considered lands usually dominated by non-forest vegetation. The Society for Range Management defines rangelands as (SRM, 1998):

> Land on which the indigenous vegetation (climax or natural potential) is predominantly grasses, grass-like plants, forbs, or shrubs and is managed as a natural ecosystem. If plants are introduced, they are managed similarly. Rangelands include natural grasslands, savannas, shrublands, many deserts, tundra, alpine communities, marshes, and wet meadows.

Rangelands occupy a wide diversity of habitats and are found on every continent except Antarctica. Excluding Antarctica and barren lands, rangelands occupy 52% of the Earth’s surface based on the land cover analysis presented in Figure 11.1. Figure 11.1 is based on the 2018 MODIS

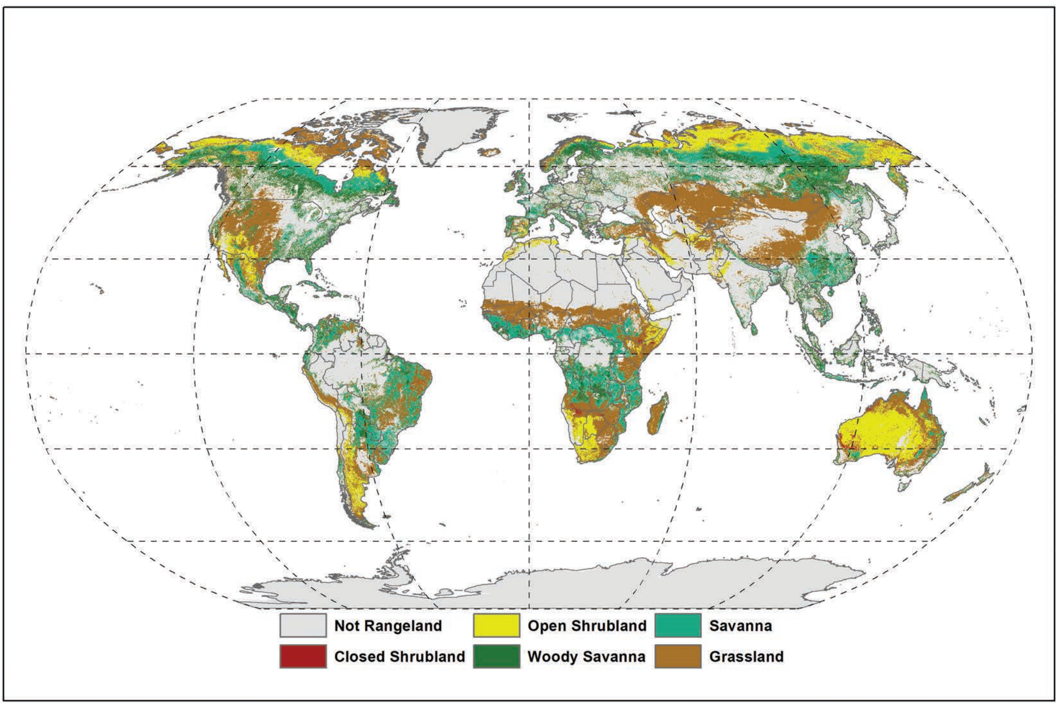

FIGURE 11.1 Global distribution of rangeland land cover types (collection 6 MODIS land cover (MCD12Q1 and MCD12C1) considered rangelands for this chapter. (Sulla-Menashe and Fiedl, 2018.)

Collection 6.0, 1 km land cover (the University of Maryland "UMD" classification) and suggested rangeland classes for this dataset are closed shrubland, open shrubland, woody savanna, savanna, and grassland. Using these classes, Russia, Australia, and Canada are the top three countries with the most rangelands (Table 11.1) representing 18, 10, and 8% of the global extent, respectively. The large areal extent of rangelands, high cost of ground data collection and quest for societal well-being have, for decades, provided rich opportunity for remote sensing to aid in answering pressing questions. Collectively, these lands provide nearly 18 trillion dollars to the global economy each year (Costanza et al., 2014).

11.2 HISTORY AND EVOLUTION OF GLOBAL REMOTE SENSING

The application of digital remote sensing to rangelands is as long as the history of digital remote sensing itself. Before the launch of the Earth Resources Technology Satellite (ERTS)—later renamed Landsat, scientists were evaluating the use of multispectral aerial imagery to map soils and range vegetation (Yost and Wenderoth, 1969). During the late 1960s, the promise of ERTS, designed to drastically improve our ability to update maps and study Earth resources, particularly in developing countries, was eagerly anticipated by a number of government agencies (Carter, 1969). With the ERTS launch on July 23, 1972, a flurry of research activity aimed at the application of this new data source to map Earth resources began. Practitioners who pioneered the use of satellite based digital remote sensing found the new data source a significant value for rangeland assessments (e.g., Rouse et al., 1973, Rouse et al., 1974, Bauer, 1976). This early work established many of the basic techniques still in use today to assess and monitor global rangelands. The following subsections discuss the evolution of remote sensing data, methods, and approaches in various decades.

11.2.1 Beginning of Landsat MSS Era, 1970s

In this first decade of satellite-based digital remote sensing, rangeland scientists quickly assessed the capabilities of this new tool across the globe (Graetz et al., 1976, Rouse et al., 1973). Work

TABLE 11.1

Global Area of Rangeland Vegetation Types Estimated Using MODIS Land Cover Data (Mod12Q1, Collection 6.1) for the Top 10 Countries with the Most Rangeland. CSL is closed shrubland, OSL is open shrubland and rangeland proportion is the rangeland area column divided by the Area column divided by 100.

Country	Area	CSL	Grassland	OSL	Savanna	Woody Savanna	Rangeland area	Rangeland Proportion
				Km^2				%
Russia	16,911,018	19,331	2,376,004	3,341,197	2,879,614	2,819,843	11,435,990	68
Australia	7,701,679	277,052	1,859,416	4,190,891	475,195	101,371	6,903,926	90
Canada	9,901,655	398	2,028,688	893,386	1,733,698	1,863,027	6,519,196	66
United States	9,449,630	19,604	2,999,071	890,464	898,098	1,265,172	6,072,409	64
China	9,403,880	1,601	2,786,941	8,019	960,887	833,217	4,590,665	49
Brazil	8,504,556	19,493	1,937,084	1,425	2,096,610	370,273	4,424,885	52
Kazakhstan	2,834,000	179	2,318,399	5,103	9,374	12,748	2,345,802	83
Argentina	2,781,182	1,297	873,035	667,471	413,937	86,635	2,042,375	73
Mexico	1,961,256	7,658	513,387	398,736	323,783	218,373	1,461,938	75
Angola	1,252,148	16,052	453,782	19,959	421,079	217,768	1,128,640	90

by Rouse et al. (1973), in what would later become the Normalized Difference Vegetation Index (NDVI) (Rouse et al., 1974), applied multi-temporal ERTS (Landsat 1) at 79 m spatial resolution data to the grasslands of the central Great Plains of the United States and documented that the normalized ratio of the Multispectral Scanner (MSS) near infrared (NIR) (band 7) and Red band (band 5) was sensitive to vegetation dry biomass, percent green, and moisture content (Figure 11.2). They also determined that within uniform grasslands, ground-based estimates of moisture content and percent green cover accounted for 99% of the variation in their "Transformed Vegetation Index" (TVI). The TVI was later renamed to the Transformed Normalized Difference Vegetation Index (TNDVI) (Deering et al., 1975) and is calculated as the square-root of the NDVI plus an arbitrary constant (0.5 in their case). This transformation of the NDVI was done to avoid negative values.

The NDVI is, to date, one of the most widely used vegetation index on a global basis. Figure 11.2 shows the graphic published by Rouse et al. (1973) identifying the tight relationship between ground derived green biomass and the TVI. The significance of Figure 11.2 is demonstration of potential to track vegetation growth across time, thus documenting the ability for remote sensing instruments to monitor vegetation dynamics and the importance of systematic and uninterrupted collection of remotely sensed imagery.

Another significant development during this first decade of satellite based remote sensing was the "Tasseled Cap Transformation" (Kauth and Thomas, 1976). The Tasseled Cap (or "Kauth-Thomas Transformation" to some) employed principal component analysis to understand the covariate nature of the four MSS spectral bands and extract from those data the primary ground features, or components, influencing the spectral signature. The Tasseled Cap and its eventual successor—the Brightness-Greenness-Wetness Transform (Crist and Cicone, 1984) applied to the Landsat Thematic Mapper sensor, has been a widely used tool for many land resource applications (Todd et al., 1998, Hacker, 1980, Graetz et al., 1986). The NDVI and the Tasseled-Cap provided the ability to convert reflectance values collected across multiple spectral bands into biophysically focused data layers, thus giving range managers and ecologists a tool by which to directly assess and monitor vegetation growth.

11.2.2 Multiple Sensor Era, 1980s

With the development of the NDVI and the launch of the Television Infrared Observation Satellite Next Generation (TIROSN) satellite carrying the Advanced Very High Resolution Radiometer

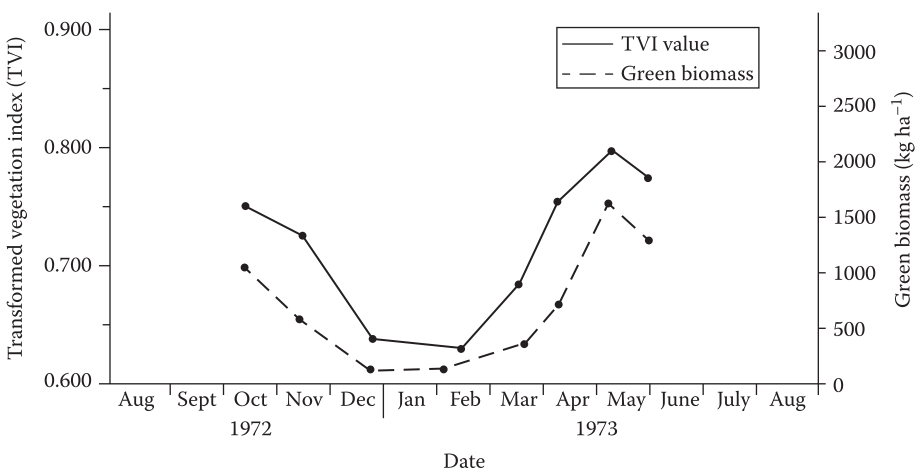

FIGURE 11.2 Earth Resources Technology Satellite (ERTS)-1 Transformed Vegetation Index values versus green biomass. (Original from Rouse et al., 1973.)

(AVHRR) in October of 1978, remote sensing practitioners now had the means to monitor temporal vegetation dynamics across very large areas (Tucker, 1979). The 1 km resolution of the AVHRR was ideal for continental scale monitoring, which was not possible with Landsat images given the computing power and data storage capacities of that era. Further, a 1day global repeat cycle provided the ability to track phenological changes in vegetation growth within and between years—a feature also not possible with the 18 and 16 day repeat cycles of the Landsat platforms. Gray and McCrary (1981) showed the utility of the AVHRR for vegetation mapping and noted that vegetation indices derived from this sensor could be related to plant growth stress due to water deficits. This relationship, coupled with the high temporal repeat interval of the TIROSN, led to the use of the NDVI to monitor the impact of drought on grasslands across the Sahel region of Africa (Tucker et al., 1983) and by direct inference predict the impact of drought to local human populations (Prince and Tucker, 1986).

The application of the NDVI to semiarid landscapes was somewhat problematic due to generally low vegetation canopy cover in these environments and the fact that background soil brightness tended to influence the resulting NDVI values (Elvidge and Lyon, 1985). Moreover, Reeves et al. (2021) estimate that the rather linear relationship between NDVI and aboveground annual productivity became asymptotic above approximately 2,300 kg ha^{-1} suggesting the need for other types of indices in higher productivity environments. The soil adjusted vegetation index (SAVI) (Huete, 1988) was developed as a simple modification to the NDVI to account for the influence of soil on the reflectance properties of green vegetation. The SAVI has been used widely within semiarid environments where vegetation cover is low. The 1980s also saw great strides in satellite based terrestrial remote sensing with the launch of Landsat 4 in July of 1982 and Landsat 5 in March of 1985, as well as the launch of the French Satellite Pour l'Observation de la Terre (SPOT) in 1986. Each platform carried sensors with slightly different capabilities, but each focused their spectral resolution on the red and NIR portions of the electromagnetic spectrum, save one. The Landsat TM was a significant improvement over its predecessor, the MSS. Not only were the spatial and radiometric resolutions improved, but also the TM supported two additional spectral bands calibrated to the shortwave infrared portion of the electromagnetic (EM) spectrum. This significant addition provided the ability to monitor leaf moisture (Tucker, 1980, Hunt and Rock, 1989) as well as identify and map recent wildfires (Chuvieco and Congalton, 1988, Key and Benson, 1999). While the work with AVHRR in Africa expanded and new sensors were becoming readily available, researchers in Australia were evaluating the applicability of Landsat images to monitoring and assessment of rangelands. Work by Dean Graetz, now retired from the Commonwealth Scientific and Industrial Organisation (CSIRO) of Australia, was instrumental in fostering use of satellite remote sensing to monitor rangelands (Graetz et al., 1983, 1986, 1988; Pech et al., 1986; Graetz, 1987). This work, coupled with other CSIRO scientists such as Geoff Pickup (Pickup and Nelson, 1984; Pickup and Foran, 1987; Pickup and Chewings, 1988), firmly established Australia as a leader in the use of remote sensing for rangeland monitoring and assessment. Researchers in Australia had similar problems applying digital imagery to semiarid rangelands as did the United States and Africa teams. The difficulty in applying imagery collected by the Landsat sensors to rangeland assessment is documented by Tueller et al. (1978) and McGraw and Tueller (1983), who found that the spectral differences among semiarid range plant communities were so small that they approached the noise level of the imagery. Even with these limitations, Robinove et al. (1981) and Frank (1984) developed methodologies for using albedo to measure soil erosion on rangelands. Pickup and Nelson (1984) developed the soil stability index (SSI) by using the ratio of the MSS green band divided by the NIR, plotted against the ratio of the red divided by the NIR. This comparison between the two ratios provided a quantitative measure of soil stability. Further, a temporal sequence of SSI images could be used as a monitoring tool to identify changes in landscape state (Pickup and Chewings, 1988). As research progressed in the use of imagery on rangelands through the 1980s, the US civilian remote sensing program began a transition to private sector management of the Landsat program. Issues of data cost and data licensing arose placing financial and legal limitations on research and data sharing. Still, research and application continued into the 1990s with an increased demand by federal land managers for landscape level information.

11.2.3 Advanced Multisensor Era, 1990s

In 1989 and throughout the 1990s, the US Fish and Wildlife Service (USFWS) and the US Geological Survey (USGS) embarked on several largescale land cover mapping efforts across the United States. The Gap Analysis Program initiated by the USFWS and later absorbed into the USGS was designed as a spatial database to identify landscapes of high biological diversity and evaluate their management status (Scott et al., 1993). The Gap Analysis was built around the linkage between wildlife habitat relationship (WHR) models and a detailed land cover map. This linkage allowed the WHR database to be spatially visualized by relating habitat parameters to land cover. The significance of this effort to remote sensing is that at the time, no one had attempted to map vegetation across landscapes requiring multiple frames of radiometrically normalized satellite imagery. The first digitally produced land cover map derived from a statistical classification of a 14image mosaic of radio metrically normalized Landsat TM imagery was completed for the state of Utah in 1995 by Utah State University (Homer et al., 1997). Programs like the Gap Analysis, coupled with the advent of the publicly available internet in 1991, provided the impetus for a new brand of remote sensing centering on large data and improved data access and product delivery. During the late 1980s, the National Aeronautics and Space Administration (NASA) was envisioning the need to provide rapid data access to users. At the time, image acquisition and delivery to the end user required a minimum of a few weeks. There was a need for time critical imagery by users and to meet that demand; NASA set a goal of data delivery to within 24 h of acquisition. Even with the advent of data transfer through the internet, a 24-hour lag between acquisition and delivery is a relatively new phenomenon of the mid-2000s.

11.2.4 New Millennium Era, 2000s

In this era, noteworthy changes to the remote sensing community, including dramatic improvements in data availability, spatial and spectral resolution and temporal frequency (Figure 11.3) were made. Commonly used high spatial resolution sensors launched during this time include Ikonos, QuickBird, GeoEye1, and WorldView2 exhibit spatial resolutions in the multispectral domain of 4, 2.4, 1.65, and 2 m, respectively.

These sensors have enabled improvements in species discrimination (e.g., Everitt et al., 2008) and stand level attributes such as canopy cover (e.g., Sant et al., 2014). Use of Quickbird for identifying giant reed (*Arundo donax*) improved both user's and producer's accuracy by an average of 12% over the use of Spot 5 alone (Everitt et al., 2008). Similarly, Sant et al. (2014) used Ikonos imagery to quantify percent vegetation cover and explained 5% more variation than using Landsat (r^2 of 0.79 vs 0.84) alone. Hyperspectral data emanating from this era also enable greater discrimination of many biophysical features than multispectral sensors alone especially in the realm of invasive species mapping. Parker and Hunt (2004) distinguished leafy spurge with AVIRIS data with overall accuracy of 95% while Oldeland et al. (2010) detected bush encroachment by Acacia spp. ($r^2 = 0.53$). Gaffney et al. (2021) were able to differentiate closely related plant community classes concluding that compositional changes were owed to growing season weather and not the management regime. These improved capabilities emanate not only from improved sensor characteristics in the 2000s but also greatly improved data availability.

In 1999, the launch of Landsat 7, coupled with new sensors from a host of other countries as well as commercial, high spatial resolution sensors, ushered a new era of global assessment and monitoring of natural and human landscapes. With the end of private sector management of the Landsat program in 1999, imagery was again placed in the public domain and costs for Landsat imagery was

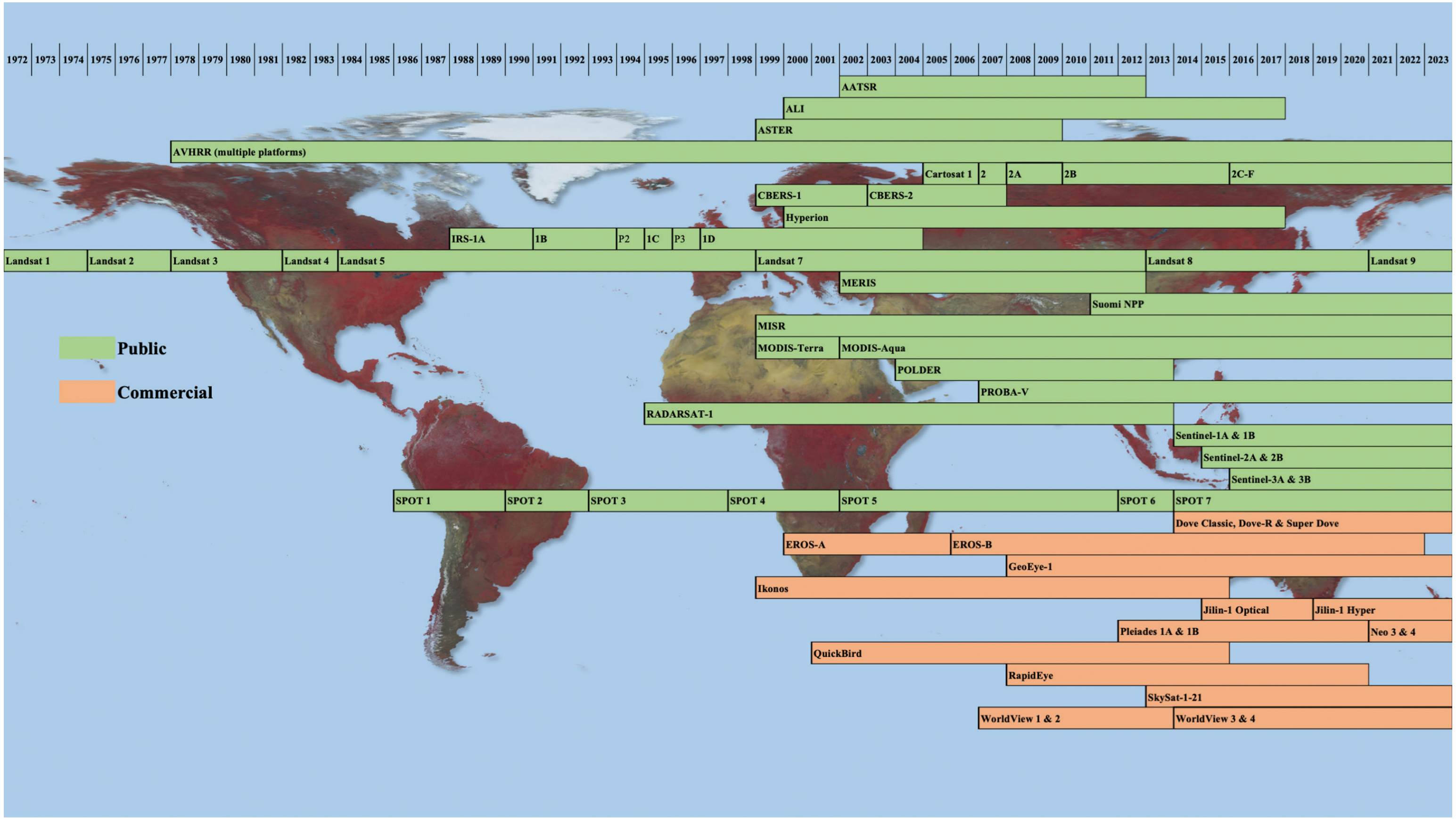

FIGURE 11.3 Temporal sequence of common remote sensing platforms relevant to mapping vegetation attributes such as cover.

reduced to $600 per scene (previously set at $4,400 per scene) for Landsat 7 Enhanced Thematic Mapper Plus (ETM+) imagery and $450 per scene for Landsat 5 TM. This reduction in cost coupled with the free exchange of data between collaborators, boosted research and application of satellite remote sensing. Further, the replacement of the AVHRR as the primary global sensor with the much-advanced Moderate Resolution Imaging Spectroradiometer (MODIS) with 36 spectral bands provided the ability for scientists to model, map, and monitor not only land cover, but net primary productivity (NPP) among other metrics. The now 23-year history of the MODIS sensor aboard two platforms (TERRA and AQUA) has provided an unprecedented source of global land cover dynamics data freely available to land managers and scientists. However, the MODIS sensors are being retired and a newer sensor called Visible Infrared Imaging Radiometer Suite (VIIRS), carried onboard the NASA-NOAA Suomi National Polar-orbiting Partnership (S-NPP) satellite, was launched in October 2011 was developed having similar sensor characteristics to MODIS. VIIRS provides moderate resolution imagery at 375m–1 km and the S-NPP orbital properties align well with MODIS sensors carried on Terra and Aqua satellites. The data collected by VIIRS are best matched to the MODIS imagery collected from the Aqua sensor (Benedict et al., 2021; Roger et al., 2017; Skakun et al., 2018; Vermote et al., 2016). For data continuity missions, key properties (e.g., equatorial crossing time, spatial, temporal, and spectral resolutions) are essential to be similar to maintain historical continuity among MODIS and VIIRS data collections. Even having the property similarities, application of a mathematical transformation between two sensors might be needed for compatible data values. Multiple studies have shown data values are higher in VIIRS products than MODIS (Benedict et al., 2021; Skakun et al., 2018). A translation formula may be applied to sensor spectral bands (Skakun et al., 2018) or calculated vegetation index (i.e., normalized difference vegetation index (NDVI)) (Benedict et al., 2021; Ji and Gallo, 2006), to transform sensor data values for VIIRS continuity in MODIS trained models. The United States Geological Survey (USGS) produces weekly NDVI composites of expedited versions of MODIS (eMODIS) and VIIRS (eVIIRS) (Benedict et al., 2021).

In 2008, The USGS made all Landsat data accessed through the internet free of charge. With this policy change, scene requests at the USGS EROS Center jumped from 53 images per day to about 5,800 images per day. This increase in data demand and delivery has arguably resulted in research in the 2000s centered on the copious use of imagery across multiple temporal and landscape scales. Commercial satellites such as the Ikonos, launched in 1999, Quickbird in 2001, and the WorldView and GeoEye satellites launched between 2007 and 2009 has provided on demand access to high spatial resolution (sub-meter to a few meters) that allows data integration between a wide array of platforms and spatial scales (Sant et al., 2014).

11.3 STATE OF THE ART

Millions of people depend on rangelands for their livelihood. This dependence raises numerous concerns about the health, maintenance, and management of rangelands from local to global perspectives. Discerning and describing how rangelands are changing at multiple spatial and temporal scales requires the integration of sensors that possess specific characteristics. The current suite of government-sponsored and commercial sensors suitable for regional to global analysis span the spatial range of sub-meter to 1 km, a temporal range of daily to bimonthly (temporal resolution is inversely proportional to spatial resolution), and all have the capacity to image landscapes in the visible and near infrared (Figure 11.4). The most commonly used sensors for global applications, however, have spatial resolutions of between 250 and 1000 m (e.g., MODIS, AVHRR, Visible Infrared Imaging Radiometer Suite (VIIRS)) and exhibit high temporal frequency, numerous spectral bands, but relatively low spatial resolution. Sensors best suited for regional to local applications (e.g., Landsat, Spot, WorldView, GeoEye) have higher spatial resolutions (sub-meter to 30 m), and lower temporal repeat cycles.

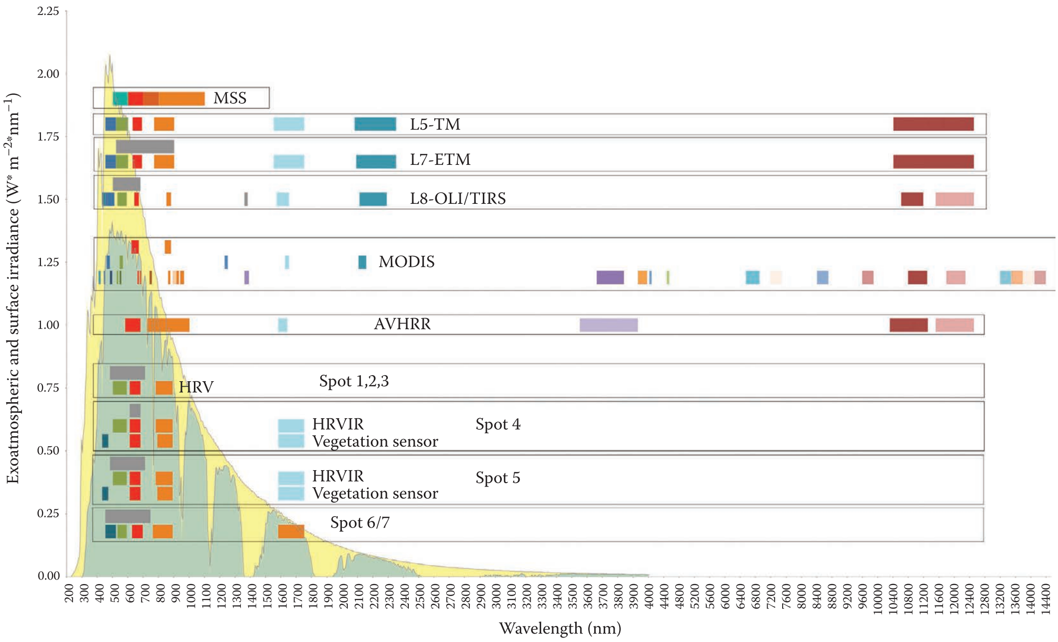

FIGURE 11.4 Comparison of the spectral bands associated with common Earth remote sensing instruments superimposed over exoatmospheric (yellow) and surface (green) solar irradiance. The list is not exhaustive and does not include coverage of radar or lidar instruments.

The present role of remote sensing for characterizing five globally significant phenomena are discussed hereafter, including land degradation, fire, food security, land cover, and vegetation response to global change (Table 11.2). These factors are not mutually exclusive and often exhibit significant interaction. Using remote sensing at global scales provides insight to what may be anticipated in the future, and indicates regions where ecological thresholds have been crossed, beyond which, decreased goods and services from rangelands can be expected.

11.3.1 Rangeland Degradation

Land and soil degradation are accelerating, and drought is escalating worldwide. At the UN Conference on Sustainable Development (Rio+20), world leaders acknowledged that desertification, land degradation, and drought (DLDD) are challenges of a global dimension affecting the sustainable development of all countries, especially developing countries. Drylands are often identified and classified according to the aridity index (AI), which is defined as P/PET where P is the annual precipitation and PET is the potential evapotranspiration. Drylands yield AI values ≤0.65. Despite decades of research, standards to measure progression of land degradation (e.g., global mapping and monitoring systems) remain elusive, but remote sensing plays a significant role.

11.3.1.1 Soil and Land Degradation and Desertification: What Is the Difference?

Land degradation and desertification have been sometimes used synonymously. Land degradation refers to any reduction or loss in the biological or economic productive capacity of the land (UNCCD, 1994) caused by human activities, exacerbated by natural processes, and often magnified by the impacts of climate change and biodiversity loss. In contrast, desertification only occurs in drylands and is considered as the last stage of land degradation (Safriel, 2009).

TABLE 11.2

The Four Most Common Sensors for Regional and Global Applications, Their Characteristics, and Example Applications. Many sensors which may have use for evaluating rangeland are not included. Svoray et al. (2013) provide a larger number of example applications in rangeland environments, but this table focuses largely on globally applicable sensors and global applications.

Satellite [sensors]	Characteristics (a is spatial resolution, b is launch date, c is swath width and d is revisit time.)	Rangeland Application Examples	References
Landsat (5, 7, 8) [Thematic Mapper, Enhanced Thematic Mapper Plus, Optical Land Imager]	a) 15 (panchromatic), 30 (multispectral), 100 (thermal), b) 1999 (Enhanced Thematic Mapper plus) (ETM+) and 2013 (Optical Land Imager) (OLI), c) 185 km × 170 km, d) 16 days	Fire (often DNBR, NBR, LWCI) 1) Burn severity (DNBR, RDNBR, Tasseled Cap Brightness) 2) Burned area mapping (Eidenshenk et al., 2007) 3) Fuel moisture (variety of indices such as NDVI, NDII, LWCI etc.)	Key and Benson (2006); Miller and Thode (2007); Loboda et al. (2013) Eidenshink et al. (2007) Chuvieco et al. (2002)
		Vegetation attributes 1) Land Cover (varied methods) 2) Leaf area index (LAI)/fraction of photo-synthetically active radiation absorbed by vegetation (fpar) (radiative transfer and vegetation indices) 3) Net primary production (multi-sensor fusion and process modeling[100]) 4) Degradation (change detection and residual trend analysis)	Gong et al. (2013); Fry et al. (2011); Rollins (2009) Shen et al. (2014) Li et al. (2012) Jabbar and Zhou (2013)
SPOT [VEGETATION]	a) 1000 b) 1998 c) 2250 km, d) 1–2 days	Fire 1) Burned area mapping Dnbr (NDVI, NDWI) 2) Fuel moisture (primarily NDVI, NDWI)	Silva et al. (2005); Tansey et al. (2004) Verbesselt et al. (2007)
		Vegetation attributes 1) Land Cover (GLC2000) 2) Net primary production/abundance (NDVI, process modeling) 3) Degradation (Trend analysis)	Bartholomé and Belward (2005) Telesca and Lasaponara (2006); Geerken et al. (2005); Jarlan et al. (2008) Fang and Ping (2010); Tchuenté et al. (2011)
Aqua and Terra [Moderate Resolution Imaging Spectroradiometer]	a) 250 (red, near-IR), 500 (multispectral), 1000 (multispectral) b) 2000 (Terra), 2002 (Aqua) c) 2230 km, d) 1–2 days	Fire (often DNBR, NBR, LWCI) 1) Active fire detection (Thermal anomalies and Fire Radiative Potential) 2) Burned area evaluation (SWIR VI and change detection) 3) Burn severity (Time integrated dNBR) 4) Fuel moisture (Empirical relations and radiative transfer modeling; many vegetation indices [GVMI, NDWI, MSI etc.])	Giglio et al. (2003); Giglio et al. (2009) Roy et al. (2008) Veraverbeke et al. (2011) Yebra et al. (2008); Sow et al. (2013)

TABLE 11.2 ***(Continued)***

The Four Most Common Sensors for Regional and Global Applications, Their Characteristics, and Example Applications. Many sensors which may have use for evaluating rangeland are not included. Svoray et al. (2013) provide a larger number of example applications in rangeland environments, but this table focuses largely on globally applicable sensors and global applications.

Satellite [sensors]	Characteristics (a is spatial resolution, b is launch date, c is swath width and d is revisit time.)	Rangeland Application Examples	References
		Vegetation attributes 1) Land Cover (varied methods) 2) Leaf area index (LAI)/fraction of photo-synthetically active radiation absorbed by vegetation (fpar) (radiative transfer modeling) 3) Net primary production (process modeling) 4) Degradation (Rain use efficiency, local NPP scaling, trend and condition analysis) 5) Livestock Early Warning System (time series analysis of NDVI, and biomass)	Friedl et al. (2010) Myneni et al. (2002); Wenze et al. (2006) Running et al. (2004); Reeves et al. (2006); Zhao et al. (2011) Bai et al. (2008); Prince et al. (2009); Reeves and Bagget (2014) Angerer (2012); Yu et al. (2011)
National Oceanic and Atmospheric Administration [Advanced Very High Resolution Radiometer]	a) 1000 m, b) NOAA-15 (1998), NOAA-16 (2000), NOAA-18 (2005), NOAA-19 (2009) satellite series (1980 to present). The approximate scene size is 2400 km × 6400 km	Fire 1) Active fire detection (Thermal anomalies and NDVI) 2) Burned area evaluation (multi-temporal multi-threshold approach) 3) Fuel moisture (NDVI) Vegetation attributes 1) Land Cover (unsupervised and supervised time series analysis) 2) Leaf area index (LAI)/fraction of photo-synthetically active radiation absorbed by vegetation (fpar) (radiative transfer modeling, Feed-Forward Neural Network) 3) Net primary production (time-integrated NDVI) 4) Degradation (NDVI and rainfall use efficiency)	Pu et al. (2004); Flasse and Ceccato (1996); Dwyer et al. (2000) Barbosa et al. (1999) Paltridge and Barber (1988); Eidenshink et al. (2007) Loveland et al. (2000); Hansen et al. (2000) Myneni et al. (2002); Ganguly et al. (2008); Zhu and Southworth (2013) An et al. (2013) Wessels et al. (2004); Bai et al. (2008)

11.3.1.2 Role of Remote Sensing for Monitoring Rangeland Degradation

Much research conducted over the last decade has been on remotely sensed biophysical indicators of land degradation processes (e.g., soil salinization, soil erosion, waterlogging, and flooding), without integration of socioeconomic indicators (Metternicht and Zinck, 2003, 2009; Allbed and Kumar, 2013). Studies from the 1970s onward have related soil erosion severity to variations in spectral response. Good reviews of spectrally based mapping of land degradation are found in

Metternicht and Zinck (2003), Bai et al. (2008), Marini and Talbi (2009), and Shoshanya et al. (2013). Moreover, research work from the 1990s and 2000s (Metternicht, 1996; Vlek et al., 2010; Le et al., 2012; Shoshanya et al., 2013) reports the benefits of a synergistic use of satellite and/or airborne remote sensing with ground-based observations to provide consistent, repeatable, cost-effective information for land degradation studies at regional and global scales. Hereafter follows a brief description of some of the most frequent applications of remote sensing applied in "global or sub global assessments" of land degradation. These remotely sensed products include biomass and vegetation health modeling via NDVI and NPP, rain use efficiency (RUE), and local NPP scaling.

11.3.1.3 Biomass and Vegetation Health Modeling As an Indicator of Degradation

The biomass produced by soil and other natural resources can be a proxy for land health (Nkonya et al., 2013). In this vein, Bai et al. (2008) framed land degradation in the context of the Land Degradation Assessment in Drylands (LADA) program as long-term loss of ecosystem function and productivity and used trends in 8 km NDVI from the Global Inventory Modeling and Mapping Studies (GIMMS) as a "proxy indicator" of changes in NPP. Figure 11.5 represents changes in NPP from 1981 to 2003 resulting from fusion of GIMMS NDVI and MODIS 1 km NPP (Bai et al., 2008). The NDVI is related to variables such as leaf area index (LAI) (Myneni et al., 1997), the fraction of photosynthetically active radiation (fPAR) absorbed by vegetation, and NPP. This explains why many NPP estimates derived from remote sensing approaches are based on LAI, and fPAR commonly from the AVHRR onboard the National Oceanic and Atmospheric Administration (NOAA) satellite, and the MODIS on the Terra and Aqua satellites (Ito, 2011). One caveat to remotely sensed estimates of NPP for degradation analyses is the need for comparison with ground measured biophysical parameters such as NPP, LAI, or soil erosion (or salinization) for accuracy assessment (Bai et al., 2008; Le et al., 2012).

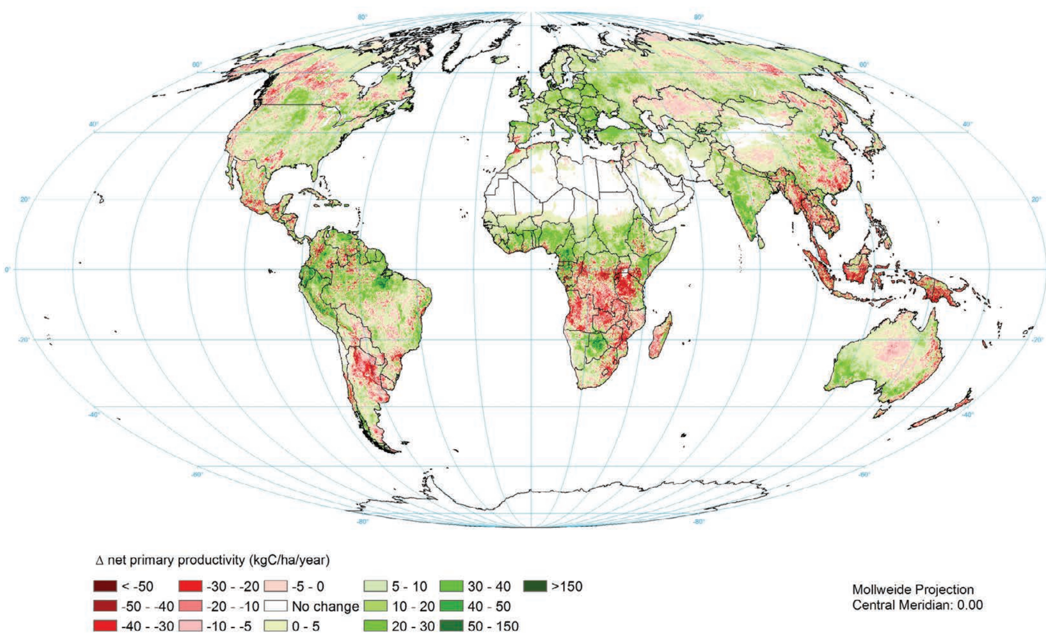

FIGURE 11.5 Global change in NDVI scaled in terms of NPP using MODIS 1 km^2 8-day composite net photosynthesis data (1981–2003). NDVI is a proxy indicator of changes in NPP. (Source: Bai et al. 2008.)

11.3.1.4 Rain Use Efficiency

RUE (ratio of NPP to rainfall) can be used to distinguish between the relatively low NPP of drylands associated with inherent moisture deficit and the additional decline in primary production due to land degradation (Le Houérou, 1984; Le Houérou et al., 1988; Pickup, 1996). In the context of the LADA project, Bai et al. (2008) estimated RUE from the ratio of the annual sum of NDVI (derived from MODIS and NOAA AVHRR) to annual rainfall and used it to identify and isolate areas where declining productivity was a function of drought (Figure 11.6). Figure 11.6 was produced using the same GIMMS NDVI data as Figure 11.5 in concert with Variability Analyses of Surface Climate Observations (VASClimO) gridded precipitation data at 0.5° resolution. This recalibration process was thought to yield a proxy index for land degradation, if a decline in vegetation for any other reason than rainfall (and temperature) differences would be an expression of some form of degradation. Statistical analysis showed 2% of the land area exhibited a negative trend at the 99% confidence level, 5% at the 95% confidence level, and 7.5% at the 90% confidence level (Bai et al., 2008).

A drawback of this mapping approach is that an area of land degradation much smaller than 8 km (pixel size of the GIMMS AVHRR) must be severe to significantly change the signal from a much larger surrounding area. In addition, the application of RUE to identify degraded landscapes has been somewhat controversial and misinterpreted as an indicator of degradation (Prince et al., 2007) since the RUE is highly variable (Fensholt and Rasmussen, 2011). In addition, errors in gridded precipitation data can add significant uncertainty, and noise to a degradation analysis suggesting analyses based solely on remotely sensed data may be beneficial (Reeves and Bagget, 2014).

11.3.1.5 Local NPP Scaling

Prince (2002) developed the local net primary productivity scaling (LNS) approach. Though the LNS approach can be applied to data of any resolution, derived from a host of sensors yielding visible and infrared bandpasses, AVHRR and Terra MODIS are commonly used. The LNS approach compares seasonally summed NDVI (ΣNDVI) of a single pixel to that of highest pixel value (or, commonly, the 90th percentile) observed in homogeneous biophysical land units (e.g., similar soils,

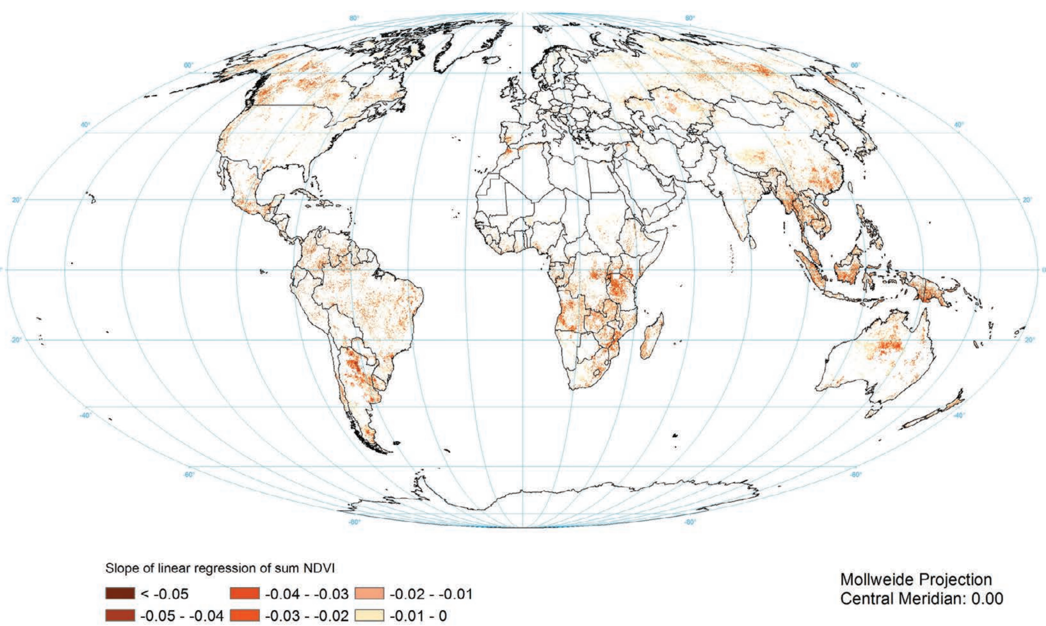

FIGURE 11.6 Average rain use efficiency (RUE) adjusted NDVI, from GIMMS-AVHRR 8 km^2 and VASClimO at 0.5° spatial resolution. (Source: Bai et al. 2008.)

climate, and landforms). The highest ΣNDVI value is assumed as a proxy for the potential aboveground NPP (ANPP) for each unit, and the other ΣNDVI values are rescaled accordingly. Prince et al. (2009) applied the LNS approach at national scales in Zimbabwe using MODIS 250 m NDVI and concluded that 17.6 Tg C year−1 were lost due to degradation. Similarly, Wessels et al. (2007) used 1 km time-integrated NDVI in northeastern South Africa. More recently, Fava et al. (2012) used annual summations of MODIS 250 m NDVI resolution in an LNS study for assessing pasture conditions in the Mediterranean resulting in a mean agreement of 65% with ground-based classes of degradation. In a variant of the LNS approach, Reeves and Bagget (2014) used the mean 250 m MODIS NDVI response of like-kind sites compared with reference conditions using a time series analysis to identify degradation on the northern and southern Great Plains, United States. With this approach, 11.5% of the region was estimated to be degraded.

11.3.1.6 Global Assessment of Land Degradation: The Evolution of Remote Sensing

The use of remote sensing data in global programs of land degradation assessment is related to the history of the global assessment of human induced soil degradation (GLASOD), the global LADA (Global Assessment of Land Degradation and Improvement [GLADA]), and the Global Land Degradation Information System (GLADIS) programs, funded by the global organizations such as United Nations Environment Program (UNEP), the UN FAO, and the Global Environmental Facility (GEF). Table 11.3 summarizes the objectives, methods, and main outputs derived from these programs, including the use of remote sensing technologies in their implementation. The GLASOD, an expert opinion based study (Table 11.3), and Oldeman (1998) had two follow up assessments, namely, the regional assessments of soil degradation status in South and Southeast Asia (Assessment of the Status of Human induced Soil Degradation in South and Southeast Asia [ASSOD]) and Central and Eastern Europe (Soil and Terrain Vulnerability in Central and Eastern Europe [SOVEUR]) and the global LADA project, under UNEP/FAO. The LADA had the objectives of developing and testing effective methodological frameworks land degradation assessment, at global, national, and subnational scales. The global component of LADA (i.e., GLADA) provided a baseline assessment of global trends in land degradation using a range of indicators collected by processing satellite data and existing global databases (NPP, RUE, AI, rainfall variability, and erosion risk) as described in Bai et al. (2008). The GLADA was implemented between 2006 and 2009, based on 22 years (1981–2003) of fortnightly NDVI data collection and processing (Table 11.3). The project developed and validated a harmonized set of methodologies for the assessment of land use, land degradation, and land management practices at global, national, subnational, and local levels.

The GLADIS was developed by FAO, UNEP, and the GEF using preexisting data and newly developed global databases to inform decision makers on all aspects of land degradation. The GLADIS developed a global land use system (LUS) classification and mapping using a set of pressures and threat indicators at the global level, allowing access to information at country, LUS, and pixel (5 arcminute resolution) levels. It accounts for socioeconomic factors of land degradation, using a variety of ancillary data to this end. Lastly, Zika and Erb (2009) produced a global estimate of NPP losses caused by human induced dryland degradation using existing datasets from GLASOD and other sources. Table 11.3 shows an evolution in the use of remote sensing technology from the first global assessments (GLASOD), expert based, with no use of remote sensing imagery, to the latest GLADIS, heavily reliant on remote sensing derived data coupled with an ecosystem approach. The GLASOD estimated that 20% of drylands ("excluding" hyperarid areas) was affected by soil degradation. A study commissioned by the Millennium Assessment based on regional datasets (including hyperarid drylands) derived from literature reviews, erosion models, field assessments, and remote sensing found lower levels of land degradation in drylands, to be around 11% (although coverage was not complete) (Lepers et al., 2005). The LADA project reported that over the period of 1981–2005, 23.5% of the global land area was being degraded. On the other hand, Zika and Erb (2009) report that approximately 2% of the global terrestrial NPP is lost each year due to dryland

TABLE 11.3

Cursory Comparison between Major Global Rangeland Degradation Efforts

Program	Objective	Methodology—Remote Sensing Usage
GLASOD-Global Assessment of Human Induced Soil Degradation (UNEP) (1987–1990)	Produce a world map of human-induced *soil degradation*, on the basis of incomplete knowledge, in the shortest possible time.	No remote sensing; expert-based approach; distinguishes "types" of soil degradation, based on perceptions; it is **not a measure** of land degradation.
LADA-GLADA Land Degradation Assessment *in Drylands* (LADA)—Global project, under UNEP/FAO. (2006–2009)	Assess (quantitative, qualitative and georeferenced) land degradation at global, national and sub-national levels to identify status, driving forces and impacts, and trends of land degradation in drylands; identify *hot* (degradation) and *bright* (improvement) spots:	The Global LADA was based on 22 years (1981–2003) of fortnightly NDVI data, derived from GIMMS and MODIS-related NPP (MOD 17). Method: 1. Identify degrading areas (negative trend in sum of NDVI) 2. Eliminate false alarms of productivity decline by: masking out urban areas; areas with a positive correlation between rainfall and NDVI, and a positive NDVI-RUE 3. Produce RUE-adjusted NDVI map 4. Calculate NDVI trends for remaining areas.
LADA-GLADIS Global Land Degradation Information System FAO-UNEP-GEF (2006–2010)	Focus on land degradation as a process resulting from pressures on a given status of the ecosystem resources.	Remote sensing is used for biomass status and trends, based on a correction factor to the GLADA-RUE-adjusted NDVI, to present trends in NDVI (1981–2006) translated in greenness losses and gains distinguished by climatic and human-induced (e.g., deforestation from FAO-FRA dataset) causes. Outputs are a series of global maps on the **status and trends** of the main ecosystem services considered, and radar graphs.

Prepared by Metternicht, G. *Sources:* Oldeman (1998); Bai et al. (2008); Nachtergaele et al. (2010).

degradation, or between 4% and 10% of the potential NPP in drylands. Figure 11.7 is a compilation of the global extent of drylands and human induced dryland degradation, produced for the fifth Global Environment Outlook (GEO5) based on research of Zika and Erb (2009) who express dryland degradation in croplands and grasslands as a function of NPP losses.

The three dryland area zones (top of the figure) are derived on basis of the AI. Only dryland areas (arid, semiarid, and dry subhumid), characterized by an AI between 0.05 and 0.65, are considered. Degradation is assessed by calculating the difference of the potential NPP (NPP_0) and current NPP (NPP_{act}). NPP losses due to human induced degradation amount to 965 Tg C year^{-1}, giving evidence that about 4%–10% of the potential pro duction in drylands is lost every year due to human induced soil degradation. The largest losses are occurring in the Sahelian and Chinese arid and semiarid regions, followed by the Iranian and Middle Eastern drylands and to a lesser extent the Australian and Southern African regions (UNEP, 2012) (Table 11.4) (Figure 11.5). A loss of NPP in the range of 20%–30% means reductions of potential productivity in that range; in most pixels of Figure 11.7, productivity losses range between 0% and 5% of their $NPP_{0.}$ The results presented in Figures 11.5 and 11.7 illustrate the scope and patterns of degradation but must only be considered as rough estimates (Zika and Erb, 2009). Major uncertainties related to the results arise from three assumptions:

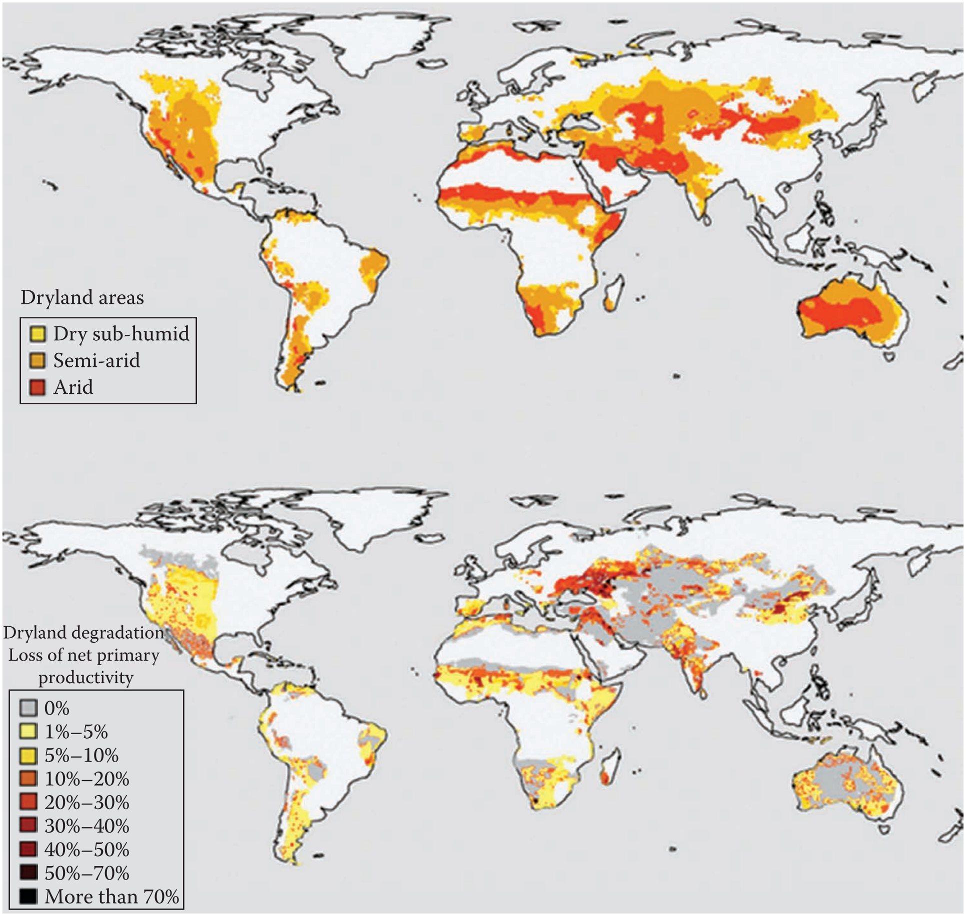

FIGURE 11.7 Global extent of drylands and human-induced dryland degradation. (Source: UNEP, 2012.) Redrawn from Zika and Erb (2009). We thank UNEP and the GEO-5 process for use of the figure.

(1) estimates of degradation extent, (2) assumptions on NPP losses due to degradation processes, and (3) potential NPP as a proxy for production potential. In recognition of the scope of degradation globally, the UN Conference on Sustainable Development (Rio+20) prompted the international community to develop universal sustainable development goals providing a timely opportunity to respond to the threat of soil and land degradation (Koch et al., 2013). Despite over 30 years of applied research in this area, however, the need to provide a baseline and method from which to measure degradation still remains (Gilbert, 2011). For regional refinements to degradation analyses, radar satellite based aboveground biomass estimations by Carreiras et al. (2012), or regional vegetation cover (Dong et al., 2014), could aid degradation analyses since cloud issues faced by LADA GLADA and GLADIS could be mitigated. Additionally, Blanco et al. (2014) propose ecological site classification of semiarid rangelands enabling more refined spatial units across which remote sensing can be conducted. Finally, engaging citizens in knowledge production (including ground verification of remotely sensed derived information), as fostered by current global (UNEPLive, Future Earth, Group on Earth Observations Biodiversity Observation Network) and sub-global initiatives (Eionet of the European Environmental Agency), could address the significant lack of ground truthing of previous global land degradation studies.

TABLE 11.4

Estimates of NPP Losses Due to Dryland dDgradation, Regional Breakdown. Source: Zika and Erb (2009).

	Degraded Dryland[a]		NPP Loss[b]	
Region	**1000 km²**	**%**	**Tg C yr⁻¹**	**%**
Central Asia and Russian Federation	1,432	19.5	250	26
Eastern and Southeastern Europe	391	55.5	73	8
Eastern Asia	1,887	45.3	50	5
Latin America and the Caribbean	1,206	18.8	98	10
Northern Africa and Western Asia	1,207	33.8	70	7
Northern America	607	11.3	51	5
Oceania and Australia	866	13.2	24	2
South-Eastern Asia	45	40.4	10	1
Southern Asia	1,437	30.9	106	11
Sub-Saharan Africa	2,597	22.8	215	22
Western Europe	128	24.7	18	2
Total	11,802	23.2	965	100

[a] % of dryland area

[b] Estimated NPP losses associated with dryland degradation. (see Zika and Erb, 2009 for more detail)

11.3.2 Fire in Global Rangeland Ecosystems

The extremely wide range of rangeland environments makes it virtually impossible to develop generalized statements about global fire regimes. However, the general composition of fuel and fuel characteristics defines some specifics of fire occurrence common for these ecosystems. Vegetation of rangelands is characterized by fast growth and slow decomposition rates (Vogl, 1979) leading to considerable buildup of surface litter. Most fuels in these ecosystems, except for chaparral systems, are flash and fine fuels (<0.25 in diameter), which dry out rapidly (i.e., 1 hour time lag fuels) and burn readily (National Wildfire Coordinating Group, 2012). Therefore, it is not unusual for these ecosystems to transition from low fire danger state to extreme fire danger state over a comparatively short period. Contiguity and loading of fuel in these ecosystems are highly variable both spatially and temporally: interannual variation in fuel loading often exceeds 110% (Ludwig, 1987). While fire is currently a common and widespread disturbance agent globally in rangelands, its prominence is expected to rise under projected climate change. Past and ongoing satellite monitoring and mapping of rangeland fire extent provide a much-needed baseline for assessment of potential future change in fire occurrence and its impact on ecosystem functioning.

11.3.2.1 Satellite Monitoring of Ongoing Burning

The hotspot detections from the nighttime top of atmosphere radiance data from the Along Track Scanning Radiometer (ATSR2) and Advanced ATSR (AATSR) were used to build the first World Fire Atlas (Jenkins et al., 1997). Neither of the source instruments was designed to support fire detection specifically, and therefore, the algorithms were based on suboptimal ranges of electromagnetic radiation (at brightness temperature [BT] centered on 3.7 and 11.8 μm) using a suite of simple thresholds (Arino et al., 2012). The MODIS was, however, designed with a specific goal to enhance fire mapping capabilities (Kaufman et al., 1998). MODIS collects daily global observations from Terra ~ 11:30 a.m. and 11:30 p.m. and Aqua at ~1:30 a.m. and 1:30 p.m. equatorial crossing time. In addition, several "fire" channels were included in the instrument to support fire monitoring:

two 4 μm channels (channel 21 with 500 K saturation level and channel 22 with 331 K saturation level) and 11 μm channel (channel 31 with 400 K saturation level) at 1 km nominal resolution (Giglio et al., 2003). The flexibility of switching the high and low saturation 4 μm channels in the contextual active fire detection algorithm is particularly important for tropical savanna environments.

The MODIS active fire product is the first product to include fire characterization metrics in addition to the binary "fire/no fire" masks. Fire radiative power (FRP), expressed in watts (W) is an instantaneous measurement of power released by ongoing burning during the satellite overpass (Kaufman et al., 1996a, 1996b) and are estimated using an empirical relationship established in Kaufman et al. (1998). FRP is directly related to the intensity of biomass burning and, when integrated overtime to fire radiative energy (FRE) expressed in joules (J), is linearly related to biomass consumption (Wooster et al., 2005).

11.3.2.2 Satellite Estimates of Burned Area

Unlike active fire detection, which is primarily based on BT in mid and long infrared spectrum, burned area estimates are most frequently based on changes in surface reflectance due to burning observable within the visible (0.4–0.6 μm), NIR (0.7–1.0 μm), and shortwave infrared (SWIR 1.1–2.4 μm) spectrum. The relatively short wavelength of radiation in this range determines that burned area mapping relies on clear surface observations and is strongly limited by considerable aerosol contamination from smoke during the burning process and high cloud cover in high northern latitudes. The first multiyear global burned area products were developed from data acquired by VEGETATION (VGT) (onboard SPOT), ATSR2 (onboard ERS2), Medium Resolution Imaging Spectrometer (MERIS), and AATSR (onboard Environmental Satellite [ENVISAT]) instruments (Plummer et al., 2006) within the GLOBCARBON initiative.

The suite of fire products developed from the MODIS 500 m data included two global burned area algorithms. The MCD45 algorithm (Roy et al., 2008), which is no longer in production, was based on the detection of rapid changes in surface reflectance within a MODIS 500 m pixel. The MCD64 algorithm (Giglio et al., 2009, 2018), the official NASA operational MODIS burned area product, relies on the detection of persistent changes in vegetation state and subsequent attribution of the change to burning by comparison to active fire occurrence within a specified spatiotemporal window (Figure 11.8).

A detailed study in Central Asia (Loboda et al., 2012) has shown that MODIS based products deliver spatially accurate estimates of burned area in Central Asia, with MCD64A1 estimates in close agreement to the Landsat based assessments (~18% underestimation). The independent accuracy assessment results within drylands of Central Asia are similar to those in North America (Giglio et al., 2009). This makes MODIS based products appear to deliver a reasonable estimate of fire impact on grasslands and shrublands of the world despite the overall higher mapping uncertainty relative to other land covers. Studies have also explored the capabilities of synthetic aperture radar (SAR) from the Sentinel-1 mission (e.g., Hosseini and Lim, 2023). However, the accuracy within rangelands is lower than optical burned area products such as MCD64A1 since the SAR backscatter variations in pre- and post-fire imagery tend to be greater in forests land covers than in grassland and shrubland landscapes (Belenguer-Plomer et al., 2019). In recent years, machine-learning and artificial intelligence have grown in popularity. At present, the majority of these studies are focused on localized analyses (e.g., Knopp et al., 2020) as these methods are still premature and require a large volume of training and validation data.

11.3.2.3 Remote Sensing Methods for Fire Impact Characterization

The characteristics of grass and shrubland fires (i.e., the large footprint of savanna fires, the remote locations of tundra fires, and the short-lived nature of these burn scars), make remote sensing the only viable source of data for consistent, global post-fire characterization of burned area. While a healthy debate about what constitutes burn severity and how much the ecological definition ranges across ecosystems is still ongoing in the fire science community (French et al., 2008; Chen et al.,

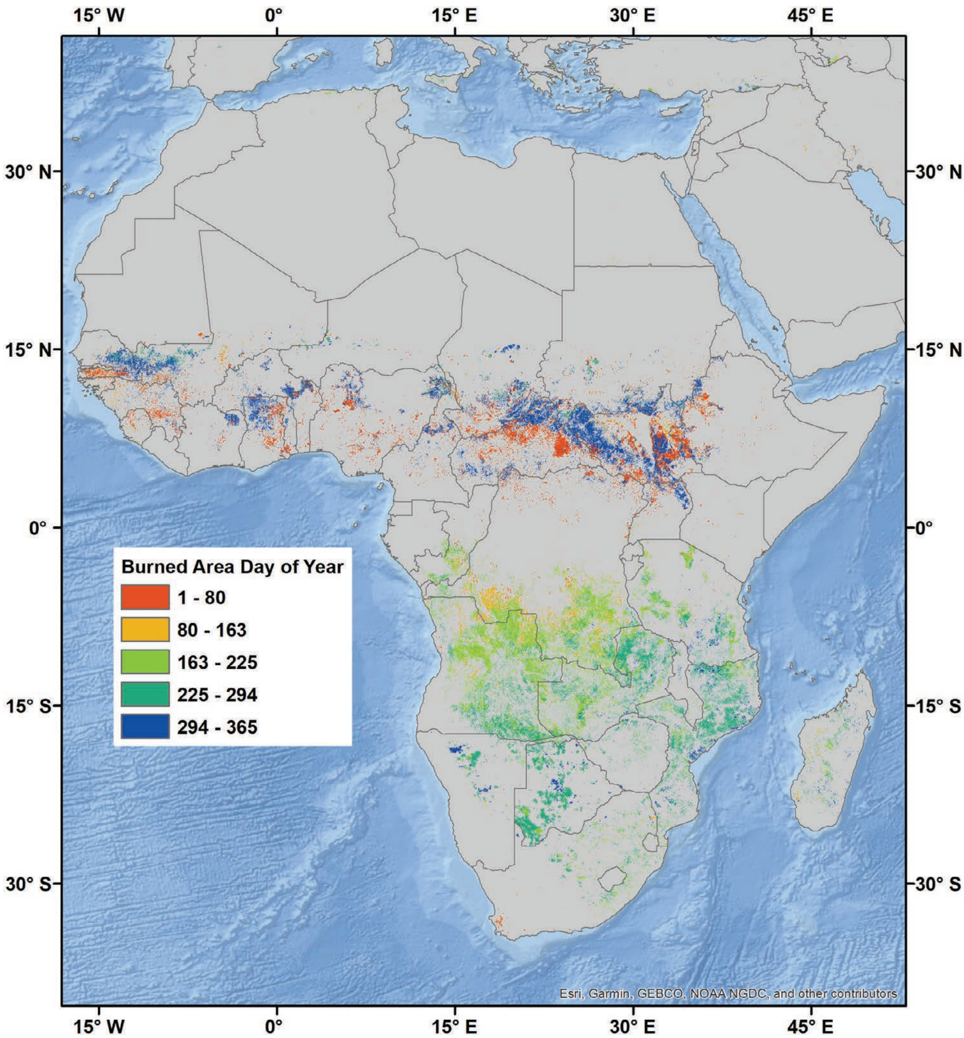

FIGURE 11.8 Example of the 2021 MCD64A1 C6.1 MODIS burned area product depicting approximate date of fire in rangelands globally. (Prepared by Joanne V. Hall.)

2021), the Monitoring Trends in Burn Severity (MTBS) program established the baseline definition. This includes the assumption that this parameter can be mapped from remotely sensed data and is ultimately based on a combination of “visible changes in living and nonliving biomass, fire byproducts (scorch, char, and ash), and soil exposure” among other components. The same ranges of electromagnetic spectrum (visible—NIR—SWIR), therefore, constitute the basis for the strongest differentiation between soil, vegetation, char, and ash components characterizing burn severity as those used most for burned area mapping. It is not surprising that the first widely applied index for mapping and quantifying burn severity is based on the normalized difference of NIR and SWIR in 2.2 μm range ($SWIR_{2.2}$) originally developed by LopezGarcia and Caselles (1991) for burned area mapping. The Normalized Difference Burn index (NDBR), as it was subsequently named by Key and Benson (1999), is calculated as follows:

$$NBR = \frac{NIR - SWIR_{2.2}}{NIR + SWIR_{2.2}} .$$

where NIR refers to the TM band 4 (0.76–0.90 µm) $SWIR_{2.2}$ refers to band 7 (2.08–2.35 µm) Key and Benson (1999) aimed to capture the fire induced changes to the proportions of soil, char, ash, and vegetation through differencing the pre-burn and post-burn NDBR measurement within a fire perimeter. This approach (differenced normalized burn ratio [dNBR], calculated as dNBR = $NBR_{pre\text{-}burn} - NBR_{Post\text{-}burn}$ has become the most widely applied index of burn severity across all ecosystems in the United States (Eidenshink et al., 2007).

Compared to forest cover, where the original assessment of dNBR were closely related to ground measurements of burn severity expressed through a composite burn index (CBI) (Key and Benson, 2006, Allen and Sorbel, 2008), these grass and shrub dominated ecosystems have a low amount of aboveground biomass and are spatially highly heterogeneous. Thus, the magnitude of change between pre-burn and post-burn surface conditions is considerably more muted and uneven. To account for the initial lower fuel loading in these ecosystems, an adjustment to dNBR, named relativized dNBR (RdNBR), was developed by Miller and Thode (2007). This index is calculated as follows:

$$RdNBR = \frac{dNBR}{\sqrt{\left| NBR_{pre-burn} / 1100 \right|}}$$

Although RdNBR versus CBI assessments show that RdNBR is more robust in assessing burn severity compared to dNBR in grass and shrub dominated ecosystems (Miller and Thode, 2007; Loboda et al., 2013), it does not overcome a major limitation of spectral signature change due to fire in NIR/SWIR spectral space within these ecosystems.

It is likely that the success rate of any one spectral index in mapping and quantifying burn severity depends strongly on the specific proportions of grass, woody biomass, exposed soil, geo graphic location (as related to frequency of observation allowing for a wider range of mapping days and different Sun sensor geometries), moisture status during image acquisition, and the timing of mapping. A recent study highlighted the importance of standardizing the pre- and post-fire image methodology for the tundra region as changes in the image acquisition seasonality (i.e., the impact of phenological differences in the image pairs) has an impact on the dNBR values (Chen et al., 2020).

11.3.3 Food Security: Role of Remote Sensing in Forage Assessment

Climate change, land degradation, landuse changes, and population growth are causing grand challenges for land managers that utilize rangelands for food production (Roche, 2016). Global demand for food is estimated to increase by 60% by 2050 with the demand for meat expected to increase by 70% (Alexandratos and Bruinsma, 2012). Meeting the food demands of a growing global population will become more difficult when coupled with the environmental and socio-economic factors (i.e., climate change, increasing land values, and limitations on land use). Changes in vegetation structure and forage quantity on rangelands due to a changing climate will have operational and economic consequences for industries reliant on these resources, such as cattle production (Klemm et al., 2020; Wold et al., 2023).

On rangelands, quantifying the amount of forage available to livestock on a near real-time basis using traditional methods (e.g., clipping vegetation along transects) can be costly, time consuming, and logistically challenging. A lack of information for making livestock management decisions at critical times could lead to loss of livestock due to lack of forage, or lead to vegetation over use, which, in turn, could result in rangeland degradation (Weber et al., 2000). Therefore, having an objective means of setting stocking rates on rangelands based on productivity will allow range land managers to better adapt to changing weather conditions. Because of the large areal cover that remote sensing products provide, in addition to the greater temporal of collection compared to traditional ground sampling over large areas, the use of remote sensing imagery is attractive for assessing vegetation production on rangelands. Multiple satellite platforms exist that are useful for rangeland forage assessments and early warning systems. Two approaches have generally been used for assessing rangeland forage conditions using remote sensing imagery. These include (1) empirical approaches that estimate the forage biomass or quality based on a statistical relationship between the spectral bands (or some combination of bands) in the imagery and ground collected vegetation data and (2) process models that use remote sensing data as inputs for predicting vegetation biomass or quality.

11.3.3.1 Empirical Approaches

Empirical approaches for assessing rangeland forage conditions using remote sensing products generally involve the use of a statistical relationship between the remote sensing spectral response or product variable and data collected from field measurements (Dungan, 1998). Using the empirical approach example in Figure 11.9, a MODIS 250 m maximum value composite and NDVI value of 7500 correspond to approximately 3414 kg ha^{-1} of annual production, after accounting for unavailability (ϕ = 0.15) and suggested utilization (υ = 0.5) results in stocking rate of 5.3 animal unit month's (AUM) ha^{-1}.

In a similar manner, Tucker et al. (1983) used both a linear and logarithmic regression between the ground collected biomass data in the Sahel region and AVHRR NDVI to predict biomass on a regional scale. AlBakri and Taylor (2003) used a linear regression approach to predict shrub biomass production for rangelands in Jordan using 7.6 km AVHRR NDVI. Both these studies reported accounting for >60% of the variation in herbaceous biomass with AVHRR NDVI alone using linear regression against biomass. In the Xilingol steppe of Inner Mongolia, Kawamura et al. (2005) used 500 m MODIS enhanced vegetation index (EVI) to predict live biomass and total biomass of livestock forage with linear regression models, which accounted for 80% of the variation in live

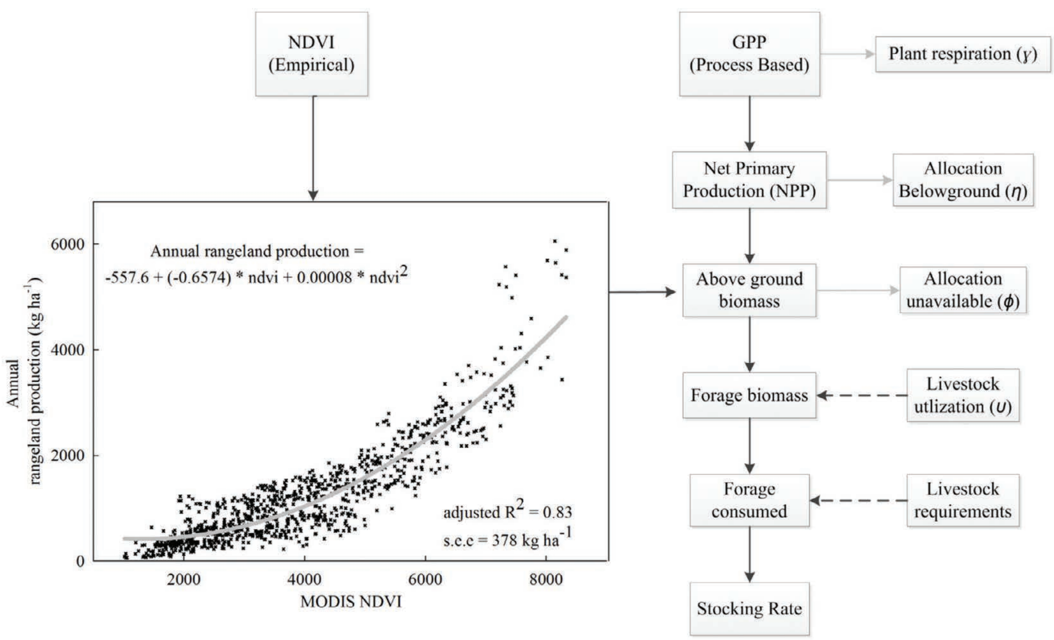

FIGURE 11.9 Process for estimating stocking rate from remote sensing data, either empirically or using a process model. Gross primary production (GPP) is determined from land cover type, spectral vegetation indices, incident photosynthetically active radiation, and climate-dependent radiation use efficiencies or empirically. Solid arrows represent reductions based on physiology while dashed arrows represent critical management decisions are determined.

biomass and 77% of the variation in total biomass. In the Tibetan Autonomous Prefecture of Golog, Qinghai, China, Yu et al. (2011) used the 250 m resolution MODIS NDVI to estimate aboveground green biomass using regression relationships between the NDVI and ground collected biomass data (r^2 of 0.51) from sites across the region.

As with forage biomass, empirical approaches can be used for forage quality assessments generally involving examining statistical relationships between forage quality variables such as crude protein or energy and spectral information from remote sensing imagery. For example, Thoma et al. (2002) used simple linear regression with AVHRR NDVI as the independent variable to predict forage quality and quantity on rangelands in Montana, United States. Their analysis indicated reasonable relationships between NDVI and live biomass ($r^2 = 0.68$) and nitrogen in standing biomass ($r^2 = 0.66$). Similarly, Kawamura et al. (2005) used regression relationships between ground collected data and MODIS EVI to predict live and dead biomass and crude protein in standing biomass. They found good predictability between standing live biomass and total biomass (live + dead) ($r^2 =$ 0.77–0.80), but correlations with crude protein were poor ($r^2 = 0.11$).

Remote sensing imagery provides a dense and exhaustive dataset that can serve as a secondary variable for geostatistical interpolation given that a correlation exists (both direct and spatial) between the primary and secondary variable (Dungan, 1998). Use of MODIS NDVI in the cokriging analysis of forage crude protein provides reasonable during the dry season ($r^2 = 0.69$) but less so during the wet season ($r^2 = 0.51$) (Awuma et al., 2007) likely because the amount of unpalatable shrub cover increased the greenness signal in the NDVI in some of the sampling areas that did not contribute to the available forage.

11.3.3.2 Process Models Using Remote Sensing Inputs

One problem that has been noted for regression models that use remote sensing variables is that they violate the regression assumption of no autocorrelation in the predictor variable(s) (Dungan, 1998; Foody, 2003). Since most remote sensing data are inherently autocorrelated, violation of this assumption may reduce the effectiveness of the regression model (Dungan, 1998). One way of overcoming the autocorrelation problems is to use process models that are driven by remotely sensed input variables on a pixel-by-pixel basis. Reeves et al. (2001) describe such an approach for predicting rangeland biomass using remote sensing products from the MODIS system and a light use efficiency model for plant growth. Hunt and Miyake (2006) used a similar light use efficiency model approach for estimating stocking rates for livestock at 1 km resolution in Wyoming, United States (Figure 11.9). Using the approach of Hunt and Miyake (2006), the stocking rate is estimated as gross primary production (GPP) $(1 - \chi)(1 - \eta)(1 - \phi)\ \upsilon$ (AUM/273 kg month^{-1}). From Hunt and Miyake (2006), the parameters for grasslands are approximately $\chi = 0.48$, $\eta = 0.79$, $\phi = 0.15$, and $\upsilon = 0.5$ where χ is autotrophic respiration, η is belowground carbon allocation, ϕ is carbon allocation to nonpalatable stems and other vegetation, and υ is an estimated accepted level of utilization. Therefore, a monthly GPP of 11,000 kg ha^{-1} month^{-1} is about 1.7 AUM's ha^{-1}, but this is just one method of using process models parameterized with remote sensing inputs. An example of a process-based modeling approach for forage quantity assessment at the regional level is the Livestock Early Warning Systems (LEWS) in East Africa (Stuth et al., 2003a, 2005) and Mongolia (Angerer, 2012) (Figure 11.10). In East Africa, the LEWS has evolved into the Predictive Livestock Early Warning System (PLEWS; Matere et al., 2019) and now encompasses Sudan, South Sudan, Ethiopia, Djibouti, Somalia, Kenya, Tanzania, and Uganda. The PLEWS platform has been incorporated into the Food and Agriculture Organization's East Africa Animal Feed Action Plan with the goal of using the system to provide information for informing drought declarations and responses, as well as providing inputs on rangeland forage availability needed for national feed inventories in each county (FAO and IGAD, 2019; Opio et al., 2020).

Coupling remotely sensed data in process models that also include economic information may provide improvements to global food security efforts in the future, For example, Wold et al. (2023) combined estimates of remotely sensed forage production on a ranch level with an economic model and assessed potential effects of climate change effects to a ranching operation. This small-scale example (coupling remote sensing estimates to an economic model) provides a framework for how we can use economic modeling in combination with remote sensing to provide a deeper understanding of land use changes, vegetation productivity, and environmental dynamics related to rangeland management. Future research could couple remotely sensed rangeland productivity at larger regions (e.g., western United States) to economic models that assess market fluctuations.

Figure 11.10 presents results of the LEWS applied in Mongolia in 2013. Note the significant decline of forage in southwestern Mongolia in 2013. The LEWS was developed to provide near real-time estimates of forage biomass and deviation from average conditions (anomalies) to provide pastoralists, policy makers, and other stakeholders with information on emerging forage conditions to improve risk management decision making. The LEWS combines MODIS 250 m NDVI, ground data collection from a series of monitoring sites, simulation model outputs, and statistical forecasting, to produce regional maps of current and forecast forage conditions and anomalies. The system uses the Phytomass Growth Simulation model (PHYGROW) (Stuth et al., 2003b), parameterized with the MODIS 250 m NDVI, as the primary tool for estimating available forage. Model verification indicates the model performs well in estimating forage biomass (Stuth et al., 2005). For example, model verification across monitoring sites in Mongolia indicated a good correspondence between the PHYGROW predicted biomass and observed ground data ($r^2 = 0.76$) with forage biomass ranging from 3 to 1230 kg ha^{-1}. PHYGROW tended to underestimate forage biomass across sites by 14% with an overall mean bias error of −18 kg ha^{-1} (Angerer, 2008).

11.3.4 Rangeland Vegetation Response to Global Change: The Role of Remote Sensing

Monitoring global change is an increasingly important endeavor (Running et al., 1999) since ecosystem goods and services, essential to human survival, are directly linked to the health of the biosphere (Fox et al., 2009). The Earth is a dynamic system with many interacting components that are complex and highly variable in space and time. Though change has always been present, human activities have influenced rates and extent of change beyond historical ranges (Vitousek, 1992; Levitus et al., 2000; Foley et al., 2005). Global change involves terrestrial, aquatic, oceanic, and atmospheric systems and cycles and is not limited to climate change alone (Beatriz and Valladares, 2008). Other factors such as invasive species, habitat change, overexploitation, and pollution are equally or even more important to the Earth's future (Millennium Ecosystem Assessment, 2005). Thus, the goal of global monitoring is aimed at characterizing "human habitability" through evaluation of vegetation that provides food, fiber, and fuel (Running et al., 1999) to a rapidly growing population. In the burgeoning field of global change monitoring, satellite remote sensing is increasingly more important. Only remote sensing offers a truly synoptic perspective of our surroundings and is therefore a critical tool for describing the type, rate, and extent of change unfolding across the globe. This is especially true for rangeland ecosystems that experienced losses of about 700 million ha by 1983 due to agriculture. In the United States alone, an estimated 75 million ha of former rangelands have been converted to agricultural land use since Euro-American settlement (Reeves and Mitchell, 2011) (Figure 11.11). The impacts of global change, such as climate impacts and land conversion, are often quantified through evaluation of vegetation cover and NPP in the context of the global carbon budget (Running et al., 1999).

11.3.4.1 Vegetation Productivity

Given the lack of ground referenced data available for determining productivity for rangelands globally, ecosystem modeling, remote sensing (Hunt and Miyake, 2006; Fensholt et al., 2006; Reeves et al., 2006), or a combination of both (Jinguo et al., 2006; Wylie et al., 2007; Xiao et al., 2008) can be used to estimate spatial and temporal trends across large areas. Many studies have evaluated the growth, total production, and health of rangeland vegetation, but two general approaches are normally applied that are very similar to the procedures outlined in the food security section. The

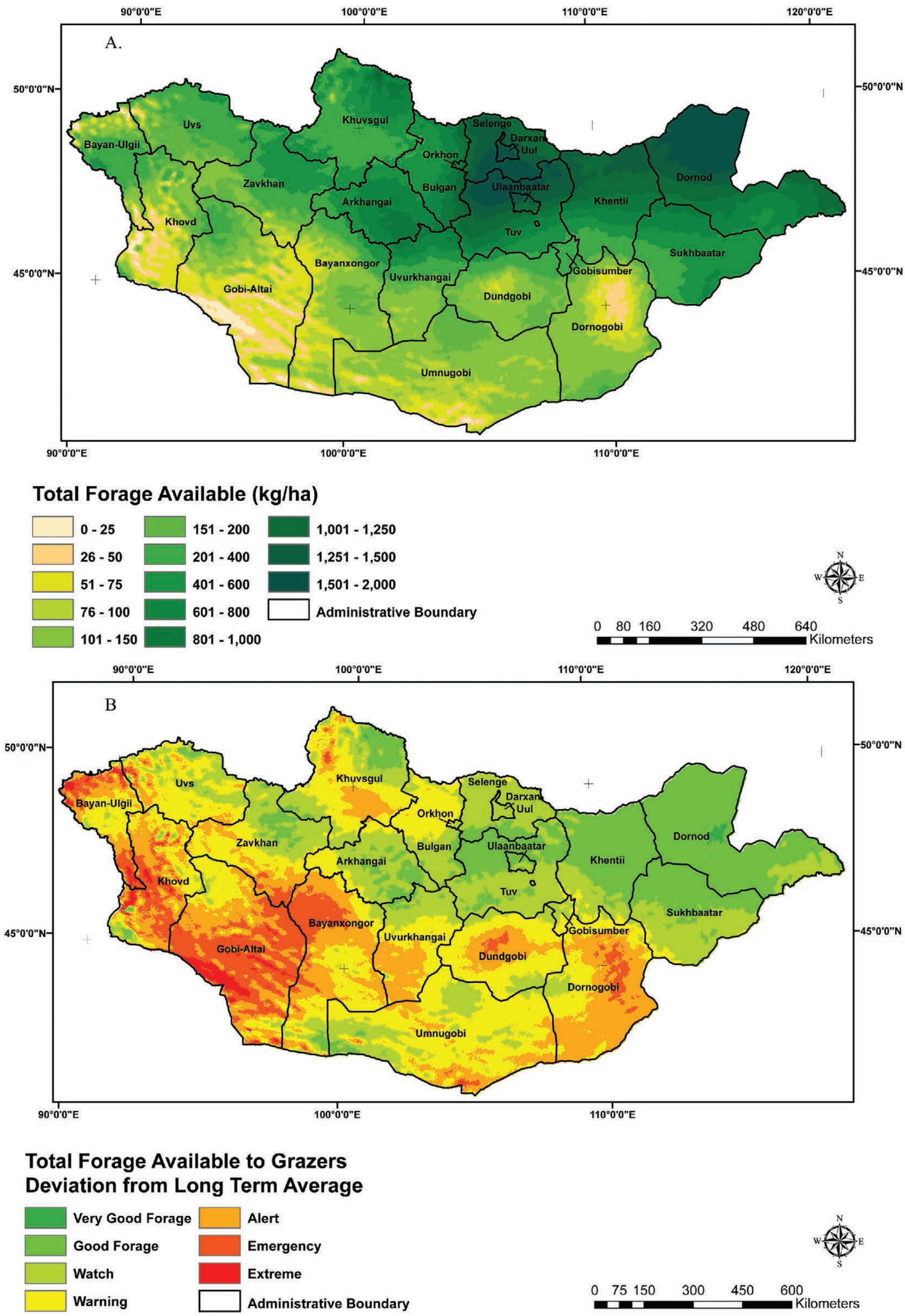

FIGURE 11.10 Panel A represents total forage available (kg ha^{-1}) during August 2013 for the Mongolia Livestock Early Warning System (LEWS). Panel B represents a map of forage deviation from long-term average (i.e., forage anomaly) for August 2013. Note areas in southwestern Mongolia experiencing Emergency to Extreme drought conditions.

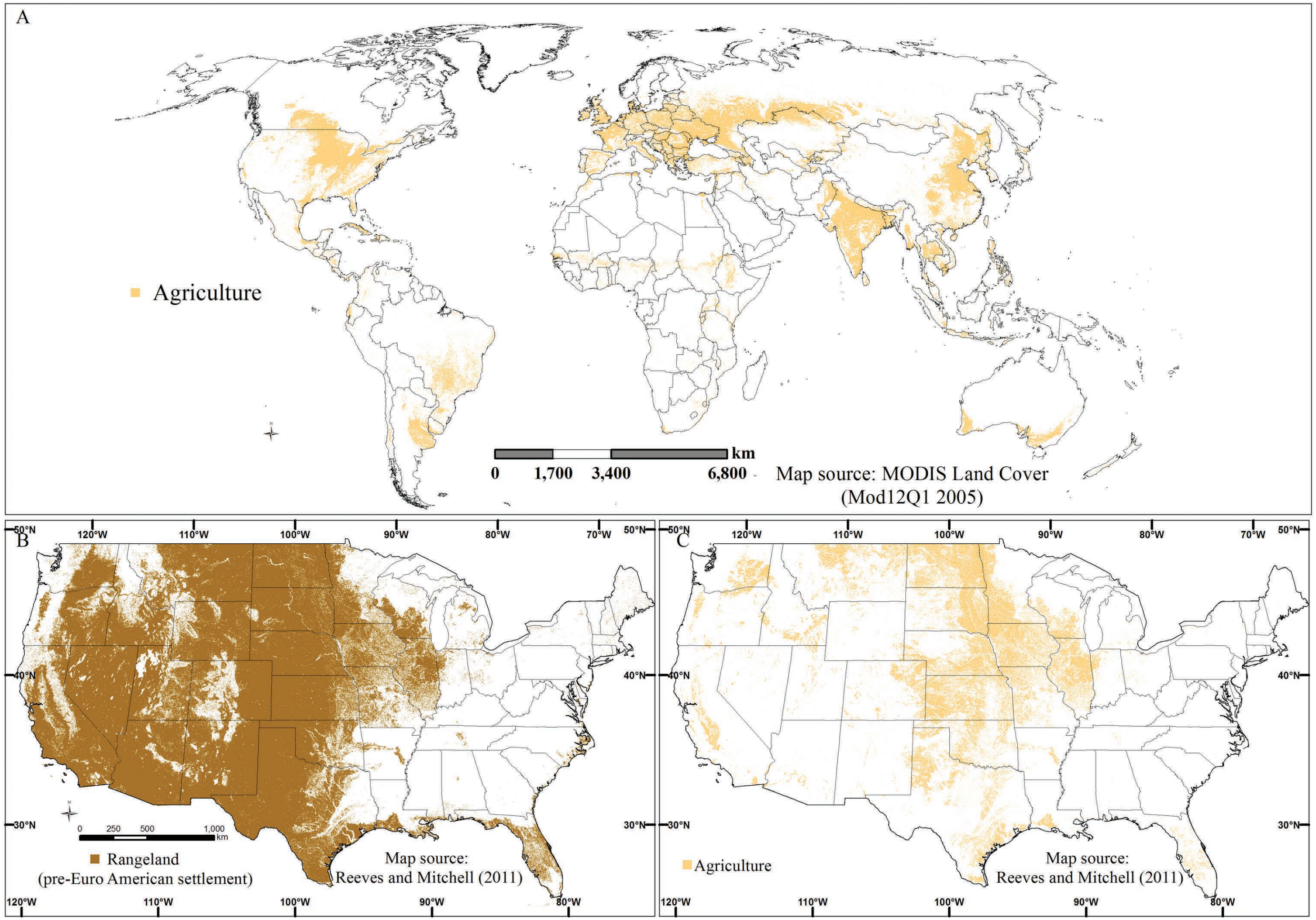

FIGURE 11.11 Panel A represents the estimated distribution of agricultural land use globally derived from MODIS MOD12Q1, 2006; University of Maryland Classification. Also shown is the hypothesized pre Euro-American extent of rangeland (Reeves and Mitchell, 2011) is shown in Panel B, while Panel C demonstrates areas of former rangeland now in agricultural production (estimated using the Biophysical Settings data product from the LANDFIRE Project (Rollins, 2009).

first approach involves directly sensing, via radiometric measurement, the amount of growth that has occurred over a given time. Direct quantification of biomass across rangeland vegetation types requires a set of spatially explicit ground samples describing the amount of peak biomass or annual production. Once ground data are collected and properly scaled, statistical models can be developed to describe the relationship between NDVI and biomass (Figure 11.12) that can, in turn, be used to monitor the response of vegetation through time. If peak biomass is estimates are sought, the annual maximum NDVI value should work reasonably well, but if annual production estimates are desired, a time integration of NDVI is usually employed (e.g., Paruelo et al., 1997).

Though NDVI has been widely used for monitoring global vegetation conditions, it exhibits well known saturation characteristics at relatively higher levels of biomass. The EVI can be used, with some success to overcome the saturation limitations inherent in NDVI. The saturation component of the NDVI signal, however, does not render it less useful for most applications. The reason for this is that across the range of productivity levels expected in most rangeland environments, the response is linear (Skidmore and Ferwerda, 2008).

The second approach for monitoring growth, total production, and health of vegetation involves use of remote sensing for quantifying canopy parameters, such as LAI, and f PAR, which, in turn, become part of a vegetation modeling system (Figure 11.12). Such a system is exemplified by the MODIS NPP algorithm (MOD17), which provides gross and net primary productivity (GPP and NPP) products at 1 km resolution for the entire globe. This approach is more sophisticated than direct sensing of biomass but enables carbon accounting for the global extent of rangelands. The modeling approach also requires a good deal more information including biome specific physiological parameters (Running et al., 2004). In addition, since this type of modeling approach requires meteorological and land cover information, it is directly informed by land cover/land use changes associated with global change. The NPP of rangeland vegetation from 2000 to 2012 is depicted in Figure 11.13, which demonstrates the type of ecosystem analysis possible with the MODIS NPP product. Figure 11.13

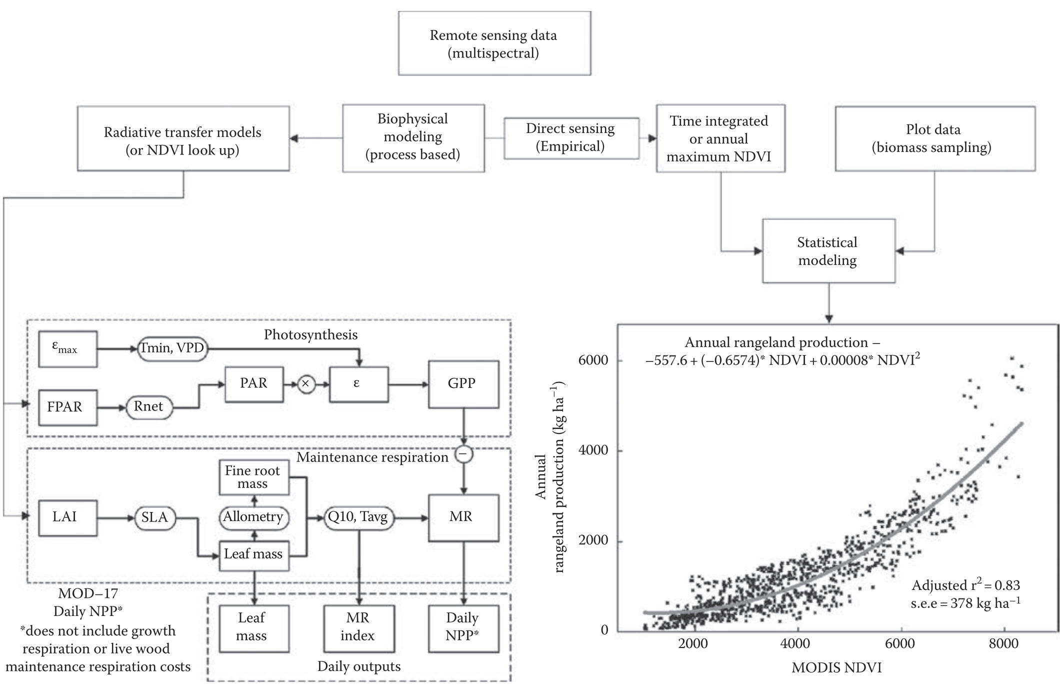

FIGURE 11.12 Direct sensing and biophysical modeling (process modeling) are two methods for estimating productivity of rangeland landscapes.

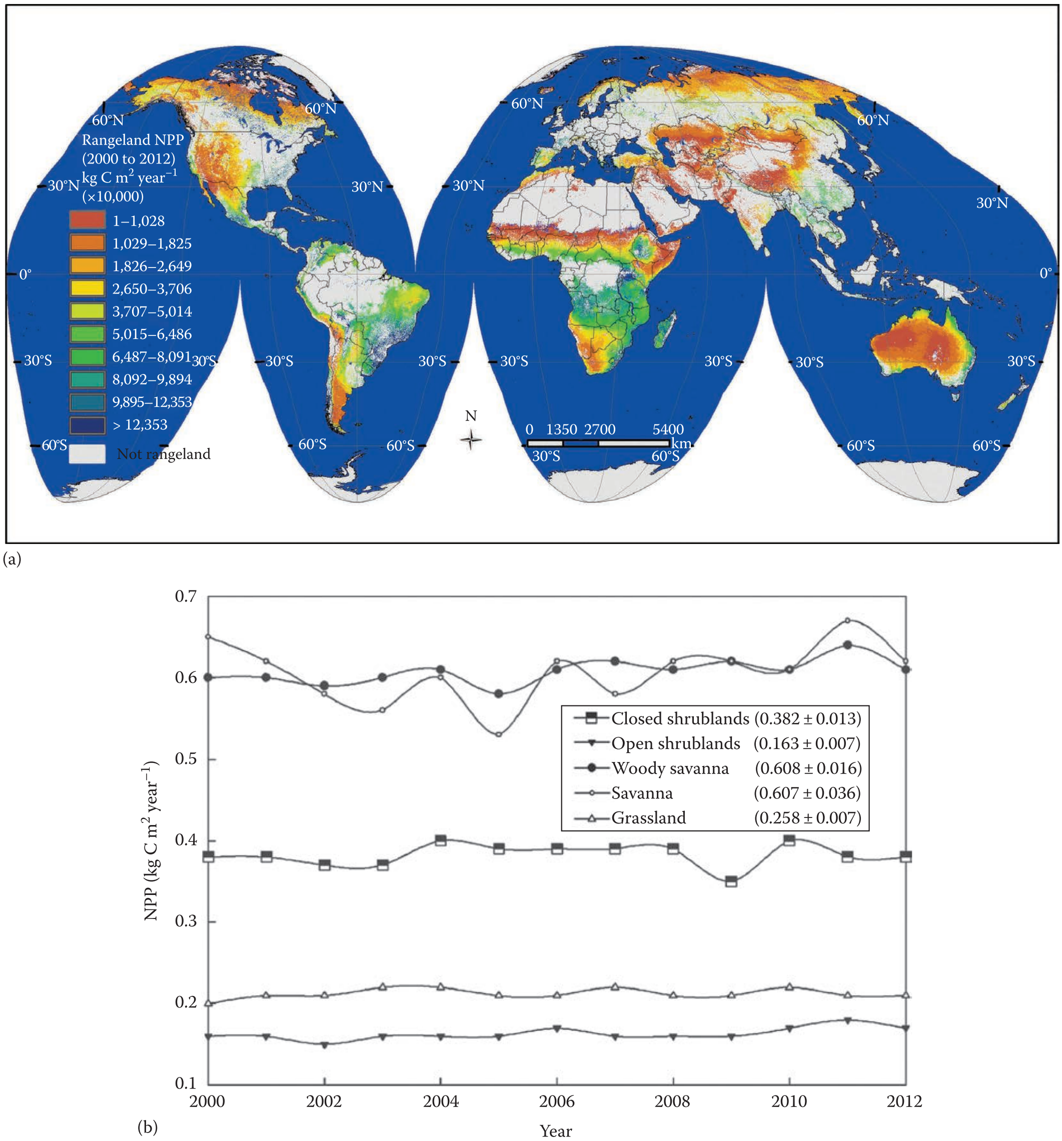

FIGURE 11.13 Panel A represents the mean (2000–2012) global distribution of rangeland NPP from the MODIS NPP (MOD17) product. Panel B represents the time series (2000–2012) of global rangeland NPP from the MOD17 product.

was created using a time series analysis from 2000 to 2012 of the MODIS derived annual NPP and Collection 4.5 land cover products. From this analysis, significant overlap and similarities between the savanna and woody savanna land cover classes are evident. These similarities suggest similar biophysical and bioclimatic conditions are present in these two classes or confusion exists between the classes. The close relationship between woody savanna and savanna could also be related to spatial commingling of the two types, which could be alleviated using higher resolution imagery. More recent analyses of (GPP) and leaf area index (LAI) suggest all major rangeland types have been greening at a significant rate. The latest long-term satellite-based leaf area index (LAI4g; Cao et al., 2023) and gross primary productivity (CEDAR-GPP; Kang et al., 2023) observations reveal widespread increases across global drylands from 1982–2020 (Figure 11.14.).

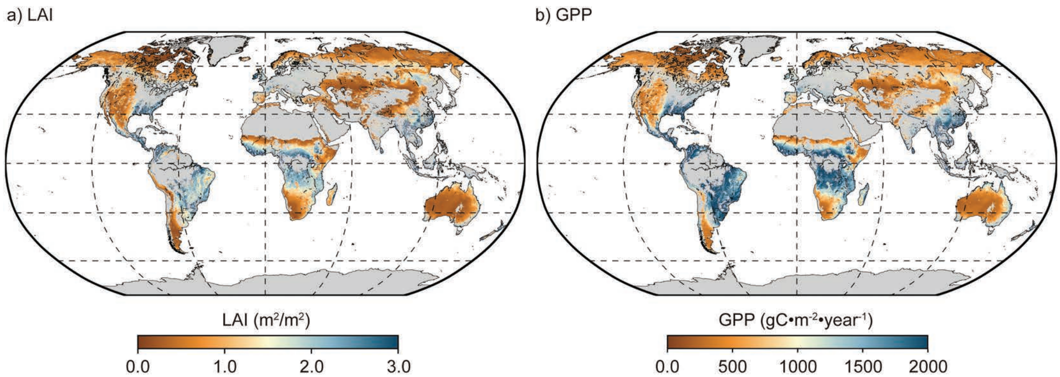

FIGURE 11.14 Long-term annual average LAI and GPP over 1982–2020. Global Inventory Modeling and Mapping Studies (GIMMS) leaf area index product (GIMMS LAI4g) is used as the proxy for vegetation greenness. GIMMS LAI4g product (version 1.1), is developed by Peking University ranging from 1982 to 2020 with a 15-day temporal resolution and ~ 8 km spatial resolution (Cao et al., 2023). GIMMS LAI4g addresses major uncertainties presented in current global long-term LAI products (e.g., GIMMS LAI3g) from NOAA satellite orbital drift and AVHRR sensor degradation and (2) insufficient LAI validation data to build robust LAI particularly before the late 1990s. For GPP dataset, upsCaling Ecosystem Dynamics with ARtificial intelligence GPP (CEDAR-GPP) is used, which incorporates the direct CO2 fertilization effect on photosynthesis. CEDAR-GPP ranging from 1982 to 2020 with monthly temporal resolution and at 0.05° resolution from 1982 to 2020 (Kang et al., 2023).

LAI has increased by an average of 0.0017 ± 0.025 $m^2\ m^{-2}$ y−1 across global rangelands. GPP has increased by an average of 1.7 ± 2.4 g C m^{-2} y−1 across global rangelands. LAI data indicate statistically significant greening ($p < 0.05$) across more than 50.1 % of rangelands, with a significant browning trend observed over 5.3 % of rangelands (Figure 11.15C). Similarly, GPP data indicates statistically significant greening ($p < 0.05$) across more than 56.5% of rangelands, with a significant browning trend observed over 3.5% of rangelands (Figure 11.15d). Notably, regions with the most pronounced increasing trend, as observed in both LAI and GPP datasets, include Central South America, Eastern China, the high-latitude Russia and Siberia landmass, and Central and South Africa. In contrast, regions exhibiting decreasing trends are found in Western US, Australia, Central Asia, and Southern South America. Generally, the spatial patterns of CEDAR-GPP consistent with those observed in GIMMS LAI4g. When considering land cover types, woody savanna experienced the largest increases in in LAI and GPP, whereas closed and open shrublands experiences relatively small increases in LAI and GPP. Often, using remotely sensed data alone, it can be difficult to assign causality but directly incorporating effects from changing climate, land cover, and associated vegetation responses simultaneously enables improved analysis of global change effects on rangeland environments. Using long time series, however, requires cross-calibration between sensors. to ensure continuity across new sensors with varying bandpasses and associated target atmospheric effects, drifts in calibration, and filter degradation (Huete et al., 2002).

11.3.4.2 Extending Remote Sensing Time Series Using Cross-Sensor Calibration

Recent ecological research has shown that declines in dryland productivity (often estimated measured using trends in NDVI and/or NPP), and increases in soil loss are due to the synergistic effects of extreme climatic events and land management practices. Livestock grazing and El Niño and La Niña events have 3 to 7 year return intervals (Holmgren and Scheffer, 2001; Holmgren et al., 2006; Washington-Allen et al., 2006) indicating that 10–20 years of continuous data is required to replicate, monitor, and assess the influence of land use practices and these extreme events (Washington-Allen et al., 2006). Sensors have finite life spans, and developing long-term observations often

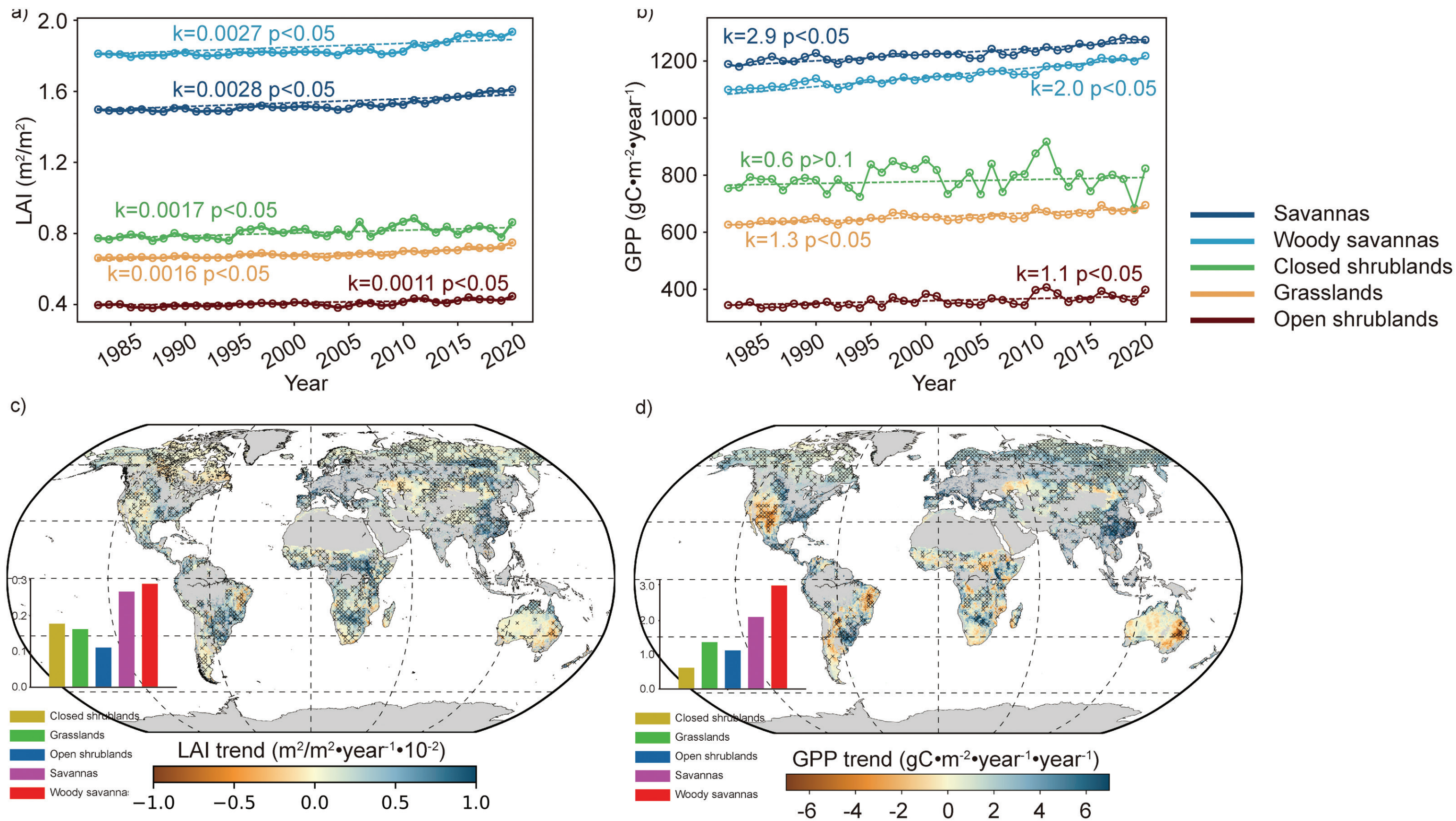

FIGURE 11.15 Interannual changes in LAI estimated by GIMMS(a) and GPP estimated by CEDAR for the period 1982–2020 over five landcovers. Spatial distribution pattern of the annual trend in LAI (c) and GPP (d) for the period 1982–2020. Regions labeled by dots have trends that are statistically significant ($p < 0.05$). The trend is calculated and evaluated using the Mann–Kendall test at the 5% significance level.

requires using multiple sources of data to develop a continuous, compatible dataset. The extension of time series is challenging due to drifts in calibration, filter degradation, and band locations (Miura et al., 2006). These characteristics create errors and uncertainties that vary with the landscape and sensors being evaluated. As examples, red and NIR spectral channels from AVHRR are relatively broad occupying the spectral space between 580–680 and 730–1,000 nm, respectively. In contrast, MODIS provides more narrow bands in the red and NIR space at 620–670 and 841–876 nm, respectively. The broader AVHRR red channel incorporates a portion of the green reflectance region (500–600 nm) (Figure 11.4) inevitably yielding a different spectral response of vegetation than MODIS.

The approaches for extending a satellite data time series via sensor (or product) cross-calibration involve remote sensing data fusion that accounts for multi-sensory, multi-temporal, multi-resolution, and multi-frequency image data from operational satellites (Pohl and Van Genderen, 1998; Zhang et al., 2010). Extension of satellite data records to produce time series of NDVI or NPP data typically involve:

1. Development of equations to simulate the spectral responses of individual channels (e.g., Suits et al., 1988)
2. Development of calibration equations to simulate the vegetation indices derived from other sensors (e.g., Steven et al., 2003; Tucker et al., 2005)
3. Crosscalibration of NDVI (e.g., from AVHRR) and NPP data products (e.g., from the MODIS sensor) to back cast the NPP record.

These techniques have been explored in a good number of studies and indicate suitable relations between sensors, but results are often inconclusive (Fensholt et al., 2009). Suits et al. (1988) determined that multiple regression analysis compared to principal component analysis was the best approach for spectral response substitution between Landsat and AVHRR sensors. Steven et al. (2003) found that vegetation indices from Landsat, SPOT, AVHRR, and MODIS were strongly linearly related, which allowed them to develop a table of conversion coefficients that allowed simulation of NDVI and SAVI across these sensors within a 1%–2% margin of error. Except for AVHRR, which was designed for other purposes, most high temporal resolution sensors have similar sensitivity to green vegetation. In addition, vegetation indices from many global platforms can be calibrated to within approximately ± 0.02 units if surface reflectance (as opposed to top of atmosphere) is used (Steven et al., 2003). Fensholt and Proud (2012) compared the GIMMS 3 g 8 km NDVI archive with MODIS 1 km NDVI and showed that global trends exhibit similar tendencies but significant local and regional differences were present, especially in more xeric environments. A comprehensive analysis of four long-term AVHRR based NDVI datasets with MODIS and SPOT NDVI datasets for the common period (from 2001 to 2008) clearly demonstrated lower correlations in more xeric regions such as the southwest and Great Basin of the United States (Scheftic et al., 2014). Similarly, Gallo et al. (2005) reported that 90% of the variation between 1 km MODIS and AVHRR NDVI can be explained by a simple linear relationship, while Miura et al. (2006) developed translation equations to emulate MODIS NDVI from AVHRR resulting in an r^2 of 0.97. Despite these successes, trend analyses from AVHRR can differ strongly from those estimated with MODIS and SPOTVGT (Steven et al., 2003) and lead to spurious conclusions. Unlike MODIS, AVHRR does not provide additional necessary channels permitting analysis of atmospheric composition for suitable atmospheric correction (Yin et al., 2012). Therefore, cross sensor calibration must be carefully planned and should leverage the strengths of previous efforts. Most efforts aimed for extending time series to improve trend analyses involve spectral calibration, either of individual band passes or indices. For monitoring global change and ecosystem performance, however, it is useful to quantify NPP trends given its link with the global carbon cycle and paramount importance to maintaining goods and services. Bai et al. (2008, 2009) developed a 23-year time series of global NPP data from 1982 to 2003 using the overlap period (2000–2003) between 1 km MODIS NPP and the mean annual sum of 8 km AVHRR GIMMS, for LADA program of FAO. Next, linear regression was applied to four-year mean, global, annual sum of NDVI from the GIMMS dataset and MODIS NPP to generate a single empirical equation between these two datasets. The resulting equation was then used to produce an 8 km NPP time series from 1982 to 2003. Wessels (2009) critiqued the approach of Bai et al. (2008) arguing that spatial variability was reduced and unaccounted for by using a single mean equation rather than a pixel-by-pixel approach. As a result, the following case study used a pixelwise regression approach for establishing relationships between 8 km GIMMS NDVI and 1 km MODIS NPP. The goal of this case study was to produce a continuous, compatible dataset describing annual NPP from 1982 to 2009 using both 8 km AVHRR GIMMS from Tucker et al. (2005) and 1 km MODIS net photosynthesis. A more recent version of GIMMS AVHRR NDVI (GIMMS 3g) data is available from 1981 to 2011 at 1/12th° spatial resolution.

11.3.4.2.1 Case Study

The strategy suggested by Steven et al. (2003) and Wessels (2009) was followed for calibrating 8 km pixel resolution GIMMS annual ΣNDVI from 1982 to 2006 to MODIS NPP data aggregated from 1 to 8 km using the 2000 to 2006 overlap period between these two separate time series. Collection 5 annual estimates of MODIS NPP from 2000 to 2006 and GIMMS ΣNDVI time series were subset to the rangeland portion of the contiguous United States and classified according to varying levels of aridity using AI (Figure 11.16). The AI of drylands (AI ≤ 0.65) is partitioned into four classes including the hyper-arid, arid, semi-arid, and dry sub-humid classes.

11.3.4.2.1.1 Application and Validation of Linear Regression Approach The Taiga Earth Trend Modeler from IDRISI was used to conduct a simple linear regression on a pixel-by-pixel basis between the two time series using the years 2000, 2002, 2004, and 2006. This was done so that a holdout dataset could be retained for comparing predicted and observed NPP. Across all pixels in

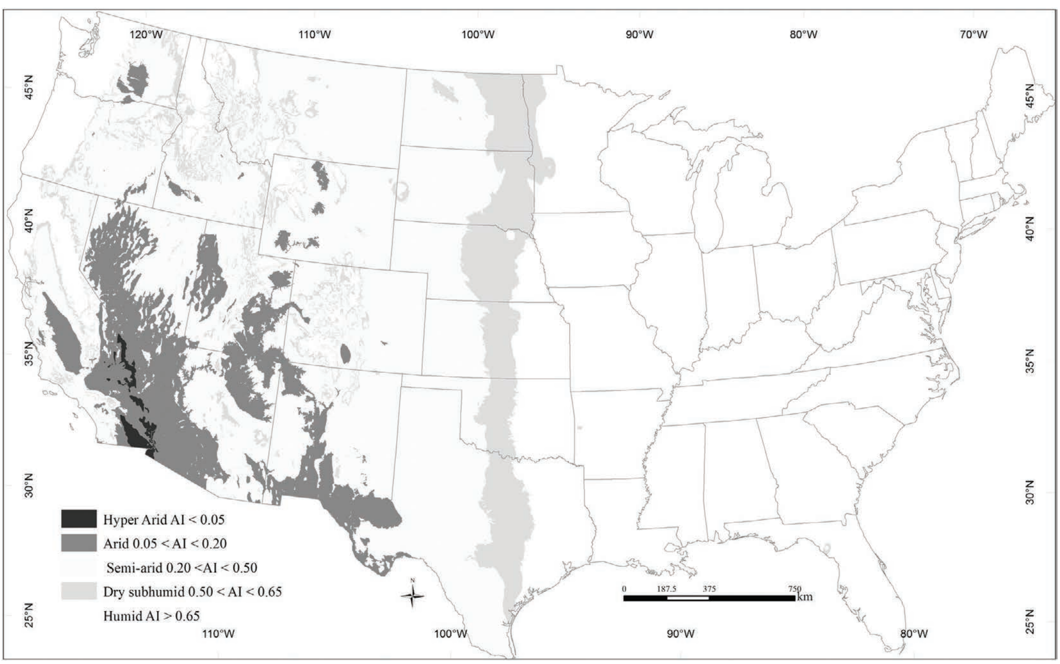

FIGURE 11.16 Distribution of aridity index (annual precipitation/potential evapotranspiration) classes throughout the United States used for aggregating NPP estimates for coterminous U.S. rangelands.

the rangeland domain, the mean NDVI was 0.03 and mean NPP was 281.6 g C m^{-2} $year^{-1}$. The mean equation across all pixels was

$$Y = 0.03 * X + (-31.7)$$

where

X is the annual GIMMS ΣNDVI

Y is the predicted 8 km MODIS NPP and $r^2 = 0.41$ (Figure 11.17)

Panels A, B, and C in Figure 11.17 represent the estimated slope, intercept, and r^2 of a linear regression for each pixel in the study area between GIMMS NDVI and MODIS NPP for the years 2000, 2002, 2004, and 2006. Predicted MODIS NPP was subsequently compared to the observed MODIS NPP (Table 11.5).

Figure 11.18 indicates a strong relationship between monthly integrated 8 km GIMMS NDVI and monthly integrated 1 km MODIS net photosynthesis (PSNnet) over the domain of coterminous US rangelands.

The net photosynthesis is a major component of the annual NPP product. To derive the final model to extend the NPP time series, the pixel level regressions developed were applied to the annual GIMMS ΣNDVI from 1982 to 1999. To these data, the MODIS NPP time series from 2000 to 2009 were added, thus extending the final time series from 1982 to 2009. Using the final time series, temporal and spatial variations in NPP response can be quantified. The mean NPP for each class from 1982 to 2009 was 95 ± 28 for hyper-arid, 115 ± 47 for arid, 218 ± 114 for semi-arid, and 370 ± 117 (g C m^{-2} $year^{-1}$) for the dry sub-humid class. In addition, the temporal trend (not accounting for temporal autocorrelation) of NPP within each AI class was as follows: hyper-arid ($r^2 = 0.08$, $p = 0.08$), arid ($r^2 = 0.01$, $p = 0.37$), semi-arid ($r^2 = 0.25$, $p = 0.004$), and dry sub-humid ($r^2 = 0.22$, $p = 0.006$) (Figure 11.19). Using this approach, significant carbon gains were detected for both semi-arid and arid systems. In addition, the positive response in arid and semiarid systems agrees with conclusions by Reeves and Bagget (2014) that significant increasing trends have been observed from 2000 to 2012 across much of the US rangeland domain, owed mostly to increased precipitation. The results portrayed in Figure 11.19 demonstrate improved chances for successfully interpreting vegetation response to global change through increasing the time series of satellite observation.

11.3.5 Remote Sensing of Global Land Cover

Global land cover data are essential to most global change research objectives, including the assessment of current global environmental conditions and the simulation of future environmental scenarios that ultimately lead to public policy development. In addition, land cover data are applied in national and sub-continental scale operational environmental and land management applications (e.g., weather forecasting, fire danger assessments, resource development planning, and the establishment of air quality standards). Land cover characteristics are integral to many Earth system processes (Hansen et al., 2000), in addition to providing information for carbon exchange and general circulation models. A common and important application of global land cover information is inference of biophysical parameters, such as LAI and fPAR, which influence global scale climate and ecosystem process models. Use of these models and monitoring the state of the Earth's rangelands is needed for global change research, especially given the influence of growing anthropogenic disturbances (Lambin et al., 2001; Jung et al., 2006; Xie et al., 2008).

One of the remote sensing community's grand challenges is to provide globally consistent but locally relevant land cover information (Estes et al., 1999). Global mapping presents special challenges since the geographic variability of both land cover and remote sensing inputs add complexity that can lead to inconsistent results. The evolution of global land cover datasets over the past 30 years has attempted to meet the grand challenge while adhering to general remote sensing land

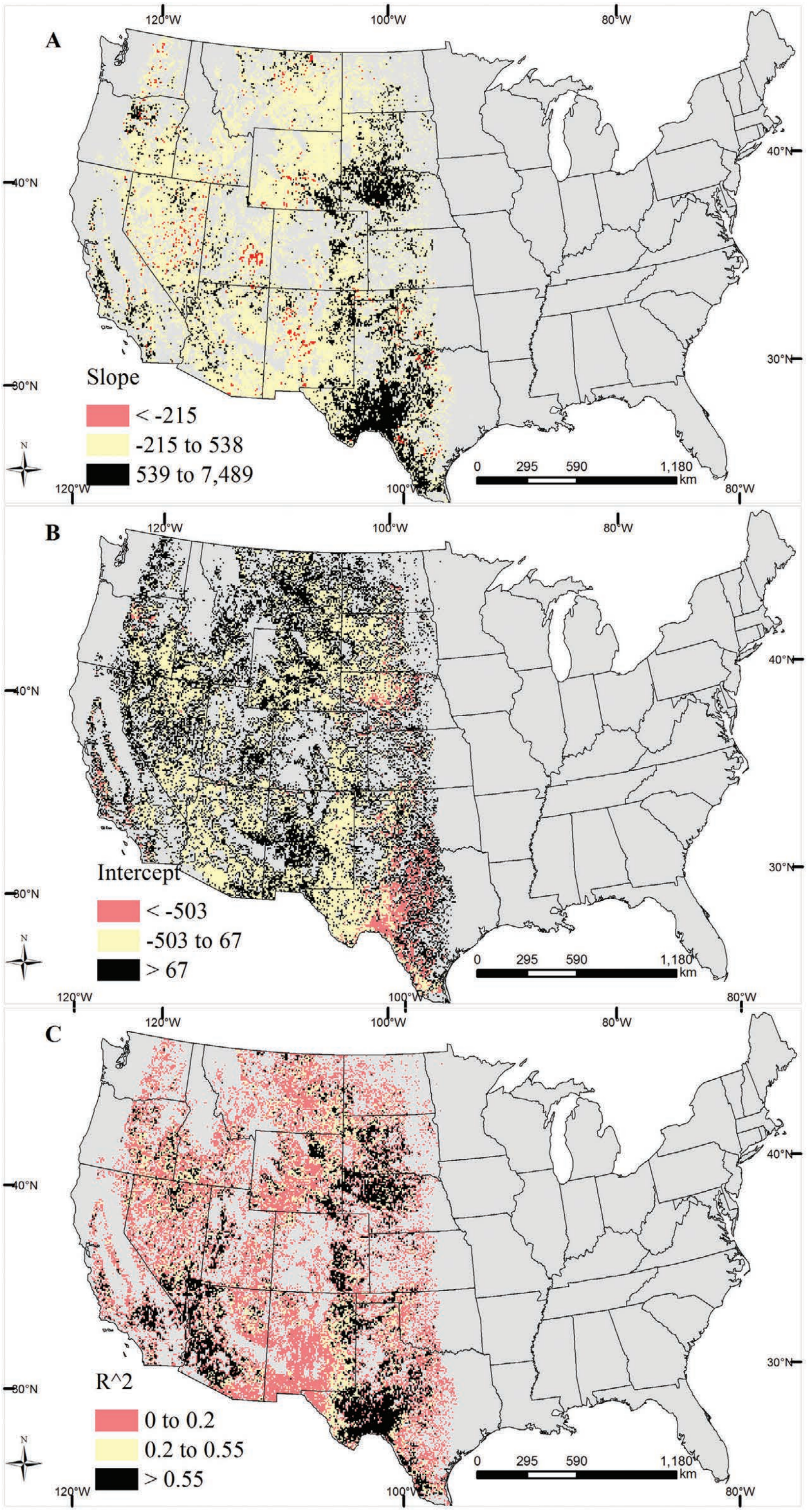

FIGURE 11.17 The resulting pixel-to-pixel linear regression models that were developed to calibrate GIMMS annual ΣNDVI to the MODIS NPP time series for the years 2000, 2002, 2004, and 2006. Panels A, B, and C represent the slope, intercept, and R^2 values for each pixel.

TABLE 11.5

Comparison of Predicted and Observed Values across the Extent of Rangelands in the Coterminous U.S. (g C m2 yr−1). Bold numbers are predicted values based on the pixel level regression equations depicted in Figure 11.15.

	Minimum	Median	Mean	SD
Year		g C m² yr⁻¹		
2001	16.5	179	211	123
	0.1	**186**	**220**	**137**
2003	15.3	189	218	131
	2.4	**184**	**217**	**131**
2005	19.8	236	126	126
	0.1	**210**	**157**	**157**

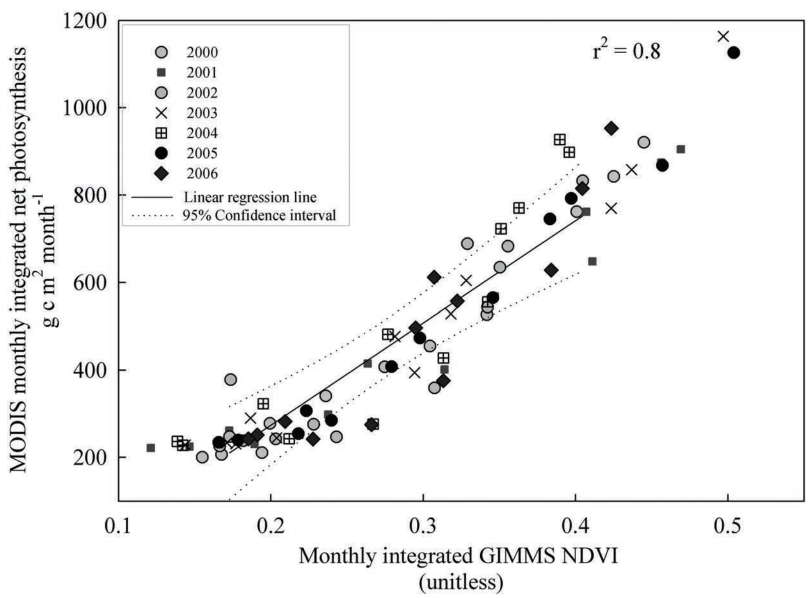

FIGURE 11.18 Relationship between monthly integrated MODIS derived 1 km² net photosynthesis and GIMMS 4 km² NDVI aggregated across all coterminous U.S. rangelands.

cover—mapping standards dealing with accuracy, consistency, and repeatability. The earliest contemporary efforts to provide global land cover data did not rely on remote sensing inputs but instead was based on the developer's expertise and the quality of information from best available sources (Matthews, 1983; Olson, 1983; Wilson and Henderson-Sellers, 1985). These maps were coarse (i.e., 1° × 1°) in resolution but thematically detailed. Global land cover mapping based on remote sensing advanced rapidly in the 1990s when NOAA polar-orbiting data from the AHVRR were compiled into global coverage. Initially, 4 km AVHRR Global Area Coverage Pathfinder data aggregated to 1° × 1° (DeFries and Townshend, 1994) and later to 8 km resolution (DeFries et al., 1998) were inputs to the first remote sensing—based global land cover products. The International Geosphere Biosphere Programme (IGBP) served as the catalyst for a worldwide effort led by the USGS to generate a 1992–1993 set of 1 km resolution AVHRR global 11-day maximum NDVI composites

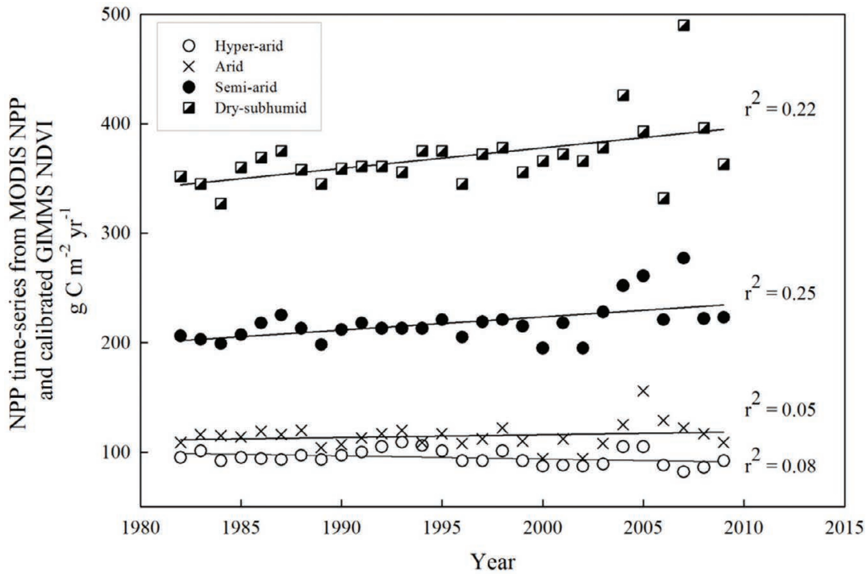

FIGURE 11.19 Rangeland mean net primary productivity (NPP) from 1982 to 2009 across four zones of aridity index (AI) including hyper arid, arid, semi-arid, and dry subhumid.

(Eidenshink and Faundeen, 1994). Also under IGBP auspices, these data were used to produce the first 1 km resolution global land cover dataset using the 17 class International Geosphere-Biosphere Programme Global Land Cover Classification (IGBP DISCover) legend (Loveland et al., 2000) (Figure 11.20). Hansen et al. (2000) followed with the completion of a 1 km, 12 class land cover dataset (UMD land cover map).

These two maps served as the foundation for future global mapping initiatives since their development experiences and map strength and weaknesses provided valuable lessons for the next generation of maps. The NASA Earth Observing System's ambitious global land product program based on multiresolution MODIS data established a new state of the art in global land cover mapping. MODIS global land cover based on 500 m resolution imagery and the 17 class IGBP DISCover legend started in the 2001 and since then has been updated annually (Friedl et al., 2002). This ongoing activity represents the only sustained global land cover initiative. In the 2000s, European global land cover projects contributed significantly to advancing global land cover understanding. The Global Land Cover 2000 (GLC2000) project used SPOT vegetation instrument data to produce a 22 class 1 km resolution land cover dataset (Bartholomé and Belward, 2005). In a follow-on effort, the European Space Agency sponsored a follow-on project, GlobCover, that used ENVISAT MERIS imagery to generate the highest resolution (300 m) global land dataset ever. The MERIS-based map contained 22 land cover classes based on the United Nations sponsored international standard land cover classification system (LCCS).

The China led Fine Resolution Observation and Monitoring Global Land Cover (FROMGLC) dataset was a groundbreaking effort to map global land cover based on Landsat 5 and 7 Thematic Mapper/ETM+ and other high resolution Earth observation data spanning the first decade of the 21st century (Gong et al., 2013). The FROMGLC dataset established new standards for high resolution land cover mapping and monitoring, with 29 land cover classes.

With new accessibility to free remote sensing data in the cloud and cloud-based computing that facilitates rapid generation of land cover across broad regional extents, there has been a proliferation of new global land cover datasets at high resolution. With these new tools, the academic community

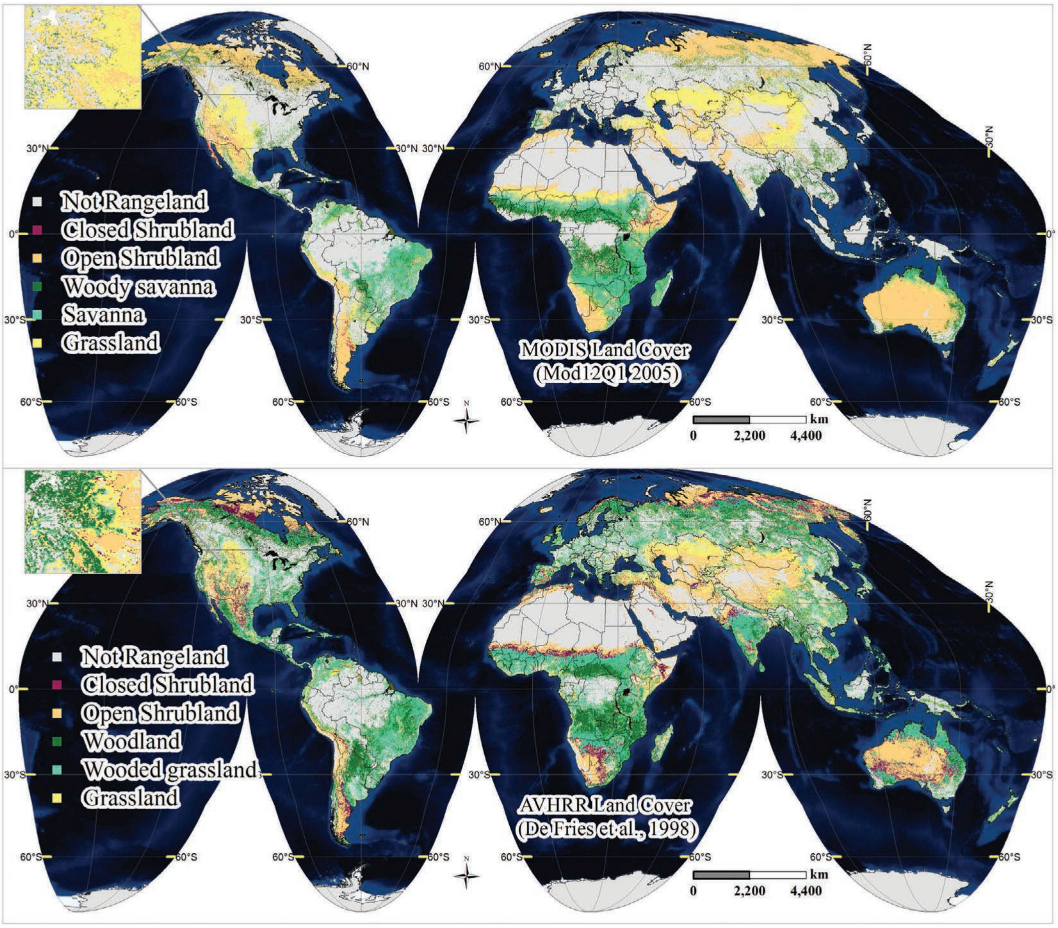

FIGURE 11.20 Comparison between 1 km^2 MODIS land cover data (Mod12Q1; UMD classification) and AVHRR derived land cover (DeFries et al., 1998) using the Simple Biosphere Model legend (Table 11.6).

produced a global land cover, land use, and ecozone map using Landsat and topographic data and defined a potential approach for multitemporal monitoring of change (Hansen et al., 2022), The European Space Agency initiated the WorldCover project in 2017 and released the first global land cover product at 10m resolution for 2020 and 2021, based on Sentinel1 and Sentinel2 data (Zanaga et al., 2020, 2021). Not only was the product the first to map land cover at 10 m resolution, but it marked a paradigm shift in the use of multimodal platforms (optical with Sentinel2, Sentinel1 based radar) for global mapping of land cover. By the early 2020s, for the first time the commercial sector began development of independent global, high resolution land cover. The Environmental Systems Research Institute (ESRI) in partnership with Impact Observatory (IO) created a Sentinel2 based 10 m global land cover product, including mapping change from 2017 to 2022 (ESRI, 2023). Google partnered with the World Resources Institute to produce Dynamic World, a global, 10 m, nine land cover class land cover dataset based on Sentinel2 (Brown et al., 2022).

In addition to the thematic land cover mapping efforts described earlier (Table 11.6), global "continuous fields" products provide quantitative estimates of the percent tree cover within each grid cell. DeFries et al. (1999) developed global percent tree cover data using 1 km AVHRR imagery, and Hansen et al. (2003) created similar products using MODIS.

TABLE 11.6
Summary of Characteristics of the Major Remote Sensing Global Land Cover Datasets

Database	Source	Vintage	Resolution	Land Cover Content (Suggested Rangeland Classes)	Strengths	Weaknesses
Global AVHRR NDVI Land Cover (DeFries and Townshend, 1994)	AVHRR	1987	1.0°^{2} Latitude	11 (3) land cover classes—based on Simple Biosphere Model	First remote sensing-based depiction of global land cover	Coarse resolution, applications limited to Global Circulation Model applications
Global AVHRR Land Cover (DeFries et al., 1998)	AVHRR Global Area Coverage Pathfinder	1987	8 km^2	14 (5) land cover classes—based on Simple Biosphere Model	Improved spatial resolution provided more realistic view of global land cover	Land cover classes were general and specific to one application requirement
IGBP DISCover (Loveland et al., 2000)	AVHRR Local Area Coverage	1992–93	1 km^2	17 (5) IGBP DISCover land cover classes, and other land cover legends	Highest resolution global land cover to date, validated based on statistical design	Variable image quality contributed to unevenness of land cover accuracy
UMD Global Land Cover (Hansen et al., 2000)	AVHRR Local Area Coverage	1992–93	1 km^2	12 (5) land cover classes	Based on an automated analysis strategy	Not validated, affected by variable image quality
MODIS Global Land Cover (Friedl et al., 2002)	MODIS	2001-present, produced annually	500 m^2	17 (5) IGBP DISCover land cover	Uses highest quality remotely sensed inputs available, based on rigorous automated methods	Unknown accuracy due to the lack of a design-based map validation
GLC2000 (Bartholomé and Belward, 2005)	SPOT 4 VEGETATION	2000	1 km^2	22 (5) land cover classes	Based on standardized land cover legend, validated results	Affected by variable image quality
GlobCover (Arino et al., 2007)	ENVISAT MERIS	2005–2006	300 m^2	22 (4) land cover classes, UN Land Cover Classification System	Based on standardized land cover legend, validated results, and highest resolution imagery to-date	Regional variability in image quality increased uncertainty of results in some part of the world
Fine Resolution Global Land Cover (Gong et al., 2013)	Landsat 5 and 7	Nominally 2005–2006	30 m^2	29 (6) land cover classes	Highest resolution dataset ever produced	Limited temporal inputs resulted in regional inconsistencies
GLC2000 (Bartholomé and Belward, 2005)	SPOT 4 Vegetation	2000	1 km^2	22 (5) land cover classes	Based on standardized land cover legend, validated results	Affected by variable image quality
GlobCover (Arino et al., 2007)	ENVISAT MERIS	2005–2006	300 m^2	22 (4) land cover classes, UN Land Cover Classification System	Based on standardized land cover legend, validated results, and highest-resolution imagery to date	Regional variability in image quality increased uncertainty of results in some parts of the world

(*Continued*)

TABLE 11.6 (*Continued*)
Summary of Characteristics of the Major Remote Sensing Global Land Cover Datasets

Database	Source	Vintage	Resolution	Land Cover Content (Suggested Rangeland Classes)	Strengths	Weaknesses
Fine resolution global land cover (Gong et al., 2013)	Landsat 5 and 7	Nominally 2005–2006	30 m^2	29 (6) land cover classes	Highest-resolution data produced to date	Limited temporal inputs resulted in regional inconsistencies
Global Land Cover and Land use 2019 (Hansen et al., 2022)	Landsat 7 and 8	2019	30 m^2	19 (5) land cover and use classes	Hybrid of land cover and land use; Validated with probability sample	Land use does not include pastures despite acknowledgment of their status as most widespread human landuse
WorldCover (Zanaga et al., 2020, 2021)	Sentinel-2, Sentinel 1	2020, 2021	10 m^2	11 (3) land cover classes	First 10 m^2 global land cover product; Multi-modal with optical and active remote sensing systems	Thematically coarse
ESRI Land Cover (ESRI, 2023)	Sentinel 2	2017–2022	10 m^2	9 (1) land cover classes	Multi-temporal mapping of global land cover at high resolution	Thematically coarse with 1 rangeland class, Questionable representation of change
Dynamic World (Brown et al., 2022)	Sentinel 2	On Demand (limited to Sentinel 2 data availability)	10 m^2	9 (2) land cover classes	First near real-time capability for global land cover	Thematically coarse, questionable representation of change

11.3.5.1 Comparative Investigations of Global Land Cover Datasets

With a relatively large number of global land cover datasets available, users face a challenge in understanding which one is best suited for their application. The differences in spatial resolution, temporal properties, land cover legend, and quality complicate the selection. Land cover legend and quality are particularly significant factors. Accuracy assessments that provide insights into data quality are available for some of the global products. For example, both the IGBP DISCover and GLC2000 datasets were evaluated using an independent accuracy assessment. DISCover accuracy was measured at 66.9% (Scepan, 1999). Mayaux et al. (2006) determined that the overall GLC2000 product accuracy was 68.6%. The MODIS land cover dataset accuracy was assessed based on a comparison with training data, with the results showing 78.3% agreement (Friedl et al., 2002). The more recent GlobCover land cover dataset's (Table 11.6) independent accuracy was measured to be 73.0%. Finally, the China led fine resolution global land cover product was determined to have an overall accuracy of 71.5% (Gong et al., 2013). Accuracy assessments were not produced for UMD global land cover datasets.

The overall accuracies mask the significant variations in per class accuracies (e.g., Scepan, 1999 estimates that the DISCover individual class accuracies varied from 40% to 100%). The class accuracy variations, as well as variations in land cover legends and class definitions, make cover specific applications problematic. As a response to this problem, several global dataset comparison studies have been undertaken, which focus on determining dataset strengths and weaknesses. Some have used independent datasets to look at regions or continents, such as Achuete et al.'s (2011) evaluation of GLC2000, GlobCover, and MODIS land cover for Africa and Frey and Smith's (2007) evaluation of IGBP DISCover and MODIS land cover over western Siberia. Other comparisons have looked at agreement between datasets across the globe. For example, Hansen and Reed (2000) compared UMD and IGBP DISCover products; Giri et al. (2005) compared MODIS and GLC2000; McCullum et al. (2006) compared IGBP, UMD, GLC2000, and MODIS products; and Fritz and See (2007) compared MODIS, GLC2000, and GlobCover. McCullum et al. (2006) concluded that while there is general agreement at the global level in total area and general land cover patterns; there is limited agreement when looking at specific spatial distributions.

A more comprehensive and definitive effort to understand the difference in global datasets comes from Wang and Mountrakis (2023). They assessed the accuracy of 11 global land cover products and several national scale products in the conterminous US. The different datasets had resolutions from 10m to 1km, and mapping dates from 1992 through 2023 and were validated using a consistent reference dataset of 25,000 manually interpreted reference points over the conterminous United States. Differences in thematic class definitions make precise comparisons difficult, but in general the study found wide discrepancies in landcover accuracies. Thematic class accuracies were highest on average for a "treed" cover class, at 78%, but average accuracies for other classes ranged from 55% to 70%. Spatial discrepancies were apparent as well, with the best performing datasets often differing among different geographies. The regional products generally performed better than global products at the scale of the conterminous United States, demonstrating the challenge of achieving regional scale accuracy with a global scale product. The study also found that accuracy across all products decreased when assessing "edge" samples that may represent boundaries among multiple land cover classes.

One of the remote sensing community's grand challenges is to provide globally consistent but locally relevant land cover information (Estes et al., 1999). Evaluations of remote sensing based global land cover datasets have shown general agreement of patterns and total area of different land covers at the global level, but have more limited agreement in spatial patterns at local to regional levels (McCullum et al., 2006) As the quality and resolution of remotely sensed data used for global land cover mapping improves, the logical expectation is that overall and individual class accuracies will also improve. However, Fritz et al. (2011a,b) emphasized the continued uncertainty in global land cover products, especially in land cover classes associated with agriculture and some forest groups. They suggest that increased use of in situ data is the key to improving global land cover datasets. Wang and Mountrakis (2023) similarly noted general room for improvement in mapping accuracy for global scale land cover products. As global high resolution products such as the ESRI and WorldCover products become increasingly available for multiple dates, there is also a need for rigorous validation of not only land cover, but land cover change.

11.4 FUTURE PATHWAYS OF GLOBAL SENSING IN RANGELAND ENVIRONMENTS

Remote sensing has created unprecedented capacity to study the Earth by providing repeated measurements of biological phenomena at global scales. Since the first regional applications of NDVI (one of the earliest regional applications found is Rouse et al., 1973) (Section 10.2), the study of the global rangeland situation has benefitted greatly from advancements made in a relatively short period of time. Degradation of global rangelands because of climate change and anthropogenic land use requires accurate, objective and repeatable measures of land condition across broad spatial scales. As presented in this chapter, the use of remote sensing over previous decades has largely focused on broad-scale satellite-based products that have been used in many international and national monitoring programs, based on trust built over many years of use. While satellite remote sensing has provided the backbone of rangeland assessment and monitoring at global and broad regional scales, condition assessments based on ground-referenced data have widely served as the dominant approach for many rangeland managers at regional and localized scales (Kachergis et al., 2022; Lawley et al., 2016; Sparrow et al., 2020). Tueller (1989) suggested that the majority of monitoring data in rangelands would be collected using remote sensing by 2010, but this still not the case, with a notable lack of uptake for fine-scale remote sensing methods for condition assessment (Retallack et al., 2023). However, recent increases in the accessibility of ultra-high-resolution data have led to the development of corresponding methods for extracting fine-scale indicators of ecosystem condition. Though future uses of remotely sensed data will be used in unexpected ways, obvious areas of enhancement and progress are anticipated. These future pathways can be expressed in distinct areas including improvements in data availability and processing, biophysical product improvement with emphasis on operational conversion of data to information.

The design and intended application of spaceborne sensors will continue to evolve, and a wider variety of satellite systems including radar and lidar could be quite beneficial in the future. If the past provides a glimpse into the future, new sensors with improved capabilities will be developed, but it is unclear, however, whether improved spatial, spectral, and temporal resolution of satellite remote sensing will provide the greatest advancements in the evaluations of rangelands on a global scale. The ability to extract surface features and quantify biophysical properties will still be limited by the same factors presently hindering remote sensing of rangelands. Characteristics such as bright soil background, leaf anatomy and physiology, and relatively low biomass conspire to hinder remote sensing of rangelands. Very little can be done to change these situations, and as a result, future pathways should include a focus on data continuity, increased data availability, better computer processing systems, and global campaigns for collecting ground referenced data and greater use of unmanned aerial vehicles for scaling ground referenced data.

Remote-sensing data continuity is important to monitoring global rangelands, and loss of this critical aspect will significantly weaken our ability to understand what the biosphere is indicating. The need for continuity is recognized in the Land Remote Sensing Policy Act of 1992, which states:

> The continuous collection and utilization of land remote sensing data from space are of major benefit in studying and understanding human impacts on the global environment, in managing the Earth's resources, in carrying out national security functions, and in planning and conducting many other activities of scientific, economic, and social importance.

Since the first civilian spaceborne missions (e.g., Landsat 1), the global monitoring community and government agencies have been reasonably successful in providing the needed continuity. The

Landsat program is a good example of the flow and continuity with incremental improvements with each successive launch generally maintaining a 30 m resolution benchmark. If archive data from Landsat 4 (deployed in 1982) are included, 41 years of 30 m spatial resolution from the TM sensor in visible and NIR (at the minimum) are available. Landsat 8, launched on February 11, 2013, is the most recent addition to the suite of Landsat satellite launches and provides an example of maintaining continuity with previous missions while improving capability. Landsat 8 contains the Operational Land Imager (OLI) and the Thermal Infrared Sensor (TIRS), which provide global coverage at varying resolutions. The OLI provides two new spectral bands for detecting cirrus clouds and the other for coastal zone observations. Now that the entire archive of Landsat data has been made freely and publicly available, usage has increased exponentially. The unprecedented data availability has and will continue to lead to new algorithmic and ecological discoveries. Increased data usage may signal greater interest in remote sensing but certainly tracks the increased microprocessor speed over the last decade (Figure 11.21). As processing speed and memory have increased so has the level of algorithmic sophistication and spatial domain for analysis. Indeed, the global remote-sensing community is poised for improved characterization capabilities, due to new data policies and concurrent advances in computing (Hansen and Loveland, 2011).

Even a decade ago, it would have been unthinkable to regularly process and store a global time series of satellite imagery with a pixel resolution of less than about 250 m. Although it is certainly possible to monitor rangelands globally at 30 m, it will be a monumental task. Each TM path/row contains 0.534 GB in the seven multispectral and thermal channels and approximately 0.234 GB for the panchromatic band. Since roughly 16,396 scenes are required for global coverage (including oceans), that is an estimated 12.3 TB of data for a single 16-day period. The repeat frequency or revisit cycle is 16 days (~22 periods per year), so the total amount of data since 1999 is near 6224 TB. Based on an online storage price of $0.05 per month per GB (https://cloud.google.com/products/cloud-storage/), the storage cost is tantamount to roughly 311,000 dollars per year. While this represents a significant amount of data and resources, a growing number of global applications at 30 m spatial resolution can be expected. Sexton et al. (2013) produced a Landsat-based global database of tree cover at 30 m resolution (Sexton et al., 2013), while Potapov et al.

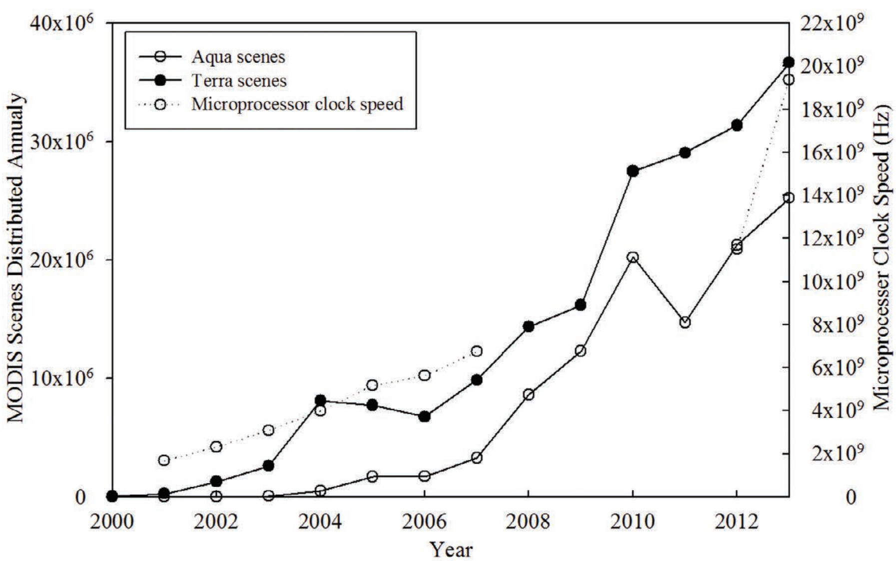

FIGURE 11.21 Microprocessor speed and MODIS data usage (Microprocessor speed data courtesy of www.raptureready.com/ (accessed 1, April 2014), MODIS usage data courtesy of B. Ramachandran NASA Earth Observing System | LP DAAC).

(2022) created the Global Land Cover and Land Use Change (GLAD) dataset quantifying changes in forest extent and height, cropland, built-up lands, surface water, and perennial snow and ice extent from the year 2000 to 2020 at 30 m spatial resolution. Moreover the fractional cover of lifeforms including those in the rangeland domain, have been quantified and made available as Google Earth Engine assets (projects/glad/GLCLU2020/). Global efforts like these will be further enhanced with Landsat 9 (27 September, 2021) as fusion between L8/OLI and S2/MSI enables revisit cycles of about 2 days (Wulder et al., 2019) compared with the nominal revisit of 3 days prior to 2021 (Bolton et al., 2020). This is important for global applications in rangeland domains when one considers the prevalence of cloud cover derived from monsoon periods across much the Earth. Presently, most efforts aimed at global remote sensing of rangelands are based on MODIS sensors aboard the Terra and Aqua satellites. Since 2006, the number of scenes annually distributed from MODIS data from both Aqua and Terra has increased by 7.6 million per year (about 181 TB year^{-1}) (Figure 11.21). This use is a testament to the breadth of vetted science data products offered globally.

Satellite sensors degrade with age, therefore new sensors are essential to continue collecting data within the same quality and usability ranges. Recently, data collected using MODIS sensors have shown degradation caused by time and orbital drift. This degradation has led to the decision to retire these satellites with continuity being supplied by the VIIRS through 2031. A visual comparison between expedited MODIS and VIIRS can be seen in Figure 11.22.

A transformation may lengthen the historical data compatible with VIIRS as it continues to monitor Earth's surface. NOAA leadership plans to continue VIIRS through 2031 with four missions called NASA-NOAA Joint Polar Satellite System (JPSS). The JPSS is a joint program between NOAA, NASA, and the Defense Weather Satellite System, tasked with developing the next generation requirements for environmental research, weather forecasting, and climate monitoring (npp.gsfc.nasa.gov/viirs.html). The JPSS provides operational continuity of satellite-based observations and products through a series of advanced spacecraft of which Suomi NPoP is a member. Suomi NPoP was launched in 2011 with five key instruments, but the instrument with greatest application, to rangelands globally, and similarity with the AVHRR and MODIS predecessors is the VIIRS. The VIIRS instrument observes the Earth and atmosphere at 22 visible and infrared wavelengths (Table 11.7). The continuity of land remote-sensing instruments is well established and provides a critical component to researchers involved with global change research in rangeland environments. Most future global issues will emulate present concerns. In other words, the problems, or area of focus, today (e.g., vegetation trends, land degradation, and fire processes) will continue and perhaps intensify in the future.

Regardless of the increasingly important roles remote sensing will play, georeferenced ground data will play an equally critical aspect of biospheric monitoring (Baccini et al., 2007). Fritz and See (2007) suggest that increased use of in situ data is the key to improving global datasets. The collection, maintenance, analysis, and distribution of georeferenced ground data, however, are a time-consuming and resource-intensive exercise, especially over regional or global domains. In this vein, the citizen scientist is an underutilized concept that can be cheaply and effectively employed to globally collect biospheric observations.

Citizen science can be defined as

> the systematic collection and analysis of data; development of technology; testing of natural phenomena; and the dissemination of these activities by researchers on a primarily avocational basis.
>
> *OpenScientist (2011)*

These open networks promote interactions between scientists, society, and policymakers leading to decision making by scientific research conducted by amateur or nonprofessional scientists (Socientize, 2013). Advancements in communication and technology are credited with aiding the growth of citizen scientists (Silverton, 2009). Collectively, citizen science efforts from around the

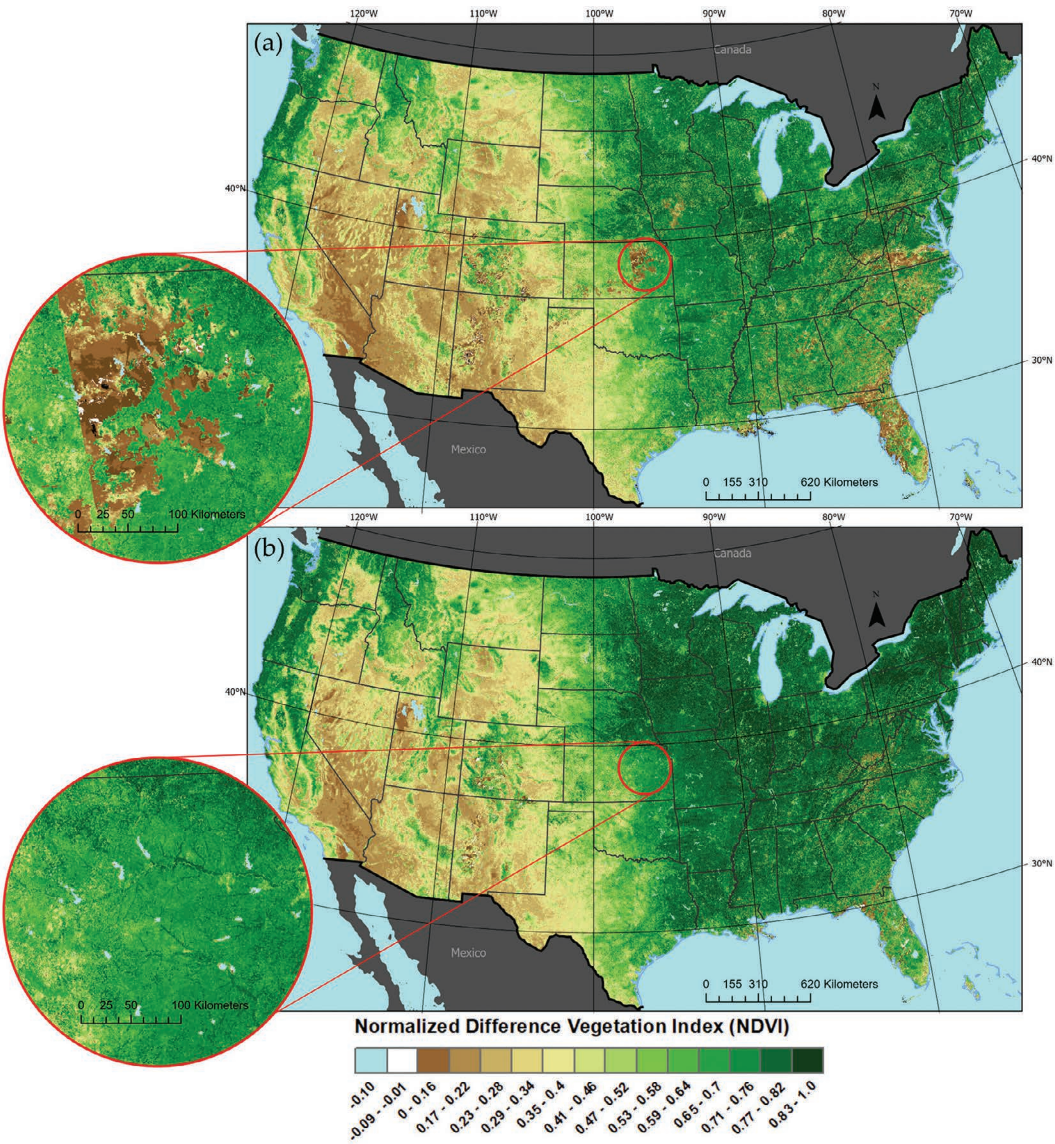

FIGURE 11.22 Expedited Moderate Resolution Imaging Spectroradiometer (eMODIS) 250-m Normalized Difference Vegetation Index (NDVI) (a) and expedited Visible Infrared Imaging Radiometer Suite (eVIIRS) 375-m NDVI (b) for composite (Julian day of year 215–221), 2016. Highlighted location in eastern Kansas shows an example of how eVIIRS composites have less noise artifacts than eMODIS composites. (Benedict et al., 2021.)

globe could possibly provide powerful venues for validating and calibrating future remote-sensing efforts. Both citizen science and crowdsourcing are valuable sources of data for calibrating or validating rangeland remote sensing but both have yet to be fully exploited Fritz et al. (2017). Fritz et al. (2017) provided a special issue dedicated to citizen science and Earth observation. A recent example of using citizen science to aid remote sensing of nonforest landscapes include mapping presence and phenological status of Buffelgrass in southern Arizona where the species is considered a major threat to desert ecosystems (Wallace et al., 2016). The Geo-Wiki project, established in 2010 by the International Institute for Applied Systems Analysis (IIASA), enables anyone with the means to

TABLE 11.7

VIIRS Spectral Channels and Suggested Usefulness. The LWIR are long wave infrared bands while the S/MWIR are short to mid wave infrared bands (adapted from http://cimss.ssec.wisc.edu/itwg/itsc/itsc13/proceedings/session10/10_2_schueler.pdf) (Schueler et al., 2003).

		Band No.	Driving EDR(s)	Spectral Range (um)	Horiz. Sample Interval (km) (Track × Scan)	
					Nadir	End of Scan
Reflective Bands	VisNIR	M1	Ocean Color Aerosol	0.402–0.422	0.742 × 0.259	1.60 × 1.58
		M2	Ocean Color Aerosol	0.436–0.454	0.742 × 0.259	1.60 × 1.58
		M3	Ocean Color Aerosol	0.478–0.498	0.742 × 0.259	1.60 × 1.58
		M4	Ocean Color Aerosol	0.545–0.565	0.742 × 0.259	1.60 × 1.58
		I1	Imagery EDR	0.600–0.680	0.371 × 0.387	0.80 × 0.789
		M5	Ocean Color Aerosol	0.662–0.682	0.742 × 0.259	1.60 × 1.58
		M6	Atmospheric Correction	0.739–0.754	0.742 × 0.776	1.60 × 1.58
		I2	NDVI	0.846–0.885	0.371 × 0.387	0.80 × 0.789
		M7	Ocean Color Aerosol	0.846–0.885	0.742 × 0.259	1.60 × 1.58
	S/WMIR	M8	Cloud Particle Size	1.230–1.250	0.742 × 0.776	1.60 × 1.58
		M9	Cirrus/Cloud Cover	1.371–1.386	0.742 × 0.776	1.60 × 1.58
		I3	Binary Snow Map	1.580–1.640	0.371 × 0.387	0.80 × 0.789
		M10	Snow Fraction	1.580–1.640	0.742 × 0.776	1.60 × 1.58
		M11	Clouds	2.225–2.275	0.742 × 0.776	1.60 × 1.58
Emissive Bands		I4	Imagery Clouds	3.550–3.930	0.371 × 0.387	0.80 × 0.789
		M12	SST	3.660–3.840	0.742 × 0.776	1.60 × 1.58
		M13	SST Fires	3.973–4.128	0.742 × 0.259	1.60 × 1.58
	LWIR	M14	Cloud Top Properties	8.400–8.700	0.742 × 0.776	1.60 × 1.58
		M15	SST	10.263–11.263	0.742 × 0.776	1.60 × 1.58
		I5	Cloud Imagery	10.500–12.400	0.371 × 0.387	0.80 × 0.789
		M16	SST	11.538–12.488	0.742 × 0.776	1.60 × 1.58

classify satellite, drone or ground-level imagery. This novel system has grown rapidly and currently has 22,000 contributors and over 18 million crowdsourced image classifications have been uploaded. In addition to Geo-Wiki, the Global Geo-Referenced Field Photo Library (Xiao et al., 2011) enables visualization and archival of geo-referenced photos. This system, managed by the Center for Earth Observation and Monitoring, also includes a smartphone app. Similarly, the NASA-funded Global Learning and Observations to Benefit the Environment (GLOBE) Observer (GO) program is a smartphone app that enables citizen-collected land cover photos to be tagged and archived with location, date and time, and, in some cases, land cover type (Kohl et al., 2021). Despite a promising future, Fritz et al. (2022) identified grand challenges facing environmental citizen science spanning methodological, technological, political and ethical domains. Lastly, while remote sensing of rangelands has undergone major advances since inception, the need for quickly accessible information targeted for land managers is increasing. Tueller (1989) stated:

> Remote sensing has been recommended for at least 30 years for assisting with rangeland resources development and management on a worldwide basis.

That was 35 years ago and yet while numerous examples of remote sensing to improve our understanding and management rangelands are discussed in this chapter, there remains a great need for operational products for meeting specific end user's needs. The suite of global biophysical products derived from MODIS since 2000 is closely aligned with this idea. The relatively coarse resolution and academic, not managerial, focus limits their usefulness for land management endeavors. However, in recent years, deep learning-based classifications have proven valuable for extracting conservation-relevant information from this high-resolution imagery, including accurate classifications of certain plants to the species-level (Retallack et al., 2023). A new example of this is the inception of the Rangeland Analysis Platform (RAP; https://rangelands.app/) has begun to change this situation as it offers fast information for user defined areas of interest, for most rangelands in the United States regarding plant functional types from 1986 to 2022 and beyond (Allred et al., 2021). While not global the RAP, leveraging the Google Earth Engine, has demonstrated the capability of converting data to information at 30 m since it emanates from the Landsat time series. Similar efforts by Rigge et al. (2020) have used machine learning techniques to classify sagebrush to the genus for sagebrush (*Artemisia* spp.) cover and these products are available for the United States through LandCART which led to development of the Rangeland Condition Monitoring Assessment and Projection data product (Zhou et al., 2020). Potapov et al. (2023) provide an excellent overview of techniques for evaluating rangeland condition using remote sensing.

These recent developments have also led to the development of novel analytical methods, where machine deep-learning has been employed to great effect for extracting information from data collected at all spatial scales, which may prove to be exceptionally useful for scaling ground-referenced data. The analysis of high-resolution UAV or aerial imagery has often been approached using object based image analysis (Lu et al., 2016; Oldeland et al., 2021; Wilson et al., 2022). The collection of this high-resolution data has been enabled by a rapid rise in the accessibility of UAV (uncrewed aerial vehicle) technology over the past decade. UAV platforms have also enabled the collection of high-resolution three-dimensional data using methods such as lidar and structure from motion (SfM). This three-dimensional data has proven invaluable in measuring and mapping changes in erosion at fine scales compared with previous aerial or satellite-based approaches (Chakrabortty and Pal, 2023). UAV-derived SfM and lidar have also been used for the prediction of aboveground biomass in rangeland systems (Anderson et al., 2018; Barnetson et al., 2020; Grüner et al., 2019; Ku and Popescu, 2019), as well as canopy structural attributes (Hillman et al., 2021). While UAV-derived lidar data have proven useful in rangelands, in terms of global applications with spaceborne lidar, the picture is less clear. The launch of the new spaceborne laser altimeter missions ICESat-2 (Ice, Cloud, and Land Elevation Satellite-2) and GEDI (Global Ecosystem Dynamics Investigation) in September and December 2018, has significantly improved observational coverage, providing more accurate estimates with footprint sizes better suited for forest observations, particularly when combined with optical or radar data. The application of spaceborne lidar systems to measure ecosystems characterized by short-stature vegetation, including rangelands (e.g., grasslands, shrublands, and savannas) and wetlands (e.g., mangroves, bogs, and swamps) is still in its infancy, as ICESat-2 and GEDI sensors are not optimized to these types of ecosystems. Ilangakoon (2020), using GEDI measurements from rangeland sites in Idaho, highlighted its capability to capture trends and patterns of functional diversity in semi-arid ecosystems and potential to identify critical biophysical and ecological shifts in similar ecosystems, which can be useful for monitoring changes in carbon-cycle dynamics, habitats and biodiversity. In African savanna ecosystems, Li et al. (2023) concluded that GEDI data products could not estimate canopy heights of shrubs below 2.34 m but accurately estimated the canopy height of trees between 3 and 15 m. In comparison studies ICESat-2 exhibited greater precision in terrain height retrieval than GEDI, contradicting previous observations favoring GEDI in forested regions over ICESat-2. This disparity can be attributed to the challenges faced by GEDI in distinguishing ground and canopy returns, especially in areas with short-stature vegetation (Zhu et al., 2023; Latifi, 2023; Singh et al., 2023). According to Liu et al. (2021) GEDI still outperforms

ICESat-2 for canopy height measurements, because ICESat-2 tends to overestimate the canopy height of dwarf shrublands and underestimate the canopy height of forest ecosystems.

11.5 CONCLUSIONS

Rangelands are found extensively throughout the world covering about 50% of the global land mass. The remoteness, harsh conditions, and high interannual variation in productivity make remote sensing the most cost effective and efficacious tool for evaluating the status and health of rangelands globally. Global remote sensing has unique constraints from a remote sensing perspective and spatial resolution is often sacrificed in place of temporal resolution. A broad suite of sensors possessing various spectral channels, revisit times, and spatial resolutions are available for regional to global rangeland applications. However, most global applications, especially those sponsored for national or international applications (e.g., LADA, IGBP), use AVHRR, SPOTVGT, MODIS, and to a lesser degree TM. Additionally, many biophysical phenomena can be investigated with the myriad of sensors, but as discussed in this chapter, we focused on the globally relevant issues of degradation, fire, land cover, food security, and global change. In this chapter, we demonstrate sensors, data, algorithms, strengths, and limitations of various methods to address these globally significant issues. Though estimates vary, the proportion of degraded rangelands is around 23% globally (Table 11.4). The use and interpretation of RUE for evaluating degradation patterns is controversial (Prince et al., 2007), but alternative techniques are subject to similar issues and assumptions. Thus, when considering degradation, especially in a global context, a model ensemble approach (e.g., combine local NPP scaling, rainfall use efficiency, and NPP trend analysis) may be most useful to indicate trends and identify where action is needed to lessen detrimental effects on goods and services.

Most global land cover efforts have limited thematic resolution of rangeland classes (average number of rangeland classes is 4.75; Table 11.6). However, computational resources and algorithmic complexity is sufficient to produce higher spatial and thematic resolution land cover maps as inaugurated by studies such as Gong et al. (2013) and Hansen et al. (2013). Land cover and land use will continue to evolve in response to broad-scale disturbance and global change. As a result, monitoring global change and extent and severity of fire has been the focus of many algorithms, national programs, and sensors. As an example, the MODIS sensor aboard both the Terra and Aqua platforms was designed with fire monitoring in mind with channels 21, 22, 31, and 33, but given the sensor drift and lifespan, MODIS is being replaced by VIIRS and other sensors. Burn severity evaluation is a relatively new capability since the AVHRR and SPOTVGT sensors lack the spectral channels necessary for contemporary algorithms. Likewise, the advent of the MODIS-derived NPP product (Running et al., 2004)—has spawned numerous studies aimed at evaluating NPP patterns globally. More recently, regional and national tools that enable visualization of aboveground annual production and fractional abundance of various lifeforms has been made possible with Google Earth Engine through the Rangeland Analysis Platform. In this chapter, we demonstrate that from 1982 to 2020, rangelands have become more productive, on average increasing in GPP by 1.7 ± 2.4 g C m^{-2} $y^{-1.}$ Despite increasing temporal trajectories globally, drought and degradation are detrimental on a regional basis and regularly threaten the security of food derived from rangelands, especially since much of the greening around the Earth is due to increasing abundance of woody species. In this vein, tools like the LEWS, driven by MODIS derived 250 m NDVI, is a useful program to provide guidance local governments and international aid organizations. As world population continues to grow, it is likely that the programs like LEWS will become increasingly important. These issues emphasize the critical importance of mission and spectral continuity.

REFERENCES

AlBakri, J. T., J. C. Taylor. 2003. Application of NOAA AVHRR for monitoring vegetation conditions and biomass in Jordan. *Journal of Arid Environments*, 54, 579–593.

Alexandratos, N., J. Bruinsma. 2012. *World Agriculture Towards 2030/2050: The 2012 Revision Ch.4(ESA/12-03, FAO,2012)*. www.fao.org/3/ap106e/ap106e.pdf.

Allbed, A., L. Kumar. 2013. Soil salinity mapping and monitoring in arid and semiarid regions using remote sensing technology: A review. *Advances in Remote Sensing*, 2, 373–385.

Allen, J. L., B. Sorbel. 2008. Assessing the differenced Normalized Burn Ratio's ability to map burn severity in the boreal forest and tundra ecosystems of Alaska's national parks. *International Journal of Wildland Fire*, 17, 463–475.

Allred, B. W., B. T. Bestelmeyer, C. S. Boyd, C. Brown, K. W. Davies, M. C. Duniway, L. M. Ellsworth, T. A. Erickson, S. D. Fuhlendorf, T. V. Griffiths, V. Jansen, M. O. Jones, J. Karl, A. Knight, J. D. Maestas, J. J. Maynard, S. E. McCord, D. E. Naugle, H. D. Starns, D. Twidwell, D. R. Uden. 2021. Improving Landsat predictions of rangeland fractional cover with multitask learning and uncertainty. *Methods in Ecology and Evolution*. https://doi.org/10.1111/2041-210X.13564.

An, N., K. P. Price, J. M. Blair. 2013. Estimating aboveground net primary productivity of the tallgrass prairie ecosystem of the Central Great Plains using AVHRR NDVI. *International Journal of Remote Sensing*, 34, 3717–3735.

Anderson, K. E., N. F. Glenn, L. P. Spaete, D. J. Shinneman, D. S. Pilliod, R. S. Arkle, S. K. McIlroy, D. R. Derryberry. 2018. Estimating vegetation biomass and cover across large plots in shrub and grass dominated drylands using terrestrial lidar and machine learning. *Ecological Indicators*, 84, 793–802. https://doi.org/10.1016/j.ecolind.2017.09.034.

Angerer, J. P. 2008. Examination of high-resolution rainfall products and satellite greenness indices for estimating patch and landscape forage biomass. PhD Dissertation. College Station, TX: Texas A&M University.

Angerer, J. P. 2012. Gobi forage livestock early warning system. In *Conducting National Feed Assessments*, eds. M. B. Coughenour, H. P. S. Makkar, pp. 115–130. Rome, Italy: Food and Agriculture Organization.

Arino, O., S. Casadio, D. Serpe. 2012. Global nighttime fire season timing and fire count trends using the ATSR instrument series. *Remote Sensing of Environment*, 116, 226–238.

Arino, O., D. Gross, F. Ranera, L. Bourg, M. Leroy, P. Bicheron, R. Whit. 2007. Globcover: ESA service for global land cover from MERIS. In *International Geoscience and Remote Sensing Symposium*, pp. 2412–2415. Barcelona, Spain.

Awuma, K. S., J. W. Stuth, R. Kaitho, J. Angerer. 2007. Application of Normalized Differential Vegetation Index and geostatistical techniques in cattle diet quality mapping in Ghana. *Outlook on Agriculture*, 36, 205–213.

Baccini, A., M. A. Friedl, C. E. Woodcock, Z. Zhu. 2007. Scaling field data to calibrate and validate moderate spatial resolution remote sensing models. *Photogrammetric Engineering and Remote Sensing*, 73, 945–954.

Bai, E., T. W. Boutton, X. B. Wu, F. Liu, S. R. Archer. 2009. Landscape scale vegetation dynamics inferred from spatial patterns of soil δ13C in a subtropical savanna parkland. *Journal of Geophysical Research*, 114, G01019.

Bai, Z. G., D. L. Dent, L. Olsson, M. E. Schaepman. 2008. Proxy global assessment of land degradation. *Soil Use and Management*, 24, 223–234.

Barbosa, P. M., J. M. Grégoire, J. M. C. Pereira. 1999. An algorithm for extracting burned areas from time series of AVHRR GAC data applied at a continental scale. *Remote Sensing of Environment*, 69, 253–263.

Barnetson, J., S. Phinn, P. Scarth. 2020. Estimating plant pasture biomass and quality from UAV imaging across queensland's rangelands. *AgriEngineering*, 2, 523–543.

Bartholomé, E., A. S. Belward. 2005. GLC2000: A new approach to global land cover mapping from Earth observation data. *International Journal of Remote Sensing*, 26, 1959–1977. https://doi.org/10.1080/01431160412331291297.

Bauer, M. E. 1976. Technological basis and applications of remote sensing of the Earth's resources. *IEEE Transactions on Geoscience Electronics*, 14, 3–9.

Beatriz, A., F. Valladares. 2008. International efforts on global change research. In *Earth Observation of Global Change: The Role of Satellite Remote Sensing in Monitoring the Global Environment*, ed. E. Chuvieco, pp. 1–21. Dordrecht, the Netherlands: Springer.

Belenguer-Plomer, M. A., A. Tanase Fernandez-Carrillo, E. Chuvieco. 2019. Burned area detection and mapping using Sentinel-1 backscatter coefficient and thermal anomalies. *Remote Sensing of Environment*, 233, 111345.

Benedict, T. D., J. F. Brown, S. P. Boyte et al. 2021. Exploring VIIRS continuity with MODIS in an expedited capability for monitoring drought-related vegetation conditions. *Remote Sensing*, 13. https://doi.org/10.3390/rs13061210.

Blanco, P., H. D. Valle, P. Bouza, G. Metternicht, L. Hardtke. 2014. Ecological site classification of semiarid range lands: Synergistic use of Landsat and Hyperion imagery. *International Journal of Applied Earth Observation and Geoinformation*, 29, 11–21.

Bolton, D. K., J. M. Gray, E. K. Melaas, M. Moon, L. Eklundh, M. A. Friedl. 2020. Continental scale land surface phenology from harmonized Landsat 8 and Sentinel-2 imagery. *Remote Sensing ofEnvironment*, 240, 111685.

Brown, C. F., S. P. Brumby, B. Guerrillas, T. Birch, S. B. Hyde, J. Mazzariello, W. Czerwinski, V. J. Pasquarella, R. Haertel, S. Ilyushchenko, K. Schwehr, M. Weisse, F. Stolle, C. Hanson, O. Guinan, R. Moore, A. M. Tait. 2022. Dynamic world, near realtime global 10m land use land cover mapping. *ScientificData*, 9, 251.

Cao, S., M. Li, Z. Zhu, J. Zha, W. Zhao, Z. Duanmu, Y. Chen. 2023. Spatiotemporally consistent global dataset of the GIMMS Leaf Area Index (GIMMS LAI4g) from 1982 to 2020. *Earth System Science Data Discussions*, 1–31. https://doi.org/10.5194/essd-2023-68.

Carreiras, A., M. Vasconcelos, R. Lucas. 2012. Understanding the relationship between aboveground biomass and ALOS PALSAR data in the forests of Guinea-Bissau (West Africa). *Remote Sensing of Environment*, 121, 426–442.

Carter, L. J. 1969. Earth resources satellite: Finally off the ground? *Science*, 163, 796–798.

Chakrabortty, R., S. C. Pal. 2023. Systematic review on gully erosion measurement, modelling and management: Mitigation alternatives and policy recommendations. *Geological Journal*, 58, 3544–3576. https://doi.org/10.1002/gj.4709.

Chen, D., C. Fu, J. Hall, E. E. Hoy, T. V. Loboda. 2021. Spatio-temporal patterns of optimal Landsat data for burn severity index calculations: Implications for high northern latitudes wildfire research. *Remote Sensing of Environment*, 258, 112393.

Chen, D., T. V. Loboda, J. V. Hall. 2020. A systematic evaluation of influence of image selection process on remote sensing-based burn severity indices in North American boreal forest and tundra ecosystems. *ISPRS Journal of Photogrammetry and Remote Sensing*, 159, 63–77. https://doi.org/10.1016/j.isprsjprs.2019.11.011.

Chuvieco, E., R. G. Congalton. 1988. Mapping and inventory of forest fires from digital processing of TM data. *Geocarto International*, 3, 41–53.

Chuvieco, E., D. Riano, I. Aguado, D. Cocero. 2002. Estimation of fuel moisture content from multitemporal analysis of Landsat Thematic Mapper reflectance data: Applications in fire danger assessment. *International Journal of Remote Sensing*, 23, 2145–2162.

Costanza, R., R. Groot, P. Sutton, S. Van der Ploeg, S. Anderson, S. Farber, R. Turner. 2014. Changes in the global value of ecosystem services. *Global Environmental Change*, 26, 152–158.

Crist, E. P., R. C. Cicone. 1984. Application of the tasseled cap concept to simulated Thematic Mapper data. *Photogrammetric Engineering and Remote Sensing*, 50, 343–352.

Deering, D. W., J. W. Rouse, R. H. Haas, J. A. Schell. 1975. Measuring forage production of grazing units from Landsat MSS data. In *Tenth International Symposium on Remote Sensing of Environment*, pp. 1169–1178. Ann Arbor, MI: University of Michigan.

DeFries, R. S., M. Hansen, J. R. G. Townshend, R. Solberg. 1998. Global land cover classifications at 8 km spatial resolution: The use of training data derived from Landsat imagery in decision tree classifiers. *International Journal of Remote Sensing*, 19, 3141–3168.

DeFries, R. S., J. R. G. Townshend. 1994. NDVI derived land cover classifications at a global scale. *International Journal of Remote Sensing*, 15, 3567–3586.

DeFries, R. S., J. R. G. Townshend, M. C. Hansen. 1999. Continuous fields of vegetation characteristics at the global scale at 1km resolution. *Journal of Geophysical Research:Atmospheres*, 104, 16911–16923.

Dong, J., X. Xiao, S. Sheldon, C. Biradar, G. Zhang, N. D. Duong, M. Hazarika, K. Wikantika et al. 2014. A 50m forest cover map in southeast Asia from ALOS/PALSAR and its application on forest fragmentation assessment. *PLoS One*, 9, e8580. https://doi.org/10.1371/journal.pone.0085801.

Dungan, J. 1998. Spatial prediction of vegetation quantities using ground and image data. *Remote Sensing*, 19, 267–285.

Dwyer, E., S. Pinnock, J. M. Gregorie, J. M. C. Pereira. 2000. Global spatial and temporal distribution of vegetation fire as determined from satellite observations. *International Journal of Remote Sensing*, 21, 1289–1302.

Eidenshink, J. C., J. L. Faundeen. 1994. The 1 km AVHRR global land data set: First stages in implementation. *International Journal of Remote Sensing*, 104, 3443–3462.

Eidenshink, J. C., B. Schwind, K. Brewer, Z. Zhu, B. Quayle, S. Howard. 2007. A project for monitoring trends in burn severity. *Fire Ecology*, 3, 3–19.

Elvidge, C. D., R. J. P. Lyon. 1985. Influence of rock soil spectral variation on the assessment of green biomass. *Remote Sensing of Environment*, 17, 265–279.

Environmental Systems Research Institute (ESRI). 2023. *Sentinel2 10meter Land Use/Land Cover*. https://livingatlas.arcgis.com/landcover/ [accessed 13 Oct., 2023].

Estes, J., A. Belward, T. Loveland, J. Scepan, A. Strahler, J. Townshend, C. Justice. 1999. The way forward. *Photogrammetric Engineering and Remote Sensing*, 65, 1089–1093.

Everitt, J. H., C. Yang, R. Fletcher, C. J. Deloach. 2008. Comparison of QuickBird and SPOT 5 satellite imagery for mapping giant reed. *Journal of Aquatic Plant Management*, 46, 77–82.

Fang, H., W. Ping. 2010. Vegetation change of ecotone in west of northeast China plain using timeseries remote sensing data. *Chinese Geographical Society*, 20, 167–175.

Fava, F., R. Colombo, S. Bocchi, C. Zucca. 2012. Assessment of Mediterranean pasture condition using MODIS Normalized Difference Vegetation Index time series. *Journal of Applied Remote Sensing*, 6, 063530106353012.

Fensholt, R. I., S. R. Proud. 2012. Evaluation of Earth observation based global long term vegetation trends—comparing GIMMS and MODIS global NDVI time series. *Remote Sensing of Environment*, 119, 131–147.

Fensholt, R. I., K. Rasmussen. 2011. Analysis of trends in the Sahelian ‘rain use efficiency’ using GIMMS NDVI, RFE and GPCP rain fall data. *Remote Sensing of Environment*, 115, 438–451.

Fensholt, R. I., K. Rasmussen, T. T. Nielsen, C. Mbow. 2009. Evaluation of earth observation based long term vegetation trends inter-comparing NDVI time series trend analysis consistency of Sahel from AVHRR GIMMS, Terra MODIS and SPOT VGT data. *Remote Sensing of Environment*, 113, 1886–1898.

Fensholt, R. I., M. S. Sandholt, S. Rasmussen, S. Stisen, A. Diou. 2006. Evaluation of satellite based primary production modeling in the semiarid Sahel. *Remote Sensing of Environment*, 105, 173–188.

Flasse, S., P. Ceccato. 1996. A contextual algorithm for AVHRR fire detection. *International Journal of Remote Sensing*, 17, 419–424.

Foley, J., R. DeFries, G. P. Asner. 2005. Global consequences of land use. *Science*, 309, 570–574.

Food and Agriculture Organization (FAO), Intergovernmental Authority on Development (IGAD). 2019. *East Africa Animal Feed Action Plan*, p. 50. Rome: Food and Agriculture Organization of the United Nations (FAO) and Intergovernmental Authority on Development (IGAD). www.fao.org/3/ca5965en/ca5965en.pdf [accessed 31 Oct., 2023].

Foody, G. M. 2003. Geographical weighting as a further refinement to regression modelling: An example focused on the NDVI—rainfall relationship. *Remote Sensing of Environment*, 88, 283–293.

Fox, W. E., D. W. McCollum, J. E. Mitchell, L. E. Swanson, U. P. Kreuter, J. A. Tanaka, G. R. Evans, H. T. Heintz. 2009. An Integrated Social, Economic, and Ecologic Conceptual (ISEEC) framework for considering rangeland sustainability. *Society and Natural Resources*, 22, 593–606.

Frank, T. D. 1984. Assessing change in the surficial character of a semiarid environment with Landsat residual images. *Photogrammetric Engineering and Remote Sensing*, 50, 471–480.

French, N. H. F., J. L. Allen, R. J. Hall, E. E. Hoy, E. S. Kasischke, K. A. Murphy, D. L. Verbyla. 2008. Using Landsat data to assess fire and burn severity in the North American boreal forest region: An overview. *International Journal of Wildland Fire*, 17, 443–462.

Frey, K. E., L. C. Smith. 2007. How well do we know northern land cover? Comparison of four global vegetation and wet land products with a new ground truth database for West Siberia. *Global Biogeochemical Cycles*, 21, 1–15.

Friedl, M. A., D. K. McIver, J. C. F. Hodges, X. Y. Zhang, D. Muchoney, A. H. Strahler, C. E. Woodcock, S. Gopal et al. 2002. Global land cover mapping from MODIS: Algorithms and early results. *Remote Sensing of Environment*, 83, 287–302.

Friedl, M. A., D. Sulla-Menashe, B. Tan, A. Schneider, N. Ramankutty, A. Sibley, X. M. Huang. 2010. MODIS Collection 5 global land cover: Algorithm refinements and characterization of new datasets. *Remote Sensing of Environment*, 114, 168–182.

Fritz, S., C. C. Fonte, L. See. 2017. The role of citizen science in earth observation. *Remote Sensing*, 9, 357. https://doi.org/10.3390/rs9040357.

Fritz, S., I. McCallum, C. Schill, C. Perger, L. See, D. Schepaschenko, M. van der Velde, F. Kraxner, M. Obersteiner. 2011a. GeoWiki: An online platform for improving global land cover. *Environmental Modelling andSoftware*, 31, 110123.

Fritz, S., L. See. 2007. Identifying and quantifying uncertainty and spatial disagreement in the comparison of Global Land Cover for different applications. *Global Change Biology*, 14, 1057–1075.

Fritz, S., L. See, F. Grey. 2022. The grand challenges facing environmental citizen science. *Frontiers of Environmental and Science*, 10. https://doi.org/10.3389/fenvs.2022.1019628.

Fritz, S., L. See, I. McCallum, C. Schill, M. Obersteiner, M. van der Velde, H. Boettcher, P. Havlík et al. 2011b. Highlighting continued uncertainty in global land cover maps for the user community. *Environmental Research Letters*, 6, 1–7.

Fry, J., G. Xian, S. Jin, J. Dewitz, C. Homer, L. Yang, C. Barnes, N. Herold et al. 2011. Completion of the 2006 national land cover database for the conterminous United States. *Photogrammetric Engineering and Remote Sensing*, 77, 858–864.

Gaffney, R., D. J. Augustine, S. P. Kearney, L. M. Porensky. 2021. Using hyperspectral imagery to characterize rangeland vegetation composition at process-relevant scales. *Remote Sensing*, 13, 4603. https://doi.org/10.3390/rs13224603.

Gallo, K., L. Li, B. Reed, J. Eidenshink, J. Dwyer. 2005. Multiplatform comparisons of MODIS and AVHRR Normalized Difference Vegetation Index data. *Remote Sensing of Environment*, 99, 221–231.

Ganguly, S., A. Samanta, M. A. Schull, N. V. Shabanov, C. Milesi, R. R. Nemani, Y. Knyazikhin, R. B. Myneni. 2008. Generating vegetation leaf area index Earth system data record from multiple sensors. Part 2: Implementation, analysis and validation. *Remote Sensing of Environment*, 112, 4318–4332.

Geerken, R., N. Batikha, D. Celisj, E. Depauw. 2005. Differentiation of rangeland vegetation and assessment of its status: Field investigations and MODIS and SPOT VEGETATION data analyses. *International Journal of Remote Sensing*, 26, 4499–4526.

Giglio, L., L. Boschetti, D. P. Roy, M. L. Humber, C. O. Humber. 2018. The Collection 6 MODIS burned area mapping algorithm and product. *Remote Sensing of Environment*, 217, 72–85.

Giglio, L., J. Descloitres, C. O. Justice, Y. J. Kaufman. 2003. An enhanced contextual fire detection algorithm for MODIS. *Remote Sensing of Environment*, 87, 272–282.

Giglio, L., T. Loboda, D. P. Roy, B. Quayle, C. O. Justice. 2009. An active fire based burned area mapping algorithm for the MODIS sensor. *Remote Sensing of Environment*, 113, 408–420.

Gilbert, N. 2011. Science enters desert debate. *Nature*, 447, 262.

Giri, G., Z. L. Zhu, B. Reed. 2005. A comparative analysis of the global land cover 2000 and MODIS land cover data sets. *Remote Sensing of Environment*, 94, 123–132.

Gong, P., J. Wang, L. Yu, Y. Zhao, Y. Zhao, L. Liang, Z. Niu, X. Huang et al. 2013. Finer resolution observation and monitoring of global land cover: First mapping results with Landsat TM and ETM+ data. *International Journal of Remote Sensing*, 34, 2607–2654.

Graetz, R. D. 1987. Satellite remote sensing of Australian range lands. *Remote Sensing of Environment*, 23, 313–331.

Graetz, R. D., D. M. Carneggie, R. Hacker, C. Lendon, D. G. Wilcox. 1976. A qualitative evaluation of Landsat imagery of Australia rangelands. *Australian Rangeland Journal*, 1, 53–59.

Graetz, R. D., M. R. Gentle, R. P. Pech, J. F. O'Callaghan, G. Drewien. 1983. The application of Landsat image data to rangeland assessment and monitoring: An example from South Australia. *Australian Rangeland Journal*, 5, 63–73.

Graetz, R. D., R. P. Pech, A. W. Davis. 1988. The assessment and monitoring of sparsely vegetated rangelands using calibrated Landsat data. *International Journal of Remote Sensing*, 9, 1201–1222.

Graetz, R. D., R. P. Pech, M. R. Gentle, J. F. Ocallaghan. 1986. The application of Landsat image data to rangeland assessment and monitoring—the development and demonstration of a Land Image-Based Resource Information System (LIBRIS). *Journal of Arid Environments*, 10, 53–80.

Gray, T. I., D. G. McCrary. 1981. The environmental vegetation index, a tool potentially useful for arid land management. *AgRISTAR Report No. EWN104076*, p. 7. Houston, TX: Johnson Space Center, 17132.

Hacker, R. 1980. Prospects for satellite applications in Australian rangelands. *Tropical Grasslands*, 14, 289.

Hansen, M. C., R. S. DeFries, J. R. G. Townshend, M. Carroll, C. Dimiceli, R. A. Dimiceli. 2003. Global percent tree cover at a spatial resolution of 500 meters: First results of the MODIS vegetation continuous fields algorithm. *Earth Interactions*, 7, 1–15.

Hansen, M. C., R. S. DeFries, J. R. G. Townshend, R. Sohlberg. 2000. Global land cover classification at the 1 km spatial resolution using a classification tree approach. *International Journal of Remote Sensing*, 21, 1331–1364.

Hansen, M. C., T. R. Loveland. 2011. A review of large area monitoring of land cover change using Landsat data. *Remote Sensing of Environment*, 122, 66–74.

Hansen, M. C., P. V. Potapov, R. Moore, M. Hancher, S. A. Turubanova, A. Tyukavina, D. Thau, S. V. Stehman et al. 2013. High resolution global maps of 21stcentury forest cover change. *Science*, 342, 850–853.

Hansen, M. C., P. V. Potapov, A. H. Pickens, A. Tyukavina, A. Hernandez-Serna, V. Zalles, S. Turubanova, I. Kommareddy, S. Stehman, X. P. Song. 2022. Global land use extent and dispersion within natural land cover using Landsat data. *Environmental Research Letters*, 17, 034050. https://doi.org/10.1088/1748-9326/ac46ec.

Hansen, M. C., B. Reed. 2000. A comparison of the IGBP DISCover and University of Maryland 1 km global land cover products. *International Journal of Remote Sensing*, 21, 1365–1373.

Hillman, S., L. Wallace, A. Lucieer, K. Reinke, D. Turner, S. Jones. 2021. A comparison of terrestrial and UAS sensors for measuring fuel hazard in a dry sclerophyll forest. *International Journal of Applied Earth Observation and Geoinformation*, 95, 102261. https://doi.org/10.1016/j.jag.2020.102261.

Holmgren, M., M. Scheffer. 2001. El Niño as a Window of Opportunity for the Restoration of Degraded arid ecosystems. *Ecosystems*, 4, 151–159.

Holmgren, M., P. Stapp, C. R. Dickman, C. Gracia, S. Graham, J. R. Gutiérrez, C. Hice, F. Jaksic, D. A. Kelt, M. Letnic, M. Lima, B. C. López, P. L. Meserve, W. B. Milstead, G. A. Polis, M. A. Previtali, M. Richter, S. Sabaté, F. A. Squeo. 2006. Extreme climatic events shape arid and semiarid ecosystems. *Frontiers in Ecology and the Environment*, 4, 87–95.

Homer, C. G., R. D. Ramsey, T. C. Edwards, A. Falconer. 1997. Landscape covertype modeling using a multi scene thematic mapper mosaic. *Photogrammetric Engineering and Remote Sensing*, 63, 59–67.

Hosseini, M., S. Lim. 2023. Burned area detection using Sentinel-1 SAR data: A case study of Kangaroo Island, South Australia. *Applied Geography*, 151, 102854.

Huete, A. R. 1988. A Soil Adjusted Vegetation Index (SAVI). *Remote Sensing of Environment*, 25, 295–309.

Huete, A. R., K. Didan, T. Miura, E. P. Rodriguez, X. Gao, L. G. Ferreira. 2002. Overview of the radiometric and biophysical performance of the MODIS vegetation indices. *Remote Sensing of Environment*, 83, 195–213.

Hunt, E. R., B. A. Miyake. 2006. Comparison of stocking rates from remote sensing and geospatial data. *Rangeland Ecology andManagement*, 59, 11–18.

Hunt, E. R., B. N. Rock. 1989. Detection of changes in leaf water content using near and middle infrared reflectances. *Remote Sensing of Environment*, 30, 43–54.

Ilangakoon, G. Y. M. N. T. 2020. Complexity and dynamics of semi-arid vegetation structure, function and diversity across spatial scales from full waveform lidar. PhD Dissertation. Boise, ID: Boise State University.

Ito, A. 2011. A historical meta-analysis of global terrestrial net primary productivity: Are estimates converging? *Global Change Biology*, 17, 3161–3175.

Jabbar, M. T., J. Zhou. 2013. Environmental degradation assessment in arid areas: A case study from Basra Province, southern Iraq. *Environmental Earth Sciences*, 70, 2203–2214.

Jarlan, L., S. Mangiarotti, E. Mougin, P. Mazzega, P. Hiernaux, V. L. Dantec. 2008. Assimilation of SPOT/VEGETATION NDVI data into a Sahelian vegetation dynamics model. *Remote Sensing of Environment*, 112, 1381–1394.

Jenkins, G., K. Mohr, V. Morris, O. Arino. 1997. The role of convective processes over the Zaire Congo basin to the southern hemispheric ozone maximum. *Journal of Geophysical Research*, 102, 18963–18980.

Ji, L., K. Gallo. 2006. An agreement coefficient for image comparison. *Photogramm Engineering and Remote Sensing*, 72, 823–833.

Jinguo, Y., N. Zheng, C. Wang. 2006. Vegetation NPP distribution based on MODIS data and CASA model—a case study of northern Hebei Province. *Chinese Geographical Science*, 16, 334–341.

Jung, M., K. Henkel, M. Herold, G. Churkina. 2006. Exploiting synergies of global land cover products for carbon cycle modeling. *Remote Sensing of Environment*, 101, 534–553.

Kachergis, E., S. W. Miller, S. E. McCord, M. Dickard, S. Savage, L. V. Reynolds, N. Lepak, C. Dietrich, A. Green, A. Nafus, K. Prentice, Z. Davidson. 2022. Adaptive monitoring for multiscale land management: Lessons learned from the Assessment, Inventory, and Monitoring (AIM) principles. *Rangelands*, 44, 50–63. https://doi.org/10.1016/j.rala.2021.08.006000609802.

Kang, Y., M. Gaber, M. Bassiouni, X. Lu, T. Keenan. 2023. CEDAR-GPP: Spatiotemporally upscaled estimates of gross primary productivity incorporating CO 2 fertilization. *Earth System Science Data Discussions*, 2023, 1–51.

Kaufman, Y. J., C. O. Justice, L. P. Flynn, J. D. Kendall, E. M. Prins, L. Giglio, D. E. Ward, W. P. Menzel et al. 1996a. Potential global fire monitoring from EOSMODIS. *Journal of Geophysical Research: Atmospheres*, 103, 32215–32238.

Kaufman, Y. J., C. O. Justice, L. P. Flynn, J. D. Kendall, E. M. Prins, L. Giglio, D. E. Ward, W. P. Menzel, A. W. Setzer. 1998. Potential global fire monitoring from EOS-MODIS. *Journal of Geophysical Research*, 103(D24), 32215–32238. https://doi.org/10.1029/98JD01644.

Kaufman, Y. J., L. A. Remer, R. D. Ottmar, D. E. Ward, R. R. Li, R. Kleidman, R. S. Fraser, L. Flynn et al. 1996b. Relationship between remotely sensed fire intensity and rate of emission of smoke: SCARC experiment. In *Global Biomass Burning*, ed. J. Levin, pp. 685–696. Cambridge, MA: The MIT Press.

Kauth, R. J., G. S. Thomas. 1976. The tasseled cap—a graphic description of the spectral temporal development of agricultural crops as seen by Landsat. In *LARS Symposia*, Paper 159, pp. 4B41–4B51. West Lafayette, IN: Purdue ePubs, Purdue University.

Kawamura, K., T. Akiyama, H. Yokota, M. Tsutsumi. 2005. Monitoring of forage conditions with MODIS imagery in the Xilingol steppe, Inner Mongolia. *International Journal of Remote Sensing*, 26, 1423–1436.

Key, C. H., N. C. Benson. 1999. Measuring and remote sensing of burn severity. In *Proceedings of the Joint Fire Science Conference*, eds. L. F. Neuenschwander, K. C. Ryan, G. E. Goldberg, Vol. II, p. 284. Boise, ID: University of Idaho and the International Association of Wildland Fire.

Key, C. H., N. C. Benson. 2006. Landscape assessment: Ground measure of severity, the Composite Burn Index, and remote sensing of severity, the Normalized Burn Index. In *FIREMON: Fire Effects Monitoring and Inventory System,For. Serv. Gen. Tech. Rep. RMRSGTR164*, eds. D. C. Lutes et al., pp. CD: LA1–LA51. Ogden, UT: USDA For. Serv. Rocky Mt. Res. Stn.

Klemm, T., D. D. Briske, M. C. Reeves. 2020. Vulnerability of rangeland beef cattle production to climate-induced NPP fluctuations in the US Great Plains. *Global Change Biology*, 26, 4841–4853.

Knopp, L., M. Wieland, M. Rättich, S. Martinis. 2020. A deep learning approach for burned area segmentation with Sentinel-2 data. *Remote Sensing*, 12(15), 2422.

Koch, A., A. McBratney, M. Adams, D. Field, R. Hill, J. Crawford, B. Minasny, R. Lal et al. 2013. Soil security: Solving the global soil crisis. *Global Policy*, 4, 434–444.

Kohl, H. A., P. V. Nelson, J. Pring, K. L. Weaver, D. M. Wiley, A. B. Danielson, R. M. Cooper, H. Mortimer, D. Overoye, A. Burdick, S. Taylor, M. Haley, S. Haley, J. Lange, M. E. Lindblad. 2021. GLOBE observer and the GO on a trail data challenge: A citizen science approach to generating a global land cover land use reference dataset. *Frontiers in Climate*, 3. https://doi.org/10.3389/fclim.2021.620497.

Ku, N.-W., S. C. Popescu. 2019. A comparison of multiple methods for mapping local-scale mesquite tree aboveground biomass with remotely sensed data. *Biomass and Bioenergy*, 122, 270–279. https://doi.org/10.1016/j.biombioe.2019.01.045.

Lambin, E. F., B. L. Turner, J. Helmut. 2001. The causes of land use and landcover change: Moving beyond the myths. *Global EnvironmentalChange*, 11, 261–269.

Latifi, H., R. Valbuena, C. A. Silva. 2023. Towards complex applications of active remote sensing for ecology and conservation. *Methods in Ecology and Evolution*, 14(7), 1578–1586.

Lawley, V., M. Lewis, K. Clarke, B. Ostendorf. 2016. Site-based and remote sensing methods for monitoring indicators of vegetation condition: An Australian review. *Ecological Indicators*, 60, 1273–1283. https://doi.org/10.1016/j.ecolind.2015.03.021.

Le, Q. B., L. Tamene, P. L. G. Vlek. 2012. Multipronged assessment of land degradation in West Africa to assess the importance of atmospheric fertilization in masking the processes involved. *Global PlanetaryChange*, 92, 71–81.

Le Houérou, H. N. 1984. Rain use efficiency: A unifying concept in arid land ecology. *Journal of Arid Environments*, 7, 213–247.

Le Houérou, H. N., R. L. Bingham, W. Skerbek. 1988. Relationship between the variability of primary production and the variability of annual precipitation in world arid lands. *Journal of Arid Environments*, 15, 1–18.

Lepers, E., E. F. Lambin, A. C. Janetos, R. DeFries, F. Achard, N. Ramankutty, R. J. Scholes. 2005. A synthesis of information on rapid landcover change for the period 1981–2000. *BioScience*, 55, 115–124.

Levitus, S., J. I. Antonov, T. P. Boyer, C. Stephens. 2000. Warming of the world ocean. *Science*, 287, 2225–2229.

Li, S., C. Potter, C. Hiatt. 2012. Monitoring of net primary production in California rangelands using Landsat and MODIS satellite remote sensing. *Natural Resources*, 3(2), 10.

Li, X., K. J. Wessels, S. Armston, P. Hancock, R. Mathieu, R. Main, R. Scholes. 2023. First validation of GEDI canopy heights in African savannas. *Remote Sensing of Environment*, 285, 113402.

Liu, A., X. Cheng, Z. Chen. 2021. Performance evaluation of GEDI and ICESat-2 laser altimeter data for terrain and canopy height retrievals. *Remote Sensing of Environment*, 264, 112571.

Loboda, T. V., N. H. F. French, C. Hight-Harf, L. Jenkins, M. E. Miller. 2013. Mapping fire extent and burn severity in Alaskan tussock tundra: An analysis of the spectral response of tundra vegetation to wildland fire. *Remote Sensing of Environment*, 134, 194–209.

Loboda, T. V., L. Giglio, L. Boschetti, C. O. Justice. 2012. Regional fire monitoring and characterization using global NASA MODIS fire products in dry lands of Central Asia. *Frontiers in Earth Science*, 6, 196–205.

Lopez-Garcia, M. J., V. Caselles. 1991. Mapping burns and natural reforestation using Thematic Mapper data. *Geocarto International*, 6, 31–37.

Loveland, T. R., B. C. Reed, J. F. Brown, D. O. Ohlen, L. Yang, J. W. Merchant. 2000. Development of a global land cover characteristics database and IGBP DISCover from 1 km AVHRR data. *International Journal of Remote Sensing*, 29, 3–10.

Lu, B., Y. He, H. Liu. 2016. Investigating species composition in a temperate grassland using unmanned aerial vehicle-acquired imagery. In *20164th International Workshop on Earth Observation and Remote Sensing Applications (EORSA). Presented at the 2016 4th International Workshop on Earth Observation and Remote Sensing Applications (EORSA)*, pp. 107–111. Guangzhou, China: IEEE. https://doi.org/10.1109/EORSA.2016.7552776.

Ludwig, J. 1987. Primary productivity in arid lands: Myths and realities. *Journal of Arid Environments*, 13, 1–7.

Lund, G. H. 2007. Accounting for the worlds rangelands. *Rangelands*, 29, 3–10.

Marini, A., M. Talbi. 2009. *Desertification and Risk Analysis Using High and Medium Resolution Satellite Data*, p. 271. Dordrecht, the Netherlands: Springer.

Matere, J., P. Simpkin, J. Angerer, E. Olesambu, S. Ramasamy, F. Fasina. 2019. Predictive Livestock Early Warning System (PLEWS): Monitoring forage condition and implications for animal production in Kenya. *Weather and Climate Extremes*, 27, 1–8.

Matthews, E. 1983. Global vegetation and land use: New high resolution data bases for climate studies. *Journal of Climatology and Applied Meteorology*, 22, 474–487.

Mayaux, P., H. Eva, J. Gallego, A. H. Strahler, M. Herold, S. Agrawal, S. Naumov, E. E. D. Miranda et al. 2006. Validation of the global land cover 2000 map. *IEEE Transactions on Geoscience and Remote Sensing*, 44, 1728–1738.

McCullum, I., M. Obersteiner, S. Nilsson, A. Shvidenko. 2006. A spatial comparison of four satellite derived 1 km global land cover datasets. *International Journal of Applied Earth Observation and Geoinformation*, 8, 246–255.

McGraw, J. F., P. T. Tueller. 1983. Landsat computer aided analysis techniques for range vegetation mapping. *Journal of Range Management*, 36, 627–631.

Metternicht, G. 1996. *Detecting and Monitoring Land Degradation Features and Processes in the Cochabamba Valleys, Bolivia*. Enschede, the Netherlands: International Institute for GeoInformation Science and Earth Observation, ITC Publication No.36.

Metternicht, G., J. Zinck. 2003. Remote sensing of soil salinity: Potentials and constraints. *Remote Sensing of Environment*, 85, 1–20.

Metternicht, G., J. Zinck. 2009. *Remote Sensing of Soil Salinization—Impact on Land Management*. London, U.K.: CRC Press.

Millennium Ecosystem Assessment. 2005. *Ecosystems and Human Well-Being: Desertification Synthesis*. Washington, DC: Island Press.

Miller, J. D., A. E. Thode. 2007. Quantifying burn severity in a heterogeneous landscape with a relative version of the delta Normalized Burn Ratio (dNBR). *Remote Sensing of Environment*, 109, 66–80.

Miura, T., A. Huete, H. Yoshioka. 2006. An empirical investigation of cross sensor relationships of NDVI and red/near infrared reflectance using EO1 Hyperion data. *Remote Sensing of Environment*, 100, 223–236.

Myneni, R. B., S. Hoffman, Y. Knyazikhin, J. K. Privette, J. Glassy, Y. Tian, Y. Wang, X. Song, Y. Zhang, G. R. Smith, A. Lotsch, M. Friedl, J. T. Morisette, P. Votava, R. R. Nemani, S. W. Running. 2002. Global products of vegetation leaf area and fraction absorbed PAR from year one of MODIS data. *Remote Sensing of Environment*, 83, 214–231.

Myneni, R. B., R. R. Nemani, S. Running. 1997. Estimation of global leaf area index and absorbed PAR using radiative transfer models. *IEEE Transactions on Geoscience and Remote Sensing*, 35, 1380–1393.

Nachtergaele, F., M. Petri, R. Biancalani, G. Van Lynden, H. Van Velthuizen. 2010. Global Land Degradation Information System (GLADIS). Beta Version. An information database for land degradation assessment at global level. *Land Degradation Assessment in Drylands Technical Report*, 17, 1563.

National Wildfire Coordinating Group (NWCG). 2012. *Glossary of Wildland Fire Terminology*. www.nwcg.gov/pms/pubs/glossary/ [accessed 13 Oct., 2023].

Nkonya, E., J. von Braun, A. Mirzabaev, Q. B. Le, H. Y. Kwon, O. Kurui. 2013. Economics of land degradation initiative: Methods and approach for global and national assessments. *ZEF Discussion Papers on Development Policy No. 183*, pp. 40. Bonn, Germany.

Oldeland, J., W. Dorigo, D. Wesuls, N. Jürgens. 2010. Mapping bush encroaching species by seasonal differences in hyper spectral imagery. *Remote Sensing*, 2, 1416–1438.
Oldeland, J., R. Revermann, J. Luther-Mosebach, T. Buttschardt, J. R. K. Lehmann. 2021. New tools for old problems—comparing drone- and field-based assessments of a problematic plant species. *Environmental Monitoring and Assessment*, 193. https://doi.org/10.1007/s10661-021-08852-2.
Oldeman, L. R. 1998. Soil degradation: A threat to food security? *Report 98/01*. Wageningen: International Soil Reference and Information Centre.
Olson, J. S. 1983. *Carbon in Live Vegetation of Major World Ecosystems*, ORNL5862. Environmental Sciences Division Publication No. 1997. Oak Ridge, TN: Oak Ridge National Laboratory.
OpenScientist. 2011. *Finalizing a Definition of "Citizen Science" and "Citizen Scientists."* www.openscientist.org/2011/09/finalizingdefinitionofcitizen.html [accessed 13 Oct., 2023].
Opio, P., H. P. Makkar, M. Tibbo, S. Ahmed, A. Sebsibe, A. M. Osman, E. Olesambu, C. Ferrand, S. Munyua. 2020. Regional animal feed action plan for East Africa: Why, what, for whom, how used and benefits. *CABI Reviews*, 15(44), 1–16.
Paltridge, G. W., I. Barber. 1988. Monitoring grassland dry ness and fire potential in Australia with NOAA/AVHRR data. *Remote Sensing of Environment*, 25, 381–394.
Parker, A. E., E. R. Hunt. 2004. Accuracy assessment for detection of leafy spurge with hyperspectral imagery. *Journal of Range Management*, 57, 106–112.
Paruelo, J. M., H. E. Epstein, W. K. Lauenroth, I. C. Burke. 1997. ANPP estimates from NDVI for the central grassland region of the United States. *Ecology*, 78, 953–958.
Pech, R. P., R. D. Graetz, A. W. Davis. 1986. Reflectance modeling and the derivation of vegetation indexes for an Australian semiarid shrubland. *International Journal of Remote Sensing*, 7, 389–403.
Pickup, G. 1996. Estimating the effects of land degradation and rainfall variation on productivity in rangelands, an approach using remote sensing and models of grazing and herbage dynamics. *Journal of Applied Ecology*, 33, 819–832.
Pickup, G., V. H. Chewings. 1988. Forecasting patterns of soil erosion in arid lands from Landsat MSS data. *International Journal of Remote Sensing*, 9, 69–84.
Pickup, G., B. D. Foran. 1987. The use of spectral and spatial variability to monitor cover change on inert landscapes. *Remote Sensing of Environment*, 23, 351–363.
Pickup, G., D. J. Nelson. 1984. Use of Landsat radiance parameters to distinguish soil erosion, stability, and deposition in arid central Australia. *Remote Sensing of Environment*, 16, 195–209.
Plummer, S., O. Arino, M. Simon, W. Steffen. 2006. Establishing an earth observation product service for the terrestrial carbon community: The GLOBCARBON initiative. *Mitigation and Adaptation Strategies for Globalchange*, 11, 97–111.
Pohl, C., J. L. Van Genderen. 1998. Multi-sensor image fusion in remote sensing: Concepts, methods and applications. *International Journal of Remote Sensing*, 19, 823–854. https://doi.org/10.1080/014311698215748.
Potapov, P., M. C. Hansen, A. Pickens, A. Hernandez-Serna, A. Tyukavina, S. Turubanova, V. Zalles, X. Li, A. Khan, F. Stolle, N. Harris, X.-P. Song, A. Baggett, I. Kommareddy, A. Kommareddy. 2022. The global 2000–2020 land cover and land use change dataset derived from the Landsat archive: First results. *Frontiers in Remote Sensing*, 3. https://doi.org/10.3389/frsen.2022.856903.
Potapov, P., M. C. Hansen, A. Pickens, A. Hernandez-Serna, A. Tyukavina, S. Turubanova, V. Zalles, X. Li, A. Khan, F. Stolle, N. Harris, X.-P. Song, A. Baggett, I. Kommareddy, A. Kommareddy, A. Retallack, G. Finlayson, B. Ostendorf, K. Clarke, M. Lewis. 2023. Remote sensing for monitoring rangeland condition: Current status and development of methods. *Environmental and Sustainability Indicators*, 19, 100285. https://doi.org/10.1016/j.indic.2023.100285.
Prince, S. D. 2002. Spatial and temporal scale for detection of desertification. In *Do Humans Create Deserts*, eds. J. F. Reynolds, M. Stafford-Smith, pp. 23–40. Berlin, Germany: Dahlem University Press.
Prince, S. D., I. Becker-Reshef, K. Rishmawi. 2009. Detection and mapping of longterm land degradation using local net production scaling: Application to Zimbabwe. *Remote Sensing of Environment*, 113, 1046–1057.
Prince, S. D., C. J. Tucker. 1986. Satellite remote sensing of rangelands in Botswana 2 NOAA AVHRR and herbaceous vegetation. *International Journal of Remote Sensing*, 7, 15551570.
Prince, S. D., K. J. Wessels, C. J. Tucker, S. E. Nicholson. 2007. Desertification in the Sahel: A reinterpretation of a reinterpretation. *Global Change Biology*, 13, 1308–1313.
Pu, R., P. Gong, Z. Li, J. Scarborough. 2004. A dynamic algorithm for wildfire mapping with NOAA/AVHRR data. *International Journal of Wildland Fire*, 13, 275–285.

Reeves, M. C., L. S. Bagget. 2014. A remote sensing protocol for identifying rangelands with degraded productive capacity. *Ecological Indicators*, 43, 172–182.

Reeves, M. C., B. B. Hanberry, H. Wilmer, N. E. Kaplan, W. K. Lauenroth. 2021. An assessment of production trends on the Great Plains from 1984 to 2017. *Rangeland Ecology andManagement*, 78, 165–179.

Reeves, M. C., J. E. Mitchell. 2011. Extent of coterminous US rangelands: Quantifying implications of differing agency perspectives. *Rangeland Ecology and Management*, 64, 1–12.

Reeves, M. C., J. C. Winslow, S. W. Running. 2001. Mapping weekly rangeland vegetation productivity using MODIS algorithms. *Journal of Range Management*, 54, 90–105.

Reeves, M. C., M. Zhao, S. W. Running. 2006. Applying improved estimates of MODIS productivity to characterize grassland vegetation dynamics. *Journal of Rangeland Ecology and Management*, 59, 1–10.

Retallack, A., G. Finlayson, B. Ostendorf, K. Clarke, M. Lewis. 2023. Remote sensing for monitoring rangeland condition: Current status and development of methods. *Environmental and Sustainability Indicators*, 19, 100285. https://doi.org/10.1016/j.indic.2023.100285.

Rigge, M. B., C. Homer, L. Cleeves, D. K. Meyer, B. Bunde, H. Shi, G. Xian, S. Schell, M. Bobo. 2020. Quantifying western U.S. rangelands as fractional components with multi-resolution remote sensing and in situ data. *Remote Sensing*, 12, 412.

Robinove, C., J. P. S. Chavez, D. Gehring, R. Holmgren. 1981. Arid land monitoring using Landsat albedo difference images. *Remote Sensing of Environment*, 11, 133–156.

Roche, L. M. 2016. Adaptive rangeland decision-making and coping with drought. *Sustainability*, 8, 1334.

Roger, J. C., E. F. Vermote, S. Devadiga et al. 2017. *Suomi-NPP VIIRS Surface Reflectance User's Guide*. V1 Re-processing (NASA Land SIPS).

Rollins, M. G. 2009. LANDFIRE: A nationally consistent vegetation, wildland fire, and fuel assessment. *International Journal of Wildland Fire*, 18(3), 235–249.

Rouse, J. W., R. H. Haas, J. A. Schell, D. W. Deering. 1973. Monitoring vegetation systems in the Great Plains with ERTS. In *Proceedings of the Third ERTS Symposium*, pp. 309–317. Washington, DC.

Rouse, J. W. Jr., R. H. Hass, J. A. Schell, D. W. Deering, J. C. Harlan. 1974. *Monitoring the Vernal Advancement and Retrogradation(Greenwave Effect) I of Natural Vegetation*, p. 390. College Station, TX: Remote Sensing Center, Texas A&M University.

Roy, D. P., L. Boschetti, C. O. Justice, J. Ju. 2008. The collection 5 MODIS burned area product—global evaluation by comparison with the MODIS active fire product. *Remote Sensing of Environment*, 112, 3960–3707.

Running, S. W., D. D. Baldocchi, D. P. Turner, S. T. Gower, P. S. Bakwin, K. A. Hibbard. 1999. A global terrestrial monitoring network integrating tower fluxes, flask sampling, ecosystem modeling and EOS satellite data. *Remote Sensing of Environment*, 70, 108–127.

Running, S. W., R. R. Nemani, F. A. Heinsch, M. Zhao, M. Reeves, H. Hashimoto. 2004. A continuous satellite derived measure of global terrestrial primary production. *Bioscience*, 54, 547–560.

Safriel, U. 2009. Deserts and desertification: Challenges but also opportunities. *Land Degradation and Development*, 20, 353–366.

Sant, E. D., G. E. Simonds, R. D. Ramsey, R. T. Larsen. 2014. Assessment of sagebrush cover using remote sensing at multiple spatial and temporal scales. *Ecological Indicators*, 43, 297–305.

Scepan, J. 1999. Thematic validation of high resolution global landcover data sets. *Photogrammetric Engineering and Remote Sensing*, 65, 1051–1060.

Scheftic, W., X. Zeng, P. Broxton, M. Brunke. 2014. Intercomparison of seven NDVI products over the United States and Mexico. *Remote Sensing*, 6, 1057–1084.

Schueler, C., J. E. Clement, L. Darnton, F. DeLuccia, T. Scalione, H. Swenson. 2003. VIIRS sensor performance. In *International Geoscience and Remote Sensing Symposium Proceedings*, Vol. I, p. 369–372. Toulouse, France.

Scott, J. M., F. Davis, B. Csuti, R. Noss, B. Butterfield, C. Groves, H. Anderson, S. Caicco et al. 1993. Gap analysis—a geo graphic approach to protection of biological diversity. *Wildlife Monographs*, 123, 1–41.

Sexton, J. O., X. P. Song, M. Feng, P. Noojipady, A. Anand, C. Huang, D. Kim, K. M. Collins et al. 2013. Global, 30m resolution continuous fields of tree cover: Landsat-based rescaling of MODIS vegetation continuous fields with lidar based estimates of error. *International Journal of Digital Earth*, 6(5), 427–448.

Shen, L., Z. Li, X. Guo. 2014. Remote sensing of Leaf Area Index (LAI) and a spatiotemporally parameterized model for mixed grasslands. *International Journal of Applied Science and Technology*, 4, 46–61.

Shoshanya, M., N. Goldshleger, A. Chudnovsky. 2013. Monitoring of agricultural soil degradation by remote sensing methods: A review. *International Journal of Remote Sensing*, 34, 6152–6181.

Silva, J. M. N., A. C. L. Sá, J. M. C. Pereira. 2005. Comparison of burned area estimates derived from SPOT-VEGETATION and Landsat ETM+ data in Africa: Influence of spatial pattern and vegetation type. *Remote Sensing of Environment*, 96, 188–201.

Silverton, J. 2009. A new dawn for citizen science. *Trends in Ecological Evolution*, 24, 467–201.

Singh, J., P. B. Boucher, E. G. Hockridge, A. B. Davies. 2023. Effects of long-term fixed fire regimes on African savanna vegetation biomass, vertical structure and tree stem density. *Journal of Applied Ecology*, 60, 1223–1238. https://doi.org/10.1111/1365-2664.14435.

Skakun, S., C. O. Justice, E. Vermote et al. 2018. Transitioning from MODIS to VIIRS: An analysis of inter-consistency of NDVI data sets for agricultural monitoring. *International Journal of Remote Sensing*, 39, 971–992.

Skidmore, A. K., J. G. Ferwerda. 2008. Resource distribution and dynamics. In *Resource Ecology: Spatial and Temporal Dynamics of Foraging*, eds. H. H. T. Prins, F. van Langevelde. Wageningen, the Netherlands: Springer.

Socientize Project (2013–12–01). 2013. *Green Paper on Citizen Science: Citizen Science for Europe: Towards a Better Society of Empowered Citizens and Enhanced Research*. Socientize Consortium.

Society for Range Management [SRM], Glossary Update Task Group. 1998. *Glossary of Terms Used in Range Management* (4th edn.), p. 32. Denver, CO: Society for Range Management.

Sow, M., C. Mbow, C. Hély, R. Fensholt, B. Sambou. 2013. Estimation of herbaceous fuel moisture content using vegetation indices and land surface temperature from MODIS data. *Remote Sensing*, 5, 2617–2638.

Sparrow, B., J. Foulkes, G. Wardle, E. Leitch, S. Caddy-Retalic, S. van Leeuwen, A. Tokmakoff, N. Thurgate, G. R. Guerin, A. J. Lowe. 2020. A vegetation and soil survey method for surveillance monitoring of rangeland environments. *Frontiers in Ecology and Evolution*, 8, 157.

Steven, M. D., T. J. Malthus, F. Baret, H. Xu, M. J. Chopping. 2003. Intercalibration of vegetation indices from different sensor systems. *Remote Sensing of Environment*, 88, 412–422.

Stuth, J. W., J. Angerer, R. Kaitho, A. Jama, R. Marambii. 2005. Livestock early warning system for Africa rangelands. In *Monitoring and Predicting Agricultural Drought: A Global Study*, eds. V. K. Boken, A. P. Cracknell, R. L. Heathcote, pp. 283–294. New York: Oxford University Press.

Stuth, J. W., J. Angerer, R. Kaitho, K. Zander, A. Jama, C. Heath, J. Bucher, W. Hamilton, R. Conner, D. Inbody. 2003a. The Livestock Early Warning System (LEWS): Blending technology and the human dimension to support grazing decisions. *Arid Lands Newsletter*, University of Arizona. http://cals.arizona.edu/OALS/ALN/aln53/stuth.html [accessed 13 Oct., 2023].

Stuth, J. W., D. Schmitt, R. C. Rowan, J. P. Angerer, K. Zander. 2003b. *PHYGROW Users Guide and Technical Documentation*, Texas A&M University. http://cnrit.tamu.edu/physite/PHYGROW_userguide.pdf [accessed 13 Oct., 2023].

Suits, G., W. Malila, T. Weller. 1988. Procedures for using signals from one sensor as substitutes for signals of another. *Remote Sensing of Environment*, 25, 395–408.

Sulla-Menashe, D., M. A. Friedl. 2018. *User Guide to Collection 6 MODIS Land Cover (MCD12Q1 and MCD12C1) Product*, Vol. I, p. 18. Reston, VA, USA: US Geological Survey (USGS). https://lpdaac.usgs.gov/documents/101/MCD12_User_Guide_V6.pdf [accessed 30 Oct., 2023].

Svoray, T., A. Perevolotsky, P. M. Atkinson. 2013. Ecological sustainability in rangelands: The contribution of remote sensing. *International Journal of Remote Sensing*, 34, 6216–6242.

Tansey, K., J. M. Gregoire, E. Binaghi, L. Boschetti, P. A. Brivio, D. Ershov, S. Flasse, R. Fraser et al. 2004. A global inventory of burned area at 1 km resolution for the year 2000 derived from SPOT Vegetation data. *Climatic Change*, 67, 345–377.

Tchuenté, K., A. Thibaut, J. L. Roujean, S. M. D. Jong. 2011. Comparison and relative quality assessment of the GLC2000, GLOBCOVER, MODIS and ECOCLIMAP land cover data sets at the African continental scale. *International Journal of Applied Earth Observation and Geoinformation*, 13, 207–219.

Telesca, L., R. Lasaponara. 2006. Quantifying intra annual persistent behaviour in SPOT VEGETATION NDVI data for Mediterranean ecosystems of southern Italy. *Remote Sensing of Environment*, 101, 95–103.

Thoma, D. P., D. W. Bailey, D. S. Long, G. A. Nielsen, M. P. Henry, M. C. Breneman, C. Montagne. 2002. Short term monitoring of rangeland forage conditions with AVHRR imagery. *Journal of Range Management*, 55, 383–389.

Todd, S. W., R. M. Hoffer, D. G. Milchunas. 1998. Biomass estimation on grazed and ungrazed rangelands using spectral indices. *International Journal of Remote Sensing*, 19, 427–438.

Tucker, C. J. 1979. Red and photographic infrared linear combinations for monitoring vegetation. *Remote Sensing of Environment*, 8, 127–150.

Tucker, C. J. 1980. Remote sensing of leaf water content in the near infrared. *Remote Sensing of Environment*, 10, 23–32.

Tucker, C. J., J. E. Pinzon, M. E. Born, D. A. Slayback, E. W. Pak, R. Mahoney, E. F. Vermote, N. E. Saleous. 2005. An extended AVHRR 8km NDVI dataset compatible with MODIS and SPOT vegetation NDVI data. *International Journal of Remote Sensing*, 26, 4485–4498.

Tucker, C. J., C. Vanpraet, E. Boerwinkel, A. Gaston. 1983. Satellite remote sensing of total dry matter production in the Senegalese Sahel. *Remote Sensing of the Environment*, 13, 461–474.

Tueller, P. T. 1989. Remote sensing technology for rangeland management applications. *Journal of Range Management*, 42, 442–453.

Tueller, P. T., F. R. Honey, I. J. Tapley. 1978. Landsat and photo graphic remote sensing for arid land applications in Australia. In *International Symposium on Remote Sensing of Environment, Proceedings*, pp. 2177–2191. Ann Arbor, MI.

UNEP. 2012. *Global Environment Outlook: GEO5*, p. 551. Nairobi, Kenya: United Nations Environment Programme.

United Nations Convention to Combat Desertification (UNCCD). 1994. *Article 2 of the Text of the United Nations Convention to Combat Desertification*. https://catalogue.unccd.int/936_UNCCD_Convention_ENG.pdf [accessed 13 Oct., 2023].

Veraverbeke, S., S. Lhermitte, W. W. Verstraeten, R. Goossens. 2011. Time-integrated MODIS burn severity assessment using the multitemporal differenced Normalized Burn Ratio (dNBR(MT)). *International Journal of Applied Earth Observation and Geoinformation*, 13, 52–58.

Verbesselt, J., B. Somers, S. Lhermitte, I. Jonckheere, J. van Aardt, P. Coppin. 2007. Monitoring herbaceous fuel moisture content with SPOT VEGETATION timeseries for fire risk prediction in savanna ecosystems. *Remote Sensing of Environment*, 108, 357–368.

Vermote, E., B. Franch, M. Claverie. 2016. *VIIRS/NPP Surface Reflectance 8-Day L3 Global 500m SIN Grid V001 [Digital Data Set]*. https://lpdaac.usgs.gov/products/vnp09h1v001/#using [accessed 30 Oct., 2023].

Vitousek, P. M. 1992. Global environmental change: An introduction. *Annual Review of Ecology,Evolution,and Systematics*, 23, 1–14.

Vlek, P., Q. B. Le, L. Tamene. 2010. Assessment of land degradation, its possible causes and threat to food security in Sub-Saharan Africa. In *FoodSecurityand Soil Quality*, eds. R. Lal, B. A. Stewart, pp. 57–86. Boca Raton, FL: CRC Press.

Vogl, R. 1979. Some basic principles of grassland fire management. *Environmental Management*, 3, 51–57.

Wallace, C. S. A., J. J. Walker, S. M. Skirvin, C. Patrick-Birdwell, J. F. Weltzin, H. Raichle. 2016. Mapping presence and predicting phenological status of invasive buffelgrass in southern Arizona using MODIS, climate and citizen science observation data. *Remote Sensing*, 8, 524. https://doi.org/10.3390/rs8070524.

Wang, Z., G. Mountrakis. 2023. Accuracy assessment of eleven medium resolution global and regional land cover land use products: A case study over the conterminous United States. *Remote Sensing*, 15, 3186.

Washington-Allen, R. A., N. E. West, R. D. Ramsey, R. A. Efroymson. 2006. A protocol for retrospective remote sensing based ecological monitoring of rangelands. *Rangeland Ecology Management*, 59, 19–29.

Weber, G. E., K. Moloney, F. Jeltsch. 2000. Simulated long term vegetation response to alternative stocking strategies in savanna rangelands. *Plant Ecology*, 150, 77–96.

Wenze, Y., B. Tan, D. Huang, M. Rautiainen, N. V. Shabanov, Y. Wang, J. L. Privette, K. F. Huemmrich et al. 2006. MODIS leaf area index products: From validation to algorithm improvement. *IEEE Transactions on Geoscience and Remote Sensing*, 44, 1885–1898.

Wessels, K. J. 2009. Letter to the Editor: Comments on 'Proxy global assessment of land degradation' by Bai et al. 2008. *Soil Use and Management*, 25, 91–92.

Wessels, K. J., S. D. Prince, P. E. Frost, D. van Zyl. 2004. Assessing the effects of human-induced land degradation in the former homeland of northern South Africa with a 1 km AVHRR NDVI timeseries. *Remote Sensing of Environment*, 91, 47–67.

Wessels, K. J., S. D. Prince, J. Malherbe, J. Small, P. E. Frost, D. van Zyl. 2007. Can human induced land degradation be distinguished from the effects of rainfall variability? A case study in South Africa. *Journal of Arid Environments*, 68, 271–297.

Wilson, M. F., A. Henderson-Sellers. 1985. A global archive of land cover and soils data for use in general circulation climate models. *International Journal of Climatology*, 5, 119–143.

Wilson, L., R. Van Dongen, S. Cowen, T. P. Robinson. 2022. Mapping restoration activities on Dirk Hartog Island using remotely piloted aircraft imagery. *Remote Sensing*, 14, 1402.

Wold, A. N., A. J. Meddens, D. Lee, V. S. Jansen. 2023. Quantifying the effects of vegetation productivity and drought scenarios on livestock production decisions and income. *Rangelands*, 45(2), 21–32.

Wooster, M. J., G. Roberts, G. Perry, Y. J. Kaufman. 2005. Retrieval of biomass combustion rates and totals from fire radiative power observations: Calibration relationships between biomass consumption and fire radiative energy release. *Journal of Geophysical Research:Atmospheres*, 110, 1–24.

Wulder, M. A., T. R. Loveland, D. P. Roy, C. J. Crawford, J. G. Masek, C. E. Woodcock, R. G. Allen, M. C. Anderson, A. S. Belward, W. B. Cohen et al. 2019. Current status of Landsat program, science, and applications. *Remote Sensing of Environment*, 225, 127–147.

Wylie, B. K., E. A. Fosnight, T. G. Gilmanov, A. B. Frank, J. A. Morgan, M. R. Haferkamp, T. P. Meyers. 2007. Adaptive data driven models for estimating carbon fluxes in the northern Great Plains. *Remote Sensing of Environment*, 106, 399–413.

Xiao, X., P. Dorovskoy, C. Biradar, E. Bridge. 2011. A library of georeferenced photos from the field. *Eos, Transactions American Geophysical Union*, 92:453. https://doi.org/10.1029/2011EO490002.

Xiao, J., Q. Zhuang, D. D. Baldocchi, B. E. Law, A. D. Richardson, J. Chen, R. Oren, G. Starr et al. 2008. Estimation of net eco system carbon exchange for the conterminous United States by combining MODIS and AmeriFlux data. *Agricultural and Forest Meteorology*, 148, 1827–1847.

Xie, Y., Z. Sha, M. Yu. 2008. Remote sensing imagery in vegetation mapping: A review. *Journal of Plant Ecology*, 1, 9–23.

Yebra, M., E. Chuvieco, D. Riaño. 2008. Estimation of live fuel moisture content from MODIS images for fire risk assessment. *Agricultural and Forest Meteorology*, 148, 523–536.

Yin, H., T. Udelhoven, R. Fensholt, D. Pflugmacher, P. Hostert. 2012. How Normalized Difference Vegetation Index (NDVI) trends from Advanced Very High Resolution Radiometer (AVHRR) and Systeme Probatoire d'Observation de la Terre VEGETATION (SPOT VGT) time series differ in agricultural areas: An inner mongolian case study. *Remote Sensing*, 4, 3364–3389.

Yost, E., S. Wenderoth. 1969. Ecological applications of multispectral colour aerial photography. In *Remote Sensing in Ecology*, ed. P. L. Johnson, pp. 46–62. Athens, GA: University of Georgia Press.

Yu, L., L. Zhou, W. Liu, H. K. Zhou. 2011. Using remote sensing and GIS technologies to estimate grass yield and livestock carrying capacity of alpine grasslands in Golog Prefecture China. *Pedosphere*, 17, 419–424.

Zanaga, D., R. Van De Kerchove, D. Daems, W. De Keersmaecker, C. Brockmann, G. Kirches, J. Wevers, O. Cartus, M. Santoro, S. Fritz, M. Lesiv, M. Herold, N. E. Tsendbazar, P. Xu, F. Ramoino, O. Arino. 2020. *ESA WorldCover 10 m 2021 v200*. https://doi.org/10.5281/zenodo.7254221.

Zanaga, D., R. Van De Kerchove, W. De Keersmaecker, N. Souverijns, C. Brockmann, R. Quast, J. Wevers, A. Grosu, A. Paccini, S. Vergnaud, O. Cartus, M. Fritz, S. Santoro, I. Georgieva, M. Lesiv, S. Carter, M. Herold, L. Linlin, N. E. Tsendbazar, F. Ramoino, O. Arino. 2021. *ESA WorldCover 10 m2020v100*.

Zhang, L., D. J. Jacob, X. Liu, J. A. Logan, K. Chance, A. Eldering, B. R. Bojkov. 2010. Intercomparison methods for satellite measurements of atmospheric composition: Application to tropospheric ozone from TES and OMI. *Atmospheric Chemistry and Physics*, 10, 4725–4739.

Zhao, M., S. Running, F. Heinsch, R. R. Nemani. 2011. MODIS-derived terrestrial primary production. In *Land Remote Sensing and Global Environmental Change*, eds. B. Ramachandran, C. O. Justice, M. J. Abrams, pp. 635–660. New York: Springer.

Zhou, B., G. S. Okin, J. Zhang. 2020. Leveraging Google Earth Engine (GEE) and machine learning algorithms to incorporate in situ measurement from different times for rangelands monitoring. *Remote Sensing of Environment*, 236, 111521. https://doi.org/10.1016/j.rse.2019.111521.

Zhu, X., S. Nie, Y. Zhu, Y. Chen, B. Yang, W. Li. 2023. Evaluation and comparison of ICESat-2 and GEDI data for terrain and canopy height retrievals in short-stature vegetation. *Remote Sensing*, 15(20), 4969.

Zhu, L., J. Southworth. 2013. Disentangling the relationships between net primary production and precipitation in Southern Africa savannas using satellite observations from 1982 to 2010. *Remote Sensing*, 5, 3803–3825.

Zika, M. E., K. H. Erb. 2009. The global loss of net primary production resulting from human induced soil degradation in drylands. *Ecological Economics*, 69, 310–388.